The Measurement and Modelling of the Intracrystalline Diffusion of Cyclohexane in ZSM-5 using Zero Length Column Chromatography

Warwick Duncan

Thesis Presented for the Degree of
DOCTOR OF PHILOSOPHY
in the Department of Chemical Engineering
UNIVERSITY OF CAPE TOWN

August 2001

Synopsis

Zeolites are important solid acid catalysts largely because of their microporous nature giving them strong shape selective properties. This shape selectivity may be improved by depositing an inert (e.g. silaceous) layer on the surface of the catalyst crystals, which inertises non-shape selective surface acid sites and increases diffusional transport resistances.

This thesis presents an investigation, using the zero length column (ZLC) method, into changes in the diffusional properties of cyclohexane in ZSM-5 that has had tetraethoxysilane deposited on the surface in the liquid phase. Theoretical analyses of the ZLC technique and its use in a detailed study of cyclohexane in unmodified ZSM-5 were performed in order to prove the reliability of the technique and measure baseline behaviour of the selected system.

The ZLC method is a chromatographic technique for the measurement of diffusion coefficients in porous sorbents. Originally developed for gaseous hydrocarbon / zeolite powder systems, it has been experimentally extended to the measurement of liquid sorbate systems, macroporous zeolite pellets and resins and the measurement of self-diffusion through tracer exchange. The technique is robust against the intrusion of external heat and mass transfer effects by the use of relatively high flow rates and small catalyst samples. Analysis of the desorption curves is simple: the slope of the linear (on semilogarthmic axes) long time region gives the diffusional time constant. This so-called 'long time' analysis gives an accurate result for the diffusional time constant.

The standard analysis is based on the carrier fluid phase being well mixed throughout the sorbent bed, which is reasonable for a physically short column (i.e. with a small Peclet number) and that the sorbent particles are monosized with a linear adsorption isotherm. It is also assumed that sorbate accumulation in the fluid phase is negligible. Theoretical studies, most backed by experimental data, have shown that most deviations from these assumptions do not preclude the accurate estimation of the diffusional time constant by the 'long time' method.

By deriving an alternative model with the fluid phase showing plug flow (infinite Peclet number) behaviour, it was shown that the behaviour of the system becomes independent of the flow pattern in the column for the characteristic dimensionless group $L > 15$, irrespective of the physical length of or (axial) flow pattern in the column. This behaviour was verified through use of a third model incorporating finite axial dispersion. This gives a 'zero length' criterion, by which it may be ensured that systems conform to the 'zero length' assumptions of the standard (mixed flow) model.

To investigate the effect of a distribution of sorbent particle sizes (the standard model assumes a monosized sample) on the desorption curve and measured (using the standard model) parameters, a

model was derived which incorporates a log-mean distribution of crystal radii. It was found that, for this case, the normally linear (on semilogarithmic axes) tail of the desorption curve became convex to the time axis. This is the expected result, since the slope of that region indicates the diffusional time constant (D/R^2). A varying value of R would thus clearly lead to a varying slope and thus curvature. Analysing such a curve with the standard ZLC model would lead to an underprediction of D/R^2 and an overprediction of L. The deviation, as expected, becomes more severe with an increasing distribution width.

The size distribution model was applied to experimental data, but the fitted distribution width was found to be a function of L, indicating that the model could not describe the data consistently. This is possibly a result of the chosen distribution function not being representative of the sorbent sample. If an experimental size distribution were available, it was shown through a simple mathematical analysis that an adequate description of the desorption curve could be obtained by simply summing the responses of a number of discrete size fractions, weighted by volume fraction.

Finally, numerical analysis indicated that, in the absence of more detailed information, systematic error in the diffusion coefficient caused by analysing a sorbent sample with a size distribution by means of the standard model could be reduced by calculating the mean radius of the particles as the ratio of the total volume of the sample to the total surface area.

For the first part of the experimental study, the sorption rate of cyclohexane in three samples of ZSM-5 of different size and morphology was measured. It was found that the diffusion coefficients obtained using the standard analysis method agreed well with one another and with some literature data. The consistency between the large and small crystals' diffusion coefficients is contradictory to many results in the literature. This was attributed to the fact that most small crystals mentioned in the literature are of an industrial origin and might have been hydrothermally treated, whereas the small particles used in this work were laboratory synthesised with no such post-synthesis modification.

While the individual experimental desorption curves appeared to be well described by the simple model, it was found that the adsorption constant appeared to be a function of purge flow rate. More specifically, L was not directly proportional to flow rate as required by the model, consistent with the expected deviations caused by a crystal size distribution. There were also differences caused by changes in the sorbate concentration during the equilibration stage of the experiment, particularly at low temperatures. This was the result of the presence of a Langmuir shaped adsorption isotherm.

Finally, the effect on the diffusion behaviour of the cyclohexane / ZSM-5 system of depositing a silaceous layer on the external surface of the zeolite was investigated. Models were derived and analysed in order to determine whether the mechanisms of pore mouth narrowing (modelled by using a surface barrier approach) and pore mouth blockage (modelled as a decrease in area available for diffusive flux) could be differentiated. The former case should yield reduced values of diffusion and adsorption constants, while the latter should yield a reduced diffusion coefficient and an unchanged adsorption constant, relative to the unmodified catalyst.

Experiments with samples of ZSM-5 modified by tetraethoxysilane in the liquid phase indicated that there was a significant (up to an order of magnitude, depending on the silanisation procedure)

decrease in diffusivity. Although there was scatter in the measured adsorption constants, it appeared that these remained constant for all samples. It would thus appear that, at least for the sorbents used in this work, the change in transport rate due to silanisation was due to the pore mouth blockage mechanism.

Contents

Contents v

List of Figures ix

List of Tables xv

Nomenclature xvii

1 Introduction 1

1.1 Zeolites . . . 1

1.1.1 ZSM-5 . . . 2

1.2 The importance of diffusion in porous adsorbents . . . 2

1.3 Post-synthesis zeolite modifications . . . 3

1.3.1 Deposition of silicon alkoxides on ZSM-5 . . . 3

1.4 The theory of diffusion . . . 4

1.4.1 Fundamental principles . . . 4

1.4.2 Diffusion mechanisms . . . 5

1.4.3 Diffusion mechanisms in porous media . . . 6

1.5 Methods of measuring diffusion . . . 8

1.5.1 The measurement of transport diffusivity . . . 8

1.5.2 The measurement of self-diffusivity . . . 10

1.5.3 Computational methods . . . 11

1.6 Causes of spurious results in diffusion measurements . . . 11

1.6.1 Intrusion of extracrystalline mass transfer resistance . . . 11

1.6.2 Intrusion of extracrystalline heat transfer resistance . . . 12

1.6.3 Surface barriers to mass transfer . . . 12

1.7 Zero length column chromatography . . . 13

1.8 Purpose of this work . . . 14

2 Review of ZLC Models and Analysis Methods 15

2.1 Preliminary assumptions and equations . . . 15

2.2 The standard model . . . 17

2.2.1 Standard model in slab geometry . . . 19
2.3 Analysis methods for the standard model . . . 20
2.3.1 The long time method . . . 20
2.3.2 Short time methods . . . 20
2.3.3 Full time range model fitting . . . 22
2.3.4 Moments analysis . . . 24
2.4 Systems with external mass transfer . . . 25
2.5 External heat transfer effects . . . 26
2.6 Model for liquid systems . . . 28
2.7 Model for nonlinear systems . . . 29
2.8 Incomplete initial equilibration . . . 31
2.9 Evaluation of analysis methods . . . 32

3 A 'Zero Length' Criterion 33
3.1 Development of the models . . . 33
3.2 Results and discussion . . . 35
3.2.1 Comparison of the plug flow and standard models . . . 37
3.3 Conclusions on zero length behaviour . . . 39

4 The Effect of a Crystal Size Distribution 41
4.1 Development of the models . . . 41
4.1.1 Continuous size distribution model . . . 41
4.1.2 Discrete size distribution model . . . 44
4.2 Results and discussion . . . 45
4.2.1 Comparison of size distribution and standard models . . . 45
4.2.2 Description of experimental data with the size distribution model . . . 47
4.2.3 Approximate models to account for a particle size distribution . . . 51
4.2.4 Definition of mean particle size . . . 53
4.2.5 Some practical considerations . . . 54
4.3 Conclusions . . . 56

5 Experimental Procedures and Apparatus 57
5.1 Unmodified sorbents . . . 57
5.2 Silanised sorbents . . . 58
5.2.1 Silanisation procedure . . . 58
5.3 Apparatus and experimental procedure . . . 58
5.4 Data analysis . . . 60

6 The Diffusion of Cyclohexane in Unmodified ZSM-5 63
6.1 Results and discussion . . . 63
6.1.1 External mass transfer . . . 71

6.1.2 Particle size distribution effects . . . 71
6.1.3 Nonlinear adsorption isotherm effects . . . 72
6.1.4 Lack of variation of diffusivity with crystal size . . . 74
6.2 Conclusions . . . 75

7 Diffusion in Silanised ZSM-5 **77**
7.1 Surface barrier analysis for the ZLC . . . 77
7.1.1 Behaviour of the intercept with flow rate . . . 79
7.1.2 The effect of a surface barrier on activation energy . . . 80
7.1.3 The effect of a surface barrier on adsorption constant . . . 82
7.2 Analysis of pore blockage . . . 83
7.2.1 Decrease in surface area for flux . . . 83
7.2.2 Decrease in total area for flux . . . 84
7.2.3 Effect of pore blockage on measured parameters . . . 85
7.2.4 Limitations of the pore blockage analyses . . . 86
7.3 ZLC measurements with cyclohexane/ZSM-5 . . . 86
7.3.1 Mechanism of transport rate reduction . . . 89
7.3.2 Sorbents modified with pure TEOS . . . 91
7.4 Conclusions about diffusion in silanised ZSM-5 . . . 93

8 Concluding Remarks **95**

Bibliography **97**

A Derivation of ZLC Models **103**
A.1 Adsorbed phase mass balance . . . 103
A.2 Fluid phase mass balance . . . 105
A.3 Disperse flow model . . . 106
A.3.1 Equilibrium control . . . 108
A.4 Plug flow model . . . 109
A.4.1 Equilibrium control . . . 109
A.4.2 Approximation for large L . . . 110
A.5 Crystal size distribution model . . . 112

B Experimental Data **115**
B.1 Sample data files . . . 115
B.2 AZSM5 (Sample B) . . . 118
B.3 BZSM5 (Sample Z-L-5/H) . . . 120
B.4 DZSM5 (Sample Z-L-5/W) . . . 121
B.5 EZSM5 (Sample Z-L-0.5/W) . . . 122
B.6 FZSM5 (Sample Z-L-100/-) . . . 123

B.7 GZSM5 (Sample Z-L-5/E) . . . 124
B.8 HZSM5 (Sample Z-L-100/-(60h)) . . . 124
B.9 RZSM5 (Sample A) . . . 125
B.10 WZSM5 (Sample C, Parent sample) . . . 126

C Selected Fortran Code **127**
C.1 Standard model fitting program . . . 127
C.2 Standard ZLC model . . . 130
C.3 Plug flow model . . . 133
C.4 Disperse flow model . . . 135
C.5 Size distribution model . . . 137
C.6 Supplementary functions . . . 139
C.6.1 `cdcoth()` . . . 139
C.6.2 `fold()` . . . 140
C.6.3 `objfn()` . . . 140
C.6.4 `rddata()` . . . 141
C.6.5 `d1mach()` . . . 144
C.6.6 `cffti()` and `cfftb()` . . . 144
C.6.7 `gaussq()` . . . 144
C.6.8 `divset()` and `dmnfb()` . . . 144

List of Figures

1.1 Structure of zeolite ZSM-5 as viewed along the straight and sinusoidal channels as indicated. 2

1.2 Structure of polymeric silaceous layer on zeolite surface. 3

2.1 ZLC desorption curves generated with the standard model (Eq. 2.16) for $L = 5$, 10, 20, 50 and 100. 18

2.2 Comparison of the standard ZLC model in spherical and slab geometries for $L = 50$. The diffusion time constant (D/R^2) for the third curve was increased by a factor 4. . . 19

2.3 Approach of β_1^2 to π^2 with L. 21

2.4 Comparison of the short time approximation Eq. 2.27 (the line $y = x$) with the full ZLC model solution (Eq. 2.16, points) for various values of L. 22

2.5 ZLC desorption curves plotted as suggested by the short time approximation Eq. 2.29 for various values of L as indicated. 23

2.6 ZLC desorption curves showing the proposed method of extracting the diffusion parameters according to Eq. 2.30 for various values of L as indicated. 23

2.7 Criterion for negligible thermal effects as a function of diffusion resistance, reproduced from Brandani et al. (1998). The ordinate is given by $(\alpha\delta/\gamma) = \left(\frac{\Delta H}{R_g T_0}\right)^2 \cdot \frac{C_0 FR}{haV_s}$. . . . 27

2.8 Representative desorption curves generated with the liquid phase ZLC model (Eq. 2.44) for $L = 50$ and $\gamma = 0.1$, 0.5 and 1. The standard model (Eq. 2.16, points) is shown for reference. 29

3.1 Plot of desorption curves using the plug flow (Eq. 3.17), liquid (Eq. 2.44) and disperse flow (Eq. 3.11) models for $L = 20$ and $\gamma = 1$. The standard model (Eq. 2.16) is shown for reference. 36

3.2 Plot of equilibrium controlled desorption curves using the plug flow (Eq. 3.21), CSTR (Eq. 3.22) and disperse flow (Eq. 3.19, $N_{Pe} = 3$) models. 36

3.3 Deviation in the apparent value of D/R^2 when fitting the standard ZLC model (Eq. 2.16) to the plug flow model (Eq. 3.17). 38

3.4 Deviation in the apparent value of L when fitting the standard ZLC model (Eq. 2.16) to the plug flow model (Eq. 3.17). 38

3.5 Desorption curves plotted with the plug flow model (Eq. 3.17) and the standard model (Eq. 2.16) for $L = 5$ and $\gamma = 0$, with the standard model fitted to the plug flow model having parameters $(D/R^2)_{\text{apparent}} = 1.45(D/R^2)$ and $L_{\text{apparent}} = 3.73$. 39

3.6 Desorption curves plotted with the plug flow model (Eq. 3.17) and the standard model (Eq. 2.16) for $L = 50$ and $\gamma = 0$. 40

4.1 Particle size distribution plot in arbitrary units for $\mu = 0$ and values of σ as indicated. 43

4.2 Desorption curves generated using the size distributions model (Eq. 4.12) for $L = 20$ and various values of σ as shown. The standard ZLC model (Eq. 2.16) is shown for verification. 44

4.3 Apparent deviation in diffusional time constant when fitting the standard ZLC model to that with a crystal size distribution, for various distribution widths. 45

4.4 Apparent deviation in L when fitting the standard ZLC model to that with a crystal size distribution, for various distribution widths. 46

4.5 Model comparison for the standard model fitted to the crystal size distribution model when $\sigma = 0.3$ for L as shown. 46

4.6 Model comparison for the standard model fitted to the crystal size distribution model when $\sigma = 0.5$ for L as shown. 47

4.7 Dependence of measured L on flow rate ($L_{\text{m}} \propto F$) when fitting the standard ZLC model to that with a crystal size distribution, for various distribution widths. 48

4.8 Example of model fit for the standard and size distribution models to an experimental desorption curve ($T = 200$°C, $F = 41.6$ ml/min, $m_{\text{s}} = 2$ mg, $D/R^2 = 1.22\times10^{-2}$ cm^2/s, $L = 30.3$). 48

4.9 Temperature dependence of the diffusional time constant as determined by both the standard and size distribution models. 49

4.10 Crystal size distribution width as a function of L for all points shown in Figure 4.9. . 50

4.11 Temperature dependence of the diffusional time constant as determined by both the standard and size distribution models with fixed $\sigma = 0.3$. 50

4.12 Example model fits using the size distribution model for two and three adjustable parameters, for desorption curve with large L (standard model fit gives $D/R^2 = 3.50 \times 10^{-4}$ cm^2/s, $L = 146$). 51

4.13 Desorption curves plotted using the full and approximate size distribution models for $\sigma = 0.3$ and L as indicated. 52

4.14 Desorption curves plotted using the full and approximate size distribution models for $\sigma = 0.5$ and L as indicated. 53

4.15 Deviation in apparent diffusional time constant when fitting the standard ZLC model to that with a crystal size distribution, for various widths, including the correction factor indicated by Equation 4.26. 54

4.16 Deviation in apparent L when fitting the standard ZLC model to that with a crystal size distribution, for various widths, including the correction factor indicated by Equation 4.26. 55
4.17 Arrhenius plot showing series of experiments where the sorbent was allowed to settle (lower two data sets) or was agitated (upper data) before packing. 55

5.1 Scanning electron micrographs of sample B. 57
5.2 Flow sheet of the ZLC apparatus used in this work. 59
5.3 Blank experiments (i.e. in the absence of sorbent) performed using an 1/8" diameter reactor at various temperatures as shown. 61

6.1 Temperature dependence of the diffusivity of cyclohexane in ZSM-5 with literature data shown for reference. Experimental data at the same temperatures have been averaged. 64
6.2 Arrhenius plots of the diffusional time constants measured for the three samples with best-fit lines. Full data sets are shown. 65
6.3 Representative desorption curve for sample A with model fit. Experimental conditions: $T = 200$℃, $F = 34.7\,\mathrm{ml/min}$, $C_0 = 395\,\mathrm{Pa}$, $m_s = 22\,\mathrm{mg}$. Fitted model parameters: $D/R^2 = 2.31 \times 10^{-4}\,/\mathrm{s}$, $L = 150$. 65
6.4 Representative desorption curve for sample B with model fit. Experimental conditions: $T = 150$℃, $F = 68.2\,\mathrm{ml/min}$, $C_0 = 495\,\mathrm{Pa}$, $m_s = 2\,\mathrm{mg}$. Fitted model parameters: $D/R^2 = 2.61 \times 10^{-3}\,/\mathrm{s}$, $L = 50.4$. The dashed line indicates a blank run (i.e. in the absence of sorbent) performed at similar conditions. 66
6.5 Representative desorption curve for sample C with model fit. Experimental conditions: $T = 125$℃, $F = 87.5\,\mathrm{ml/min}$, $C_0 = 191\,\mathrm{Pa}$, $m_s = 2\,\mathrm{mg}$. Fitted model parameters: $D/R^2 = 1.55 \times 10^{-3}\,/\mathrm{s}$, $L = 61.0$. 66
6.6 Temperature dependence of the Henry adsorption constant for cyclohexane on ZSM-5 as measured for the three different samples. Pairs of points show the upper and lower limits of the data. 67
6.7 Adsorption constants measured for sample A, with the van't Hoff equation fitted to all but the two lower temperature points. The full data set is shown. Literature data are shown for comparison. 68
6.8 Dependence of L on flow rate for sample B at 150℃, measured at different initial sorbate concentration as indicated, in a 1/8 in. tube. Lines are to aid the eye. 68
6.9 Dependence of L on flow rate for sample B at 200℃, measured at different initial sorbate concentration as indicated, in a 1/8 in. tube. Lines are to aid the eye. 69
6.10 Dependence of D/R^2 on flow rate for sample B at 150℃, measured at different initial sorbate concentrations, as indicated, in a 1/8 in. tube. 69
6.11 Dependence of D/R^2 on flow rate for sample B at 200℃, measured at different initial sorbate concentrations, as indicated, in a 1/8 in. tube. 70

6.12 Dependence of $D/R^2 \times L$ on flow rate for sample B at 150℃for the same data as shown in Figures 6.8 and 6.10 to show the apparent dependence of K on flow rate. Lines are to aid the eye. 70
6.13 Desorption curves for sample A at different initial concentrations ($C_0 = 263$, 1468 and 2855 Pa). Other experimental conditions: $T = 150$℃, $F = 52.0$ ml/min, $m_s = 22$ mg. . 72
6.14 Plot to extract Langmuir isotherm parameters from apparent Henry constants. Data are for 22 mg of sample A at 200℃ and 52 ml/min. 73
6.15 Diffusional time constant as a function of the initial concentration for the same experiments as those shown in Figure 6.14. Data are for 22 mg of sample A at 200℃ and 52 ml/min. 74

7.1 Desorption curves for the surface barrier model for various $D/(k_s R)$ as shown and $L = 100$. The standard model is shown for verification. 79
7.2 Fit of the standard model (lines) to the surface barrier model (points) for $D/(k_s R) = 0.3$ and $L = 100$. 80
7.3 Variation of the initial eigenvalue of the surface barrier model with temperature for $E_a - E_{as} = -55$ kJ/mol and $k_s R/D = 10^8$. 81
7.4 Error in apparent value of K relative to true value when using the standard analysis for a system influenced by a surface barrier. Curves are for $L = 10$, 20, 30, 50, 70, 100 and 120. 82
7.5 Representations of the pore blockage models showing which areas of the sorbent particle do not allow radial diffusive flux. 83
7.6 Conceptual diffusion paths inside a porous sorbent with a fraction of blocked pore openings. 85
7.7 Arrhenius plot for the parent and all silanised ZSM-5 samples. Data have been averaged for each temperature. 87
7.8 Experimental desorption curves and model fits for parent and silanised (Z-L-5/H) catalysts for identical conditions ($T = 150$℃, $F = 93.0$ ml/min, $C_0 = 191$ Pa). 87
7.9 Arrhenius plot showing all data (except for sample Z-L-0.5/W, for which average data at each temperature are shown) for samples that have been modified with dilute TEOS. 88
7.10 Sample desorption curves for the parent ZSM-5 sample at the conditions indicated. . . 88
7.11 Sample desorption curves for 7 mg of sample Z-L-5/H at the conditions indicated. . . . 89
7.12 Van't Hoff plot showing all adsorption constant data for samples that have been modified with dilute TEOS. 90
7.13 Diffusional time constant for cyclohexane in ZSM-5 at 150℃ for modified catalyst samples (relative to parent) as a function of their 4-methyl quinoline temperature programmed desorption capacities (relative to parent). TPD data are from Weber (1998). 91
7.14 Arrhenius plot for ZSM-5 samples modified with pure liquid TEOS. 92

7.15 Desorption curves for sample Z-L-100/-(60h) at 250℃ and flow rate and initial cyclohexane concentrations as follows: $F = 79.5\,\mathrm{ml/min}$, $C_0 = 207\,\mathrm{Pa}$; $F = 98.7\,\mathrm{ml/min}$, $C_0 = 167\,\mathrm{Pa}$; $F = 117.8\,\mathrm{ml/min}$, $C_0 = 140\,\mathrm{Pa}$; $F = 137.0\,\mathrm{ml/min}$, $C_0 = 120\,\mathrm{Pa}$. 92

7.16 Desorption curves for sample Z-L-100/-(60h) at 250℃, 79.5 ml/min and initial cyclohexane concentrations of 207, 482 and 897 Pa. 93

List of Tables

4.1 Division of a continuous size distribution into discrete fraction such that all fractions have equal surface area or volume; $\mu = 0$. 52

5.1 Naming convention of silanised ZSM-5 samples used in this work. 58

6.1 Summary of measured diffusivities and diffusional activation energies. 64

Nomenclature

a	pore diameter
b	parameter in Langmuir adsorption isotherm
c	concentration
C	fluid phase sorbate concentration
C_p	heat capacity
D	intracrystalline diffusivity
$\mathcal{D}$	self-diffusivity
D_0	corrected diffusivity
D_{AB}	binary (bulk) diffusion coefficient
D_K	Knudsen diffusion coefficient
D_{L}	axial dispersion coefficient
D_{m}	molecular diffusion coefficient
E_{a}	activation energy of intracrystalline diffusion
E_{as}	activation energy of transport across surface barrier
F	carrier fluid volumetric flow rate
h	heat transfer coefficient
ΔH_{a}	enthalpy change on adsorption
J	diffusive flux
K	dimensionless Henry constant of adsorption
k_{s}	first order surface barrier rate constant
L	ratio of diffusion to convection time; eq. 2.15
L'	analogue to L for pore blockage model; eq. 7.18
L_{m}	analogue to L for model including external mass transfer; eq. 2.36
L_{s}	analogue to L for surface barrier model; eq. 7.5
L_{bed}	length of sorbent bed
M	molecular weight
m_{s}	mass of sorbent
N_{Pe}	Peclet number
N_{Sh}	Sherwood number
p	Laplace parameter with respect to τ_{e}
	partial pressure

P	size distribution function
	pressure
q	adsorbed phase sorbate concentration
q_s	saturation adsorbed phase sorbate concentration
Q	normalised adsorbed concentration; $Q = q/q_0$
r	radial position in sorbent particle
R	sorbent particle radius
R_g	universal gas constant
R_m	mean particle radius; eq. 4.10
s	Laplace parameter with respect to τ
t	time
T	temperature
v	fluid linear velocity
V_f	volume of fluid in sorbent bed
V_s	volume of sorbent
X	normalised radial coordinate; $X = r/R$
y_A	mole fraction of component A
Y	normalised fluid phase concentration; $Y = C/C_0$
z	axial position in sorbent bed
Z	normalised axial position; $Z = z/L_{bed}$

Greek Symbols

α	parameter to indicate intracrystalline tortuosity ($0 < \alpha \leq 1$)
β_n	model eigenvalue; eq. 2.17
β'_n	analogue to β_n for model with pore blockage; eq. 7.23
β_{sn}	analogue to β_n for surface barrier model; eq. 7.7
γ	ratio of carrier fluid capacity to sorbent capacity; eq. 2.46
δ	tortuosity
λ	ratio of initial loading to saturation loading; eq. 2.48
μ	number mean of normal distribution of $\ln R$
η	viscosity
σ	standard deviation of normal distribution of $\ln R$
τ	dimensionless diffusion time ($\tau = Dt/R^2$)
τ_e	dimensionless equilibrium controlled desorption time ($\tau_e = Ft/(V_s K + V_f)$)
τ_f	ratio of fluid wash-out time to diffusion time; $\tau_f = V_f D/(FR^2)$
τ_m	dimensionless time; $R_m = Dt/R_m^2$
ζ	dummy variable used in size distribution model

Chapter 1

Introduction

This chapter gives an introduction to the importance of zeolites and diffusion in chemical reaction engineering. Methods of altering the diffusional characteristics of zeolites are discussed. The theory of diffusion, particularly in microporous sorbents, and methods of measurement are described, with particular attention to zero length column chromatography. Finally, the aims and a brief outline of this thesis are given.

Sections 1.1 and 1.3 borrow heavily from Weber (1998), Sections 1.4 and 1.5 from Kärger and Ruthven (1992).

1.1 Zeolites

Zeolites are three dimensional aluminosilicates made up of linked tetrahedra with small atoms ("T atoms") at the centre of each tetrahedron and with oxygen atoms at the corners. The T atoms are normally either silicon or aluminium, such that the ratio O/(Si+Al)=2. The presence of Al atoms in the silicon based structure (which give the zeolite their Bronsted acidity required for catalysis) results in a nett negative charge on the crystal lattice, which must be balanced by a counter-ion, typically H^+ or Na^+. The arrangement of the tetrahedral units results in the formation of channels and cavities, different configurations of which yield the different zeolite types.

The zeolite characteristic of greatest interest is the channel system. Depending on the largest channel, zeolites are classified as being either small, medium or large pore types. Small pore structures (e.g. 5A) have apertures made up of eight linked tetrahedra, while medium (e.g. ZSM-5) and large pore (e.g. mordenite) zeolites have ten and twelve membered rings respectively. In addition to these pore size differences, the channels of different zeolites have differing configurations, being one- (ZSM-22), two- (ferrierite) or three- (ZSM-5) dimensional, and may be straight or tortuous. The channels of multidimensional pore structured zeolites may intersect; the three dimensional nature of ZSM-5 is in fact a result of its two intersecting two dimensional channel systems.

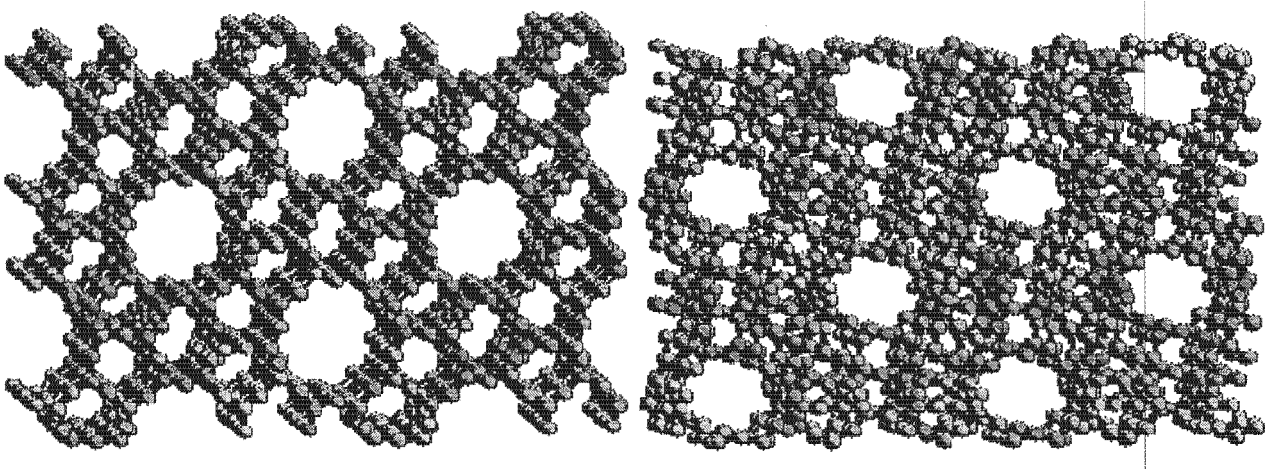

(a) straight (b) sinusoidal

Figure 1.1: Structure of zeolite ZSM-5 as viewed along the straight and sinusoidal channels as indicated.

1.1.1 ZSM-5

ZSM-5 (Figure 1.1) is a medium pore MFI type zeolite with an intersecting, three dimensional channel structure, made up of straight channels running parallel to the (100) axis and sinusoidal channels running parallel to the orthogonal (010) axis. The pores are 10 membered and elliptical, the sinusoidal channels having a size of 5.1×5.5 Å and the straight channels 5.3×5.6 Å. ZSM-5 has a crystal density of $1.76\,\mathrm{g/cm^3}$ (Szostak, 1992).

1.2 The importance of diffusion in porous adsorbents

One of the prime reasons that zeolites have become important catalysts is their shape selective nature, caused by steric hindrance of intermediates and product species in the cages and pores of the structure. The restrictive size of the zeolite cages reduces or eliminates the formation of intermediates that cannot fit into them without significant strain on their structure. In addition, some of the products of a reaction may be bulkier than others, which are then able to diffuse out faster. This creates a surplus of the unwanted products inside the catalyst structure and so the reaction is driven towards the formation of the desired products. Thus, while there may be an equilibrium product distribution within the catalyst, or close to it, transport restrictions are able to create a product spectrum different to that predicted from thermodynamic considerations. This effect, whereby selectivity is determined by the relative diffusion and adsorption parameters of the system components, has been modelled by Liang et al. (1995).

An important example of shape selective catalysis caused by the above mentioned effects is the isomerisation of C_8 aromatics over H-ZSM-5 (Kärger and Ruthven, 1992). The main industrial demand is for *p*-xylene and, to a lesser extent, *o*-xylene, while *m*-xylene and ethylbenzene are generally unwanted.

H-ZSM-5 is able to isomerise the xylenes with very little disproportionation, probably as a result

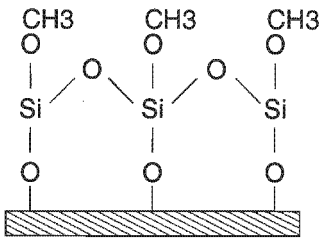

Figure 1.2: Structure of polymeric silaceous layer on zeolite surface.

of transition state selectivity favouring the unimolecular isomerisation mechanism rather than the bimolecular disproportionation path, which then has a far larger intermediate. In addition, the large difference in diffusivity between *p*-xylene and the *o*- and *m*- isomers results in the latter two being effectively trapped within the zeolite pores. *P*-xylene (and ethylbenzene) on the other hand, can easily diffuse out. As a result, the fraction of *p*-xylene in the product is greater than the equilibrium value.

Differences in species diffusivity may also be exploited for separation processes, such as the liquid phase 'Molex' process (Kärger and Ruthven, 1992), which employs zeolite 5A for the separation of linear from branched hydrocarbons by molecular sieving.

1.3 Post-synthesis zeolite modifications

Depending on the process for which it is to be used, it is sometimes beneficial to modify the zeolite to improve its behaviour. Hydrothermal treatment (steaming) can increase the activity of several zeolite types by causing dealumination of the crystal lattice and the formation of extra-framework aluminium at its surface. Acid leaching with HCl or HNO_3 may be used to remove extra-framework aluminium from zeolites. A third example of post-synthesis modification is the formation of a silicalite (Al-free ZSM-5) shell on the outer surface of ZSM-5 crystals, for the purpose of creating a catalyst with an inert surface (catalytic sites on the external surface are, of course, non-shape selective) while not reducing the catalytic activity of the shape selective crystal interior.

1.3.1 Deposition of silicon alkoxides on ZSM-5

The deposition of silicon alkoxides (using chemical vapour deposition or chemical liquid deposition) on zeolites has been intensively investigated recently. The compounds are chosen for their size, so that they do not enter the zeolite pores. Thus they deposit only on the external surface of the particle. The most commonly used silanes compounds are tetramethoxysilane (TMOS) and tetraethoxysilane (TEOS). The molecular diameter of TEOS is 9.6 Å.

Three methods of silane deposition have been reported in the literature: a static vacuum technique and vapour and liquid phase flow methods. The precise conditions vary greatly between investigations.

It has been proposed that the TMOS deposition mechanism on zeolites follows the following

scheme: first, the alkoxide reacts with the hydroxyl on the external surface, giving a trimethoxide attached to the surface and methanol. The trimethoxide is then hydrolysed (by the addition of water to the system or by residual water in the zeolite) to form new hydroxyl groups, which react further with alkoxide in the gas phase or other surface-attached trimethoxides to form a polymeric silica later on the surface (see Figure 1.2).

Various studies have shown that, while the adsorption capacities (and ammonia TPD) of silanised zeolites remain similar to the unmodified catalyst, sorption rates tend to be lower for the modified samples. This result implies that the internal structure is conserved, but the pore openings are either narrowed or blocked. Much work in the literature indicates that pore mouth narrowing does occur and that the pore mouth size can be closely controlled, but consideration of the relative sizes of the channel openings and the Si-O bonds lengths, this effect is difficult to justify on purely steric grounds.

Chemical vapour and liquid deposition methods have been widely used to improve *para*-selectivities for a range of reactions, including the isomerisation of *o*-xylene, the disproportionation of toluene and the alkylation of toluene and ethylbenzene with methanol or ethylene on ZSM-5. Selectivity toward the *para*-isomers routinely exceeds 95%, but conversion is lower than in the parent sample.

1.4 The theory of diffusion

This section will introduce the quantitative aspects of diffusion and will outline mechanisms whereby diffusion is thought to occur. A more detailed mathematical treatment may be found elsewhere in the literature (Kärger and Ruthven, 1992).

1.4.1 Fundamental principles

There are essentially two types of diffusion: transport diffusion, which occurs as a result of a concentration gradient, and self-diffusion, which describes the motion of molecules in the absence of a gradient. This is essentially Brownian motion.

In the mid-1800's, Adolf Fick recognised that the diffusion of matter could be represented by a relationship analogous to Fourier's Law of heat conduction, leading to what has become known as Fick's First Law of Diffusion (Kärger and Ruthven, 1992):

$$J = -D\nabla c \tag{1.1}$$

This equation may be taken as the definition of the transport diffusivity, or diffusion coefficient, D.

Using a mass balance and the assumption that D is not a function of concentration c, it is easy to derive Fick's Second Law:

$$\frac{\partial c}{\partial t} = -D\nabla^2 c \tag{1.2}$$

While Equation 1.1 indicates that the driving force for diffusion is a concentration gradient, it may be argued that, since diffusion is a manifestation of the tendency of systems towards thermodynamic equilibrium, the true driving force must be a gradient of chemical potential. Using this starting

point, it is possible to derive the following form of Equation 1.2:

$$J = D_0 \frac{d\ln p}{d\ln c} \nabla c \tag{1.3}$$

By comparison with Equation 1.1 it can be seen that the term D has been replaced with the product of D_0, known as the 'corrected diffusivity', and a form of derivative of the adsorption isotherm of the system. This derivative is generally known as the Darken correction factor. If a system shows Henry's Law adsorption behaviour this derivative becomes equal to unity and the transport and corrected diffusivities (D and D_0) become identical. It is found that D_0 is often independent of concentration (Kärger and Ruthven, 1992).

Using irreversible thermodynamics (i.e. considering the rate of entropy generation of a diffusive system) it is possible to derive the following relation between transport and self-diffusivities (D and $\mathcal{D}$):

$$\frac{D(c)}{\mathcal{D}(c)} = \frac{d\ln p}{d\ln c}\left[1 + \frac{\beta(c)}{\alpha(c)}c\right] \tag{1.4}$$

Here α and β are phenomenological coefficients representing sorbate-sorbent and inter-sorbate interactions respectively. Thus at low sorbate concentrations, where the adsorption isotherm is linear and sorbate-sorbate interactions are a minimum, it would be expected that the transport diffusivity should be directly comparable to the self-diffusivity.

1.4.2 Diffusion mechanisms

Mass transport in porous and adsorbing media takes place in a variety of ways depending on the sorbate interaction with the sorbent.

Molecular diffusion

This is the mechanism (also known as bulk diffusion) whereby fluids diffuse through one another without interference from any other phases. In heterogeneous systems this sort of diffusion is important in large pores (in which the mean free path of the diffusing molecules is much larger than the pore diameter) and in the transport of molecules through external fluid films.

Bulk diffusivity may be accurately calculated for gases at moderate temperatures and pressures using the Chapman-Enskog formula (Smith, 1981):

$$D_{\mathrm{AB}} = 0.0018583 \frac{T^{\frac{3}{2}}\left(\frac{1}{M_{\mathrm{A}}} + \frac{1}{M_{\mathrm{B}}}\right)^{\frac{1}{2}}}{P\sigma_{\mathrm{AB}}^2 \Omega_{\mathrm{AB}}} \tag{1.5}$$

where A and B are the two components under consideration, T is in Kelvin, M is the molecular weight, P is in atmospheres, σ_{AB} is the Lennard-Jones potential energy function for the molecule pair in Å, Ω_{AB} is the collision integral and D_{AB} is in cm^2/s. Strictly speaking, this relation should only be used for non-polar gases.

Knudsen diffusion

In small pores or at low pressures, where the mean free path of the diffusing molecules are comparable to or larger than the pore diameter, collisions between the molecules and the pore wall occur more frequently than intermolecular collisions. Knudsen diffusion is a stochastic process and is dependent only on the pore size and molecular velocity. Knudsen diffusion does not occur for liquid phases (Smith, 1981).

The following expression is generally used to calculate the Knudsen diffusivity D_K (Kärger and Ruthven, 1992):

$$D_K = 9700a\sqrt{\frac{T}{M}} \tag{1.6}$$

where a (the pore diameter) is in centimetres, T in Kelvin, M in g/mol and D_K in cm^2/s.

Poiseuille flow

If there is a pressure difference between the ends of a capillary, there will be a bulk laminar flow described by a Fickian-type relation. The Poiseuille diffusivity is given by (Kärger and Ruthven, 1992):

$$D_{\text{Poiseuille}} = \frac{\Delta P a^2}{8\eta} \tag{1.7}$$

A fair assumption would be to treat this forced flow as additive to the diffusive flux, particularly under isothermal conditions. Poiseuille flow is generally only important in large pores (diameter of the order of hundreds of Angstroms) and its contribution increases with pressure.

Surface diffusion

For systems with a high adsorbed phase concentration, there is a possibility of a diffusive flux due to the movement of fairly mobile physically adsorbed molecules. This flux may be approximately treated as additive to the gas-phase diffusive flux. Surface diffusion is generally insignificant at temperatures greater than the boiling point of the sorbate.

Application of this concept to a microporous adsorbent such as a zeolite is probably not relevant, since adsorption occurs by pore filling rather than the classical attachment of an adsorbate onto a flat surface.

1.4.3 Diffusion mechanisms in porous media

Pores may be divided into three types based on size, with the IUPAC definitions being:

- micropores: <20Å
- mesopores: 20–500Å
- macropores: >500Å

This classification is based on the different mechanisms that control sorption behaviour in the different size pore size regimes.

Macroporous diffusion

In many cases both bulk and Knudsen diffusion contribute to the mass transport rate within the macropores. The combined effective diffusivity for a binary system is given by (Smith, 1981)

$$\frac{1}{D} = \frac{1 - \left(1 - \sqrt{\frac{M_A}{M_B}}\right) y_A}{D_{AB}} + \frac{1}{(D_K)_A} \tag{1.8}$$

where A is the diffusing species, y_A is its mole fraction and B is the bulk fluid within the pore. This relation is valid for non-reacting systems under constant pressure.

When reaction occurs, the term under the radical in Equation 1.8 is determined by the reaction stoichiometry. For stoichiometry such that the diffusion is countercurrent and equimolar, the following simplified relation may be used:

$$\frac{1}{D} = \frac{1}{D_{AB}} + \frac{1}{(D_K)_A} \tag{1.9}$$

The above relationships do not, however, account for realistic geometric considerations in zeolites, such as the interconnection of pores and the fact that they are not straight cylinders; they are based on the cross-sectional area of the pores. It is therefore customary to correct these values using an adjustable factor known as the tortuosity factor δ as follows:

$$D_{\text{effective}} = \frac{\varepsilon_{\text{pellet}} D}{\delta} \tag{1.10}$$

where D is given by Equation 1.8 or 1.9. Formulae to predict δ on the basis on structural consideration of the sorbent solid (Kärger and Ruthven, 1992) give fairly good approximations.

Experimental data has shown δ to range from less than 1 to greater than 6, with the typical value being approximately 3 (Smith, 1981; Kärger and Ruthven, 1992).

Microporous diffusion

The mechanism of diffusion in micropores (microporous, configurational or intracrystalline diffusion) differs from those discussed above in that the diffusing molecules never escape the force field of the pore wall, even in the centre of the pore. It is an activated process, with similarities to surface diffusion, and thus shows an Arrhenius temperature, i.e.

$$D = D_\infty \exp\left(-\frac{E_a}{R_g T}\right) \tag{1.11}$$

where E_a is the activation energy and R_g the universal gas constant. The movement of the diffusing molecules proceeds by a series of jumps between regions of relatively low potential energy (sites).

Microporous diffusion is generally Fickian in nature, but with the Fickian diffusivity tending to show a strong increase in concentration (Kärger and Ruthven, 1992), although this is certainly not the rule (e.g. (Bülow et al., 1991; Grenier et al., 1994). It is found, however, that the corrected diffusivity is fairly concentration-independent.

Because of the constant strong interaction between the sorbing molecules and the pore walls it is usual to consider the diffusing molecules within the pores as a single adsorbed phase.

1.5 Methods of measuring diffusion

A wide variety of methods have been applied to the measurement of diffusion in zeolites. This section will give a brief overview on some of these methods, with the exception of the ZLC method, which will be dealt with in greater detail in Section 1.7.

1.5.1 The measurement of transport diffusivity

These techniques are largely transient and involve the measurement of diffusion under the influence of a concentration gradient. These include the well-known gravimetric uptake and ZLC methods, as well as the more obscure optical and X-ray techniques. It is usual, with these methods, to work under conditions of Henry's Law adsorption in order to simplify the interpretation of the experimental data. Alternatively, differential concentration changes could be used such that the isotherm is linear over the range of conditions used for the experiment.

Batch methods

In constant pressure techniques, the sorbent sample is subjected to a step change in the sorbate pressure at constant total pressure, with the approach to equilibrium being monitored either volumetrically or, more usually, gravimetrically. The constant pressure condition is easier to maintain in the latter case simply by using an experimental system with a sufficiently large volume.

Alternatively, one may conduct the experiment at constant volume and follow the approach to equilibrium by monitoring the pressure. The system volume should be small enough so that the sorption changes the pressure by a measurable amount.

A different approach to the step change methods described above is to perturb the systems periodically (Yasuda, 1982). These are known as frequency response methods.

The major disadvantage of these methods is that the sorbent sample is placed in a stagnant gas so that external heat and mass transfer resistances can be difficult to eliminate. It is thus necessary to use small samples in order to counteract these and bed diffusion effects. It is also usual to vary the sorbent configuration to ensure that consistent results are obtained.

The behaviour of batch sorption systems has been comprehensively modelled for a variety of geometries and controlling diffusion regimes, as well as for non-isothermal regimes (Kärger and Ruthven, 1992).

Flow methods

When diffusion is rapid, the results in batch experiments can often be obscured by the intrusion of external transport resistances. These effects are much less severe in flow systems where high carrier gas flow rates reduce hydrodynamic boundary layers.

In chromatographic measurements, a column is packed with sorbent over which an inert carrier gas stream is flowed. A pulse of sorbate is then injected into the column and the effluent concentration is monitored. The retention time of the peak is then a measure of the system's adsorption behaviour, while diffusion parameters are given by the peak spreading. It is also possible to apply a step change in sorbate concentration or a periodic perturbation (Deisler and Wilhelm, 1953; Boniface and Ruthven, 1985).

It is necessary, in chromatographic measurements, to eliminate or allow for the contribution of axial dispersion to peak broadening. This imposes an upper limit on the diffusion time constant (R^2/D) that can be reliably measured since, for rapid diffusion, the contribution of axial dispersion can become dominant.

The jetloop reactor method (Möller and O'Connor, 1994; Schwan and Möller, 2001) uses an internal circulation reactor, loaded with a pelletised zeolite sample, which behaves as a mixed flow reactor (CSTR, or continuous stirred tank reactor). High internal circulation rates minimise heat and mass transfer effects. The perturbation used in this technique is a pulse and the diffusion and adsorption parameters may be obtained by analysis of the effluent concentration vs. time curve.

The membrane method involves the measurement of the diffusive flux of a sorbate through a sorbent plug. A constant known pressure is applied to one side of the plug while the pressure on the other side of the plug is allowed to increase with the passage of the diffusing species through it. If the downstream side of the plug is maintained at constant volume, the variation of pressure with time on this side gives information as to the diffusional properties of the sorbent.

This technique is mostly limited to the measurement of pellets due to the practical difficulty in synthesising crystals large enough to be easily mounted. An advantage of this method is that it can provide information on the diffusional properties of different channels in non-isotropic sorbents.

An alternate method of performing the membrane experiment (Smith, 1981) is to have a carrier gas flowing past either end of the sorbent plug, then injecting a pulse on one side and monitoring its emergence on the other.

Less commonly used methods (although gaining in importance), include the wall-coated capillary chromatographic method (Jama et al., 1997), positron emission profiling (Anderson et al., 1998; Noordhoek et al., 1998) and the tapered element oscillating microbalance (Zhu et al., 1998).

Steady state methods

There is a steady state variant of the membrane technique in which the flux is measured under constant pressure conditions with a known concentration gradient across the membrane. Comparison the steady state and transient experiments could give information as to the pore structure of

the sorbent, in that dead-end pores should affect the transient experiments more severely that the stationary ones (Smith, 1981).

It is possible to determine effective diffusivity from reaction rate measurements under similar conditions using different zeolite crystal sizes. Small crystals should show no diffusion limitations and these would give the intrinsic rate. Experiments with larger crystals, in which diffusion plays a significant role, could then be done and, using the effectiveness factor and Thiele modulus (Smith, 1981; Kärger and Ruthven, 1992), an effective diffusivity could be calculated.

1.5.2 The measurement of self-diffusivity

Self-diffusivity describes diffusional behaviour in the absence of a concentration gradient, i.e. essentially Brownian motion. There are two common methods of measuring this sort of transport, namely nuclear magnetic resonance (NMR) methods and tracer exchange methods.

Tracer exchange techniques

These experiments are very similar to those transient methods described above to measure transport diffusivity, with the difference that the system is kept at constant sorbate concentration. Where above a change would be made in sorbate concentration, here a change is made in the concentration of a fraction of labelled molecules, usually being isotopically tagged. The approach toward equilibrium is generally followed by measuring the concentration of these labelled molecules in the gas phase. This approach has found application in the tracer ZLC method, giving results generally consistent with other such techniques (Brandani et al., 1995b).

NMR Gradient techniques

When a constant magnetic field is applied to a system, the individual nuclei align themselves such that the sum of their dipole moments is parallel to the field. Their individual spins would, in this case, be invisible. When a $\pi/2$ pulse is applied to the system, the total magnetisation is shifted into the plane perpendicular to the direction of the constant field where it then rotates at a certain (Larmor) frequency (Kärger and Ruthven, 1992). It is this transverse component of the total magnetisation that is considered in an NMR self-diffusion measurement.

In pulsed field gradient nuclear magnetic resonance (PFG NMR), the field gradient is superimposed on the constant field in two short pulses in opposite directions. The first pulse results in a de-phasing of the vectors of the transverse magnetisation at different positions within the sample, as a result of which the vector sum decays. If the individual molecules do not move between the signals, the second pulse should exactly counteract the first, so that the phase of the spins are re-focused and the transverse magnetisation restored to its original value. However, if the molecules have moved, then the re-focusing will be incomplete and the transverse magnetisation will not be completely restored. The decrease in the NMR signal becomes larger as the mean square displacement increases.

1.5.3 Computational methods

With the advent of powerful computers it has become practical to simulate diffusion on a microscopic scale. The advantage of this approach is that it then becomes fairly simple to investigate effects such as channel geometry on the transport behaviour of a system. Extension to multicomponent systems is also quite straightforward.

It has been shown that a random walk by a sequence of uncorrelated steps is equivalent to Fickian diffusion (Kärger and Ruthven, 1992). Computational methods which rely on this approach are generally known as Monte Carlo methods. The stochastic nature of diffusion is simulated by random number generating routines.

An alternative approach is the molecular dynamic method, in which the equations of motion are solved for a number of particles in a known force field. The force field must take into account intermolecular interactions as well as the interaction between the molecules and the surroundings.

In both the above methods it is usual to simulate the behaviour of a small volume element of the system under consideration, with the macroscopic structure being built up of repeating units of this element.

1.6 Causes of spurious results in diffusion measurements

Diffusion is a particularly difficult property to measure accurately, leading to the profusion of techniques whereby it is performed. This section will outline some of the difficulties which may be encountered when performing such experiments.

1.6.1 Intrusion of extracrystalline mass transfer resistance

External barriers to mass transfer (or film diffusion) are a result of a laminar boundary layer around the adsorbent particle where transport can only occur by molecular diffusion. The significance of this effect depends on the thickness of the boundary layer which in turn depends on the hydrodynamic conditions (Kärger and Ruthven, 1992).

External mass transfer is usually correlated in terms of a mass transfer coefficient k_f defined according to a linear rate expression as follows:

$$J = k_f(C_{bulk} - C_{surface}) \tag{1.12}$$

where C_{bulk} is the concentration in the bulk fluid phase and $C_{surface}$ is the fluid phase concentration at equilibrium with the surface of the sorbent particle. There are numerous correlations for k_f in terms of fluid and flow properties (Coulson and Richardson, 1991).

External mass transfer obviously becomes more likely to influence the overall mass transport rate as the intraparticle diffusion rate increases. It also becomes more important as the strength of adsorption (K) increases. This can easily be seen by inspecting the equation for an uptake experiment

under conditions of film diffusion control (Kärger and Ruthven, 1992):

$$\frac{\bar{q}}{q_\infty} = 1 - \exp\left(-\frac{3k_f}{KR}t\right) \tag{1.13}$$

where $\bar{q}$ is the average adsorbed phase concentration and q_∞ is the final equilibrium adsorbed phase concentration. This relation clearly shows that an increase in K causes a retarded approach to equilibrium.

External mass transfer effects are relatively easy to negate in flow systems: simply increase the linear velocity of the carrier gas in order to decrease the thickness of the laminar boundary layer. Series of experiments at different flow rates should reveal the presence (or not) of this resistance. Film diffusion in batch systems may be detected by varying the sample mass and configuration and checking for consistency of results.

1.6.2 Intrusion of extracrystalline heat transfer resistance

The majority of diffusion measurements occur under isothermal conditions in order to ease the interpretation of the experimental data. The presence of external barriers to heat transfer slows the rate at which the heat of sorption is removed (in the case of an uptake experiment) from the sorbent sample. Heat transfer through the solid particles will generally occur far more rapidly that through the fluid film (Kärger and Ruthven, 1992), so that the particles are likely to be isothermal at any one time. They may not, however, necessarily be at the bulk temperature of the system, so that temperature-dependent effects may not be accurately represented. In addition the sorption rate, and thus the rate of heat generation, generally varies during the course of an experiment, so that the sorbent temperature may vary with time, if not with position within itself.

This sort of resistance is similar in nature to that of film diffusion, i.e. there is a laminar boundary layer around the sorbent particles through which heat can only be transferred by conduction.

External heat transfer effects may be counteracted in a similar manner to that described above for film diffusion.

1.6.3 Surface barriers to mass transfer

It has been found (Kärger and Ruthven, 1992) that various catalyst pretreatment methods (e.g. steaming) cause the formation of a so-called surface barrier to diffusion, a resistance to transport localised at the surface of the sorbent particle, in series with the intracrystalline diffusion resistance. This is suspected to be a result of pore mouth narrowing, skin resistance (in pellets) or possibly window blocking. The effect is also found in coked samples. Typically, samples affected by surface barrier resistance show decreased diffusivities with little change in diffusional activation energy.

Such surface barriers are difficult to quantify absolutely since their effect on the transport properties of the sorbent varies according to the type of sorbate used (i.e. its shape and size).

In additional to the well-known structural surface barrier, the existence of a (non-structural) non-equilibrium surface barrier for the uptake of p-ethyltoluene in ZSM-5 has also been reported

(Micke et al., 1994a). It was found that the surface barrier penetration process obeyed a Langmuir kinetics mechanism.

1.7 Zero length column chromatography

Since its development by Eic and Ruthven (1988), the zero length column (ZLC) method of measuring intracrystalline diffusivity in microporous sorbents has become widely used. It is a chromatographic method in which a small sample of sorbent is equilibrated with a sorbate-carrying inert carrier stream and then subjected to a step decrease in sorbate concentration. The effluent concentration is monitored and the diffusion and adsorption constants determined by the application of an appropriate model.

The usual method of loading the catalyst into the experimental apparatus is to sandwich one or two milligrams of the sample between two frits. The bed is then assumed to be short enough (a monolayer of crystals is normally desired), so that the column may be considered well mixed.

Originally introduced for low concentration (linear adsorption isotherm) gaseous hydrocarbon systems, the method has since been both theoretically and experimentally developed to include the study of many other systems, including ion-exchange resins (Rodriguez et al., 1998), self-diffusion through tracer exchange (Brandani et al., 1995b,a, 2000a) and liquid systems (Ruthven et al., 1993; Ruthven and Stapleton, 1993; Brandani and Ruthven, 1995). The application to zeolite powders has been extended to pellet systems as well (Brandani, 1996; Silva and Rodrigues, 1996, 1997). Non-hydrocarbon sorbates have also been measured (Ruthven and Xu, 1993).

In addition, some work has been done to quantify deviations from the original simple theory. The liquid ZLC work provided a general criterion whereby sorbate accumulation in the carrier fluid phase may be neglected (Brandani and Ruthven, 1995), which may generally be done for gaseous systems. The effect of external film mass transfer resistance on the desorption curve has been briefly mentioned (Eic and Ruthven, 1989), and the effect of incomplete saturation during the equilibration stage of the experiment has been analysed (Brandani and Ruthven, 1996a). External heat transfer has been considered in a simplified way (Brandani et al., 1998).

Conflicting work has been published on the effect of a nonlinear adsorption isotherm (Micke et al., 1993; Brandani, 1998) on the ZLC. It would appear that the earlier work was in error, the latter paper providing an intuitively more correct result, i.e. that the low concentration region of the desorption curve is similar to that for a linear isotherm and the zero loading diffusivity may still be measured. One would expect the Henry Law limit to be attained in that region. In addition, the work showed that increasing the initial loading of the sorbent tends to increase L, thus decreasing the integral of the normalised curve, i.e. decreasing the mass balance compared to that for the linear isotherm case. This is again intuitively correct, as one would find less material adsorbed close to the saturation limit of the sorbent than would be calculated by a simple extrapolation of the Henry isotherm to high concentrations. The work of Brandani (1998) has been shown to be consistent with experiment (Brandani et al., 2000b).

It may be seen from the above work that, even if the system under study does not strictly conform to the assumptions of the standard, simple ZLC model, the linear tail of the desorption curve tends to have the correct slope under a number of conditions. The interept (and thus the evaluation of K) is not as reliable. Thus the 'long time' solution method (Hufton and Ruthven, 1993) is very robust for obtaining intracrystalline diffusivities. Various other 'short time' and 'intermediate time' solution methods have been suggested (Brandani and Ruthven, 1996a), largely to address the concern that the linear asymptote is obtained at very low concentrations and may be adversely affected by erroneous baselining as well as the accuracy of the measuring device. It is felt, however, that these problems may be overcome by careful experimental design and operation. Often, the deviation from the model shown by desorption curves in the literature occurs in the initial part of the experiment (for example, the work with light alkanes in silicalite presented in Hufton and Ruthven (1993)), severely limiting the usefulness of the short time methods.

The zero length column method is a widely accepted technique for the macroscopic measurement of intracrystalline diffusion coefficients and is being employed by an increasing number of research groups for this purpose. The results given by the technique are generally consistent with macroscopic method (e.g. Kärger and Ruthven (1989); Hufton and Danner (1993); Grenier et al. (1994); Brandani et al. (2000a)), and it has the advantage of being cheap and easy to deploy.

1.8 Purpose of this work

The work presented in this thesis is an attempt to differentiate between the mechanisms of pore mouth narrowing and pore mouth blockage in liquid phase silanised ZSM-5, as introduced in Section 1.3, by employing the zero length column method.

The ZLC method was investigated theoretically to assess its reliability (Chapters 2, 3 and 4). The chosen experimental system (cyclohexane/ZSM-5) was studied in detail so as to determine baseline behaviour for the unmodified zeolite case. Finally, the results of the investigation into the silanised ZSM-5 is presented in Chapter 7.

Chapter 2

Review of ZLC Models and Analysis Methods

The ZLC technique relies on comparing experimental desorption curves to a mathematical model in order to extract the relevant adsorption and diffusion parameters. This chapter provides an overview of the various models and methods of comparison that exist in the literature.

2.1 Preliminary assumptions and equations

All models are based on the solution of Fick's Second Law with a variety of boundary conditions, depending on the situation being modelled. This law is based on a mass balance for the volume within which diffusion is taking place (i.e. the sorbent particle), using Fick's First Law

$$J = -D\nabla q \tag{2.1}$$

to relate the diffusive flux (J) to the concentration gradient. The general form of Fick's Second Law is

$$\frac{\partial q}{\partial t} = D\nabla^2 q \tag{2.2}$$

with the following inherent assumptions:

- isotropic control volume (i.e. diffusivity does not vary with position);
- concentration-independent diffusivity;
- applicability of Fick's First Law.

The last condition may not be as trivial as it first appears, as it is more likely that the true driving force for diffusion is a chemical potential gradient, rather than a concentration gradient (Kärger and Ruthven, 1992).

Most ZLC models assume that the sorbent particles have spherical geometry, in which case Equation 2.2 may be written in the form

$$\frac{\partial q}{\partial t} = D\left(\frac{\partial^2 q}{\partial r^2} + \frac{2}{r}\frac{\partial q}{\partial r}\right) \tag{2.3}$$

The usual initial condition is that the sorbate is distributed uniformly throughout the sorbent volume:

$$q(r, t = 0) = q_0 \tag{2.4}$$

The form of q_0 is given by the adsorption isotherm (if one assumes thermodynamic equilibrium throughout the particle), i.e. $q_0 = KC_0$ for a linear isotherm.

All models use a symmetry condition at the centre of the particle:

$$\frac{\partial q}{\partial r}(r = 0, t) = 0 \tag{2.5}$$

The second boundary condition, at the outer edge of the sorbent particle, is derived from a sorbate mass balance for the carrier phase:

$$V_s\frac{d\bar{q}}{dt} + V_f\frac{dC}{dt} + FC = 0 \tag{2.6}$$

where $\bar{q}$ is the space-averaged adsorbed phase concentration given by

$$\bar{q}(t) = \frac{3}{R^2}\int_0^R r^2 q(r, t)\, dr \tag{2.7}$$

It is generally more convenient to work with normalised variables. Making the substitutions

$$\begin{aligned} Q &= \frac{q}{q_0} \\ X &= \frac{r}{R} \\ Y &= \frac{C}{C_0} \\ \tau &= \frac{D}{R^2}t \end{aligned} \tag{2.8}$$

one may rewrite Equation 2.3 and the initial and boundary conditions in the form

$$\frac{\partial Q}{\partial \tau} = \frac{\partial^2 Q}{\partial X^2} + \frac{2}{X}\frac{\partial Q}{\partial X} \tag{2.9}$$

$$Q(X, \tau = 0) = 1 \tag{2.10}$$

$$\frac{\partial Q}{\partial X}(X = 0, \tau) = 0 \tag{2.11}$$

The exact form of the second boundary condition depends on further assumptions as to the nature of the diffusive and adsorptive behaviour at the surface of the sorbent particle. The approach

is briefly illustrated below for the case of the standard model.

2.2 The standard model

The model most commonly used for analysing ZLC desorption curves is that presented in the initial ZLC paper (Eic and Ruthven, 1988). The sorbent bed is assumed to be well mixed, a reasonable assumption for thin sorbent layers and small particles (Ruthven, 1984). Equivalently, the bed could be assumed to be differential; see Chapter 3 for a more detailed discussion on this point. In addition, sorbate accumulation in the carrier phase is neglected; the validity of this assumption is discussed in Section 2.6. Lastly, the sorbent-sorbate interaction is assumed to be linear, i.e. a Henry Law type adsorption isotherm ($q = KC$ at $r = R$).

The fluid phase mass balance (Equation 2.6) may thus be written as

$$V_s \frac{d\bar{q}}{dt} + FC = 0 \tag{2.12}$$

Recognising that, for diffusion control,

$$\frac{\partial \bar{q}}{\partial t} = \frac{3D}{R} \left. \frac{\partial q}{\partial r} \right|_{r=R} \tag{2.13}$$

and then making use of the dimensionless variables defined above, one obtains the second boundary condition for Equation 2.3:

$$\frac{1}{L} \left. \frac{\partial Q}{\partial X} \right|_1 + Q|_1 = 0 \tag{2.14}$$

where

$$L = \frac{FR^2}{3V_s KD} \tag{2.15}$$

This set of equations has the analytical solution

$$\frac{C}{C_0} = 2L \sum_{n=1}^{\infty} \frac{\exp\left(-\beta_n^2 \tau\right)}{\beta_n^2 + L(L-1)} \tag{2.16}$$

where the eigenvalues are given by the positive roots of

$$\beta_n \cot \beta_n + L - 1 = 0 \tag{2.17}$$

The dimensionless parameter L may be interpreted as the ratio of a characteristic diffusion time (R^2/D) to a convection/adsorption or washout time ($V_s K/F$) (Ruthven and Brandani, 1997). Alternatively, one may see it as the initial concentration gradient at the surface of the sorbent particle. L gives an indication of how far removed the system is from equilibrium control, a large value implying a dominance of intracrystalline diffusion on the rate at which material is removed from the bed. Representative model curves are shown in Figure 2.1 for various values of L.

At long times, such that only the first term in Equation 2.16 is significant, the model may be

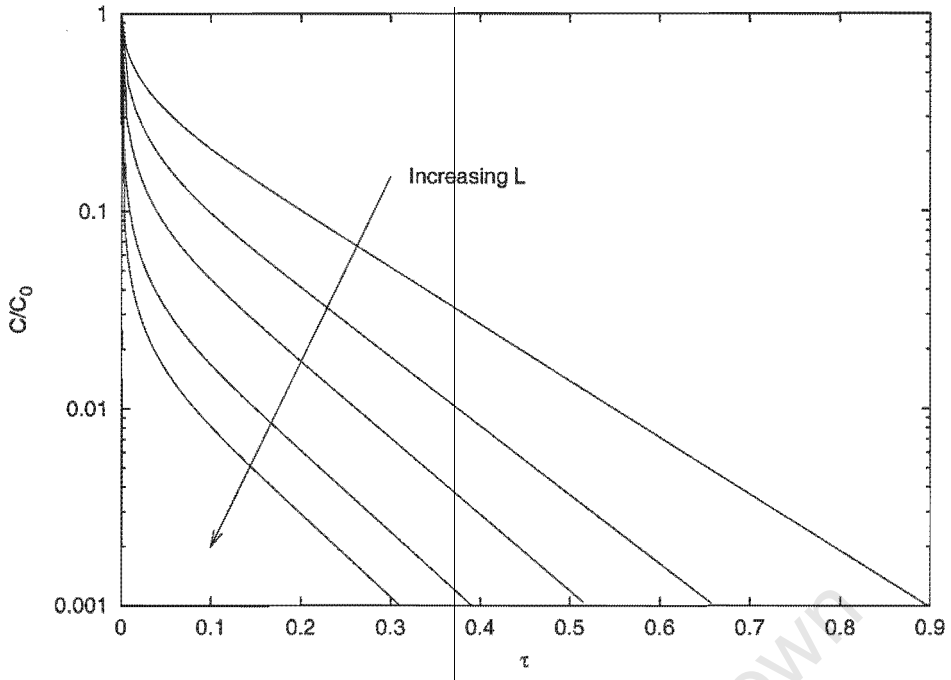

Figure 2.1: ZLC desorption curves generated with the standard model (Eq. 2.16) for $L = 5$, 10, 20, 50 and 100.

approximated as

$$\ln\left(\frac{C}{C_0}\right) = \ln\left[\frac{2L}{\beta_1^2 + L(L-1)}\right] - \beta_1^2\tau \tag{2.18}$$

For large values of L, where the concentration at the sorbent surface is kept close to zero, $\beta_n \to n\pi$ and we may simplify the model still further:

$$\ln\left(\frac{C}{C_0}\right) = \ln\left(\frac{2}{L}\right) - \pi^2\tau \tag{2.19}$$

In the limit $L \to 0$ (i.e. low flow rate or very strong adsorption), $\beta_1^2 \to 3L$ and the solution approaches the form (Eic and Ruthven, 1988)

$$\ln\left(\frac{C}{C_0}\right) = -\frac{F}{V_s K}t \tag{2.20}$$

which is simply the equation for the purging of a mixed flow reactor. This form gives no kinetic information and must thus be avoided in an experiment aimed to give diffusion data; it could conceivably be used to extract the adsorption constant. It corresponds to the situation in which the removal of the sorbate from the crystal surface is so slow compared to its transport through the crystal that a uniform intracrystalline concentration is maintained. Eic and Ruthven (1988) recommend that, for reliable kinetic control, experimental conditions should be set such that $L > 1$.

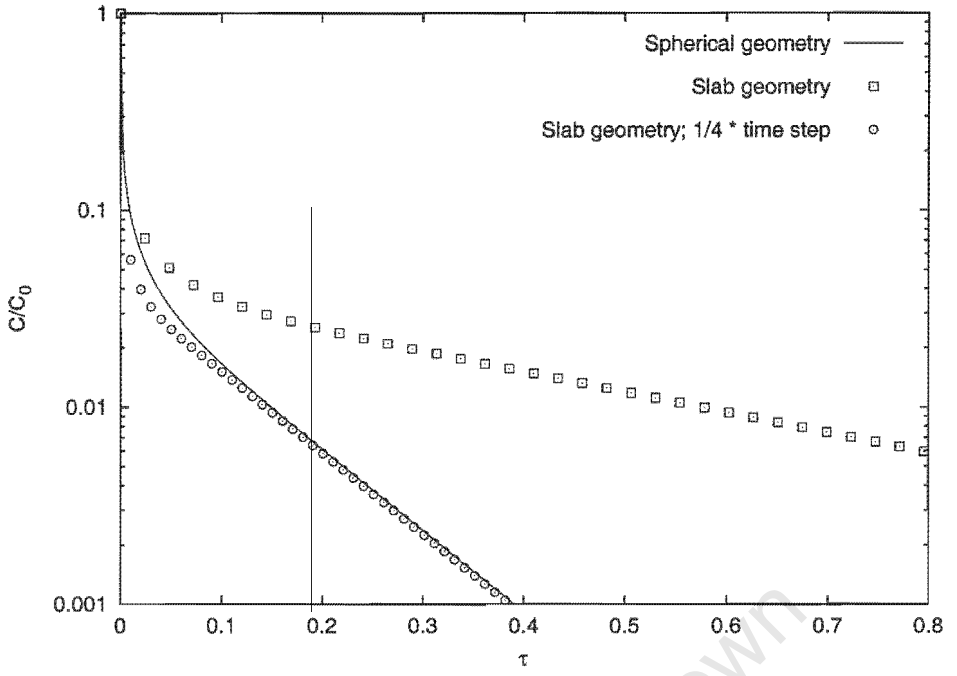

Figure 2.2: Comparison of the standard ZLC model in spherical and slab geometries for $L = 50$. The diffusion time constant (D/R^2) for the third curve was increased by a factor 4.

2.2.1 Standard model in slab geometry

For some sorbent samples the assumption of spherical symmetry is physically inaccurate, e.g. large, well formed ZSM-5 crystals, for which the main diffusion path is often considered to be parallel to the straight channels (Ruthven et al., 1991) running perpendicular to the large faces of the crystal (Haag et al., 1982). Thus it is sometimes desirable to have the ZLC model solved for the case of a parallel sided slab. Brandani and Ruthven (1996a) give the solution for an adsorbent with half-thickness l as

$$\frac{C}{C_0} = 2L \sum_{n=1}^{\infty} \frac{\exp\left(-\beta_n^2 \tau_{\text{slab}}\right)}{\beta_n^2 + L(L+1)} \tag{2.21}$$

where

$$L = \frac{Fl^2}{KV_{\text{s}}D} \tag{2.22}$$

$$\tau_{\text{slab}} = \frac{D}{l^2}t \tag{2.23}$$

and

$$\beta_n \tan \beta_n - L = 0 \tag{2.24}$$

For large L the eigenvalues tend to

$$\beta_n \simeq \left(n - \frac{1}{2}\right)\pi \tag{2.25}$$

The spherical and slab geometry variants of the simple model are compared in Figure 2.2. The limiting value of β_1 is $\pi/2$ for the slab model rather than π as for the spherical model, resulting in

the large difference in time scale between the first two curves. The third curve shows the result of effectively increasing the diffusivity of the slab case by a factor four to account for the difference in eigenvalues compared to the spherical case, resulting in the curves for the two geometries being almost identical in the long time region. There is, however, clearly a deviation between the two models in the short time region. This is probably because, for the spherical case, the sorbate diffuses through an expanding area as it moves away from the centre of the particle, while in the case of a slab the area for diffusive flux is constant throughout the crystal.

2.3 Analysis methods for the standard model

Since Equation 2.16 is the model used for the analysis of almost all experimental curves and is the standard to which all other models are compared, the development of analysis techniques has focused almost exclusively on it.

2.3.1 The long time method

Expanding the dimensionless time τ, Equation 2.19 (for long times and large L) takes the form

$$\ln\left(\frac{C}{C_0}\right) = \ln\left(\frac{2}{L}\right) - \pi^2\frac{D}{R^2}t \tag{2.26}$$

By this equation, a semilogarithmic plot of normalised concentration versus time should tend toward a straight line at long times, the slope of which gives the diffusional time constant. This solution technique is known as the 'long time' method (Hufton and Ruthven, 1993).

If the large L condition can be achieved, Equation 2.26 provides a simple (as compared to Equation 2.18) way to extract D/R^2 and L from the desorption curve as it is unnecessary to solve Equations 2.18 and 2.17 simultaneously. The concept is clearly illustrated by Figure 2.1, where the long time slopes of the desorption curves are seen to tend toward a constant slope for the larger values of L.

A criterion for which L may be considered large enough may be obtained by examining Figure 2.3, which illustrates the accuracy of the $\beta_1 = \pi$ approximation as a function of L. It can be seen that, for an accuracy of 10% in the diffusional time constant, it is necessary that $L > 20$. Ruthven and Brandani (1997) recommend $L > 10$.

It has been suggested (Han et al., 1999) that the appropriate time interval for the application of the long time method is $t \geq R^2/10D$.

2.3.2 Short time methods

During the initial part of the experiment, the following approximation to Equation 2.16 has been proposed (Hufton and Ruthven, 1993):

$$\frac{C}{C_0} = \frac{1}{L}\left(\sqrt{\frac{R^2}{\pi Dt}} - 1\right) \tag{2.27}$$

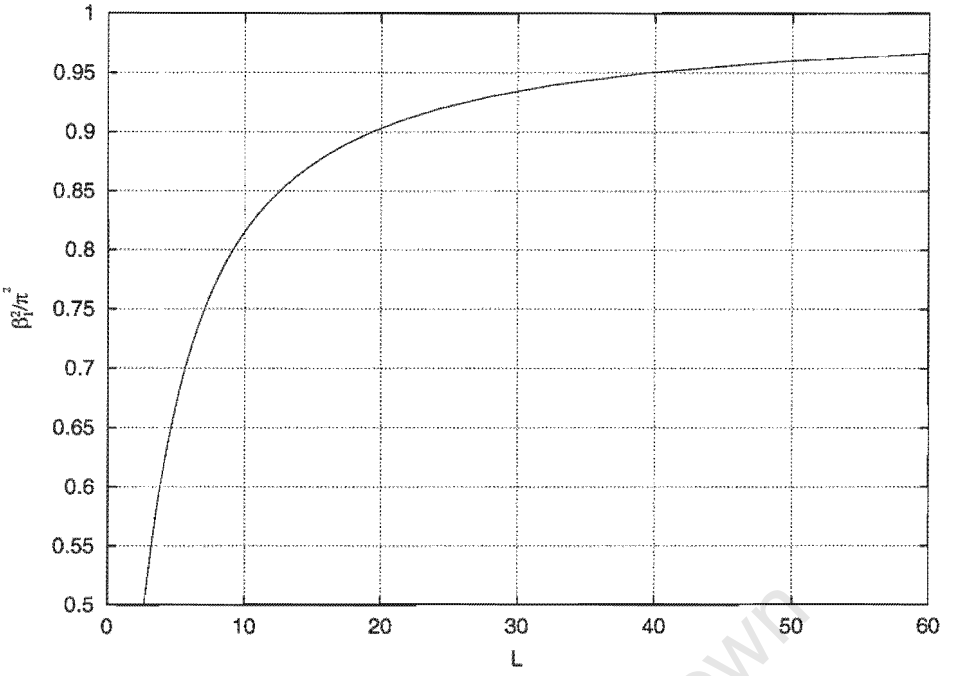

Figure 2.3: Approach of β_1^2 to π^2 with L.

This relation forms the basis for the original 'short time' solution method, in which D/R^2 and L are obtained from the slope and intercept of a plot of C/C_0 versus $1/\sqrt{t}$. Han et al. (1999) suggest that the method should be applied over the time interval $t \leq R^2/2D$. Data in the paper of Hufton and Ruthven (1993) show, however, that the model predicts the initial region of the experiment particularly badly; often the initial drop in concentration is far slower than allowed by Equation 2.16.

It has been pointed out by Brandani and Ruthven (1996a) that Equation 2.27 cannot be correct in the limit $t \to 0$ or for small L since, for these conditions, it predicts $C/C_0 \to \infty$. The authors of that paper in fact refer to it as an 'intermediate time' approximation. The approximation can only be expected to hold for large L, i.e. $L > 20$.

The analogue of Equation 2.27 for parallel-sided slab geometry is (Cavalcante et al., 1997)

$$\frac{C}{C_0} = \frac{1}{L}\sqrt{\frac{l^2}{\pi D t}} \tag{2.28}$$

It can be seen that, for the slab case, a plot of C/C_0 versus $1/\sqrt{t}$ should pass from the origin. It can be seen above that a negative intercept should occur for a spherical sorbent. This provides a possible means to discern the dominant diffusion path in a sorbent, employed successfully by Cavalcante et al. (1997).

The validity of Equation 2.27 can be evaluated by inspection of Figure 2.4. It is seen that the short time approximation is indeed more accurate for large values of L. However, the model is highly inaccurate for short times (the right hand side of the graph), so references to this as a 'short time' method are misleading. It is conceivable that this method could be used for the analysis of desorption

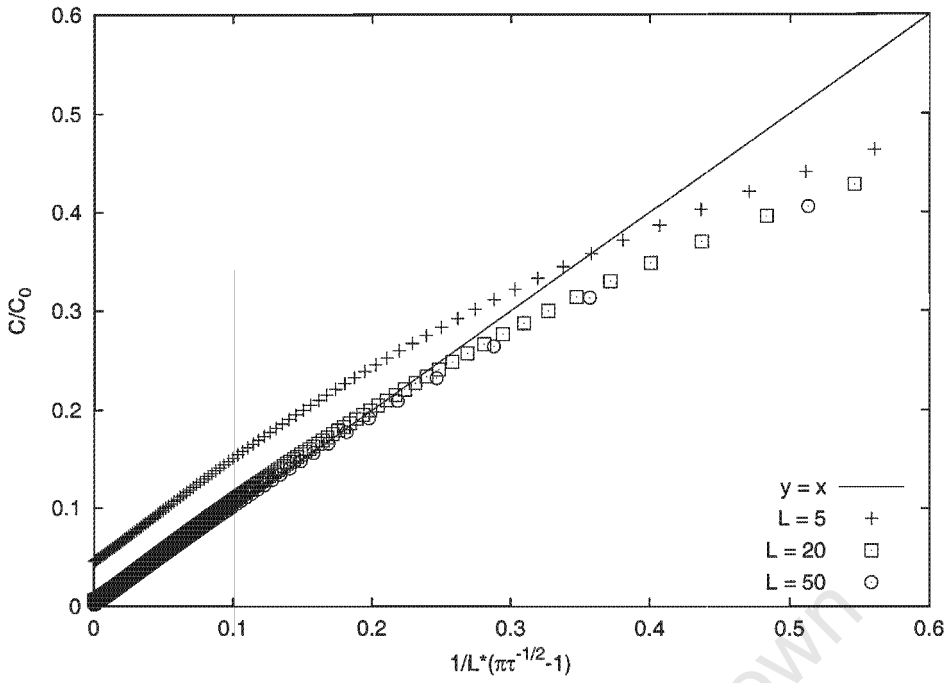

Figure 2.4: Comparison of the short time approximation Eq. 2.27 (the line $y = x$) with the full ZLC model solution (Eq. 2.16, points) for various values of L.

curves showing significant tailing in the long time region, since data in the tail would be compressed and any curvature would be reduced.

An alternative short time approximation (Brandani and Ruthven, 1996a) is

$$\frac{C}{C_0} = 1 - 2L\sqrt{\frac{Dt}{\pi R^2}} \tag{2.29}$$

which is graphically compared to the full solution on Figure 2.5. This relation provides the correct short time asymptote and is applicable for small values of L. However, the choice of zero time for a plot of C/C_0 versus $\sqrt{t}$ has a large effect on the initial slope. Brandani and Ruthven (1996a) therefore suggest that a more useful plot would be $(1 - C/C_0)/\sqrt{t}$ vs. $\sqrt{t}$, i.e. with Equation 2.29 in the form

$$\frac{1 - C/C_0}{\sqrt{t}} = 2L\sqrt{\frac{D}{\pi R^2}} \tag{2.30}$$

The value of $2L(D/\pi R^2)$ can then be directly read from the intercept and the curve is nearly linear over a wide range of t, as may be seen in Figure 2.6. Repetition of experiments with different flow rates allows the determination of D/R^2 and L individually. This method is suitable for systems where $0.5 < L < 5.0$ (Brandani and Ruthven, 1996a).

2.3.3 Full time range model fitting

It has been suggested that, since both the short and long time methods are simplifications, neither method is satisfactory for the analysis of experimental data (Han et al., 1999). The short time

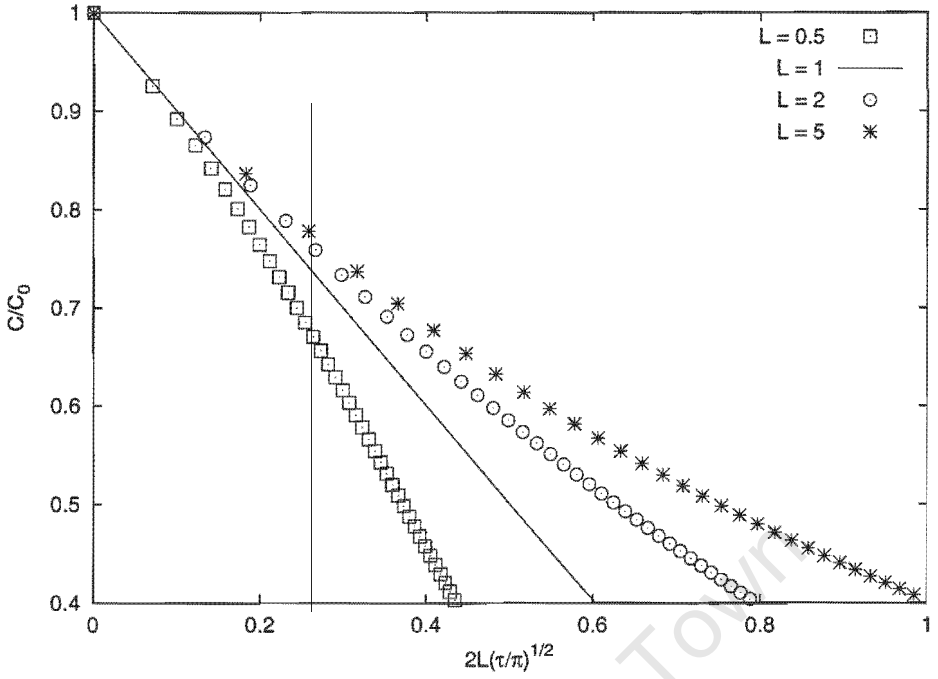

Figure 2.5: ZLC desorption curves plotted as suggested by the short time approximation Eq. 2.29 for various values of L as indicated.

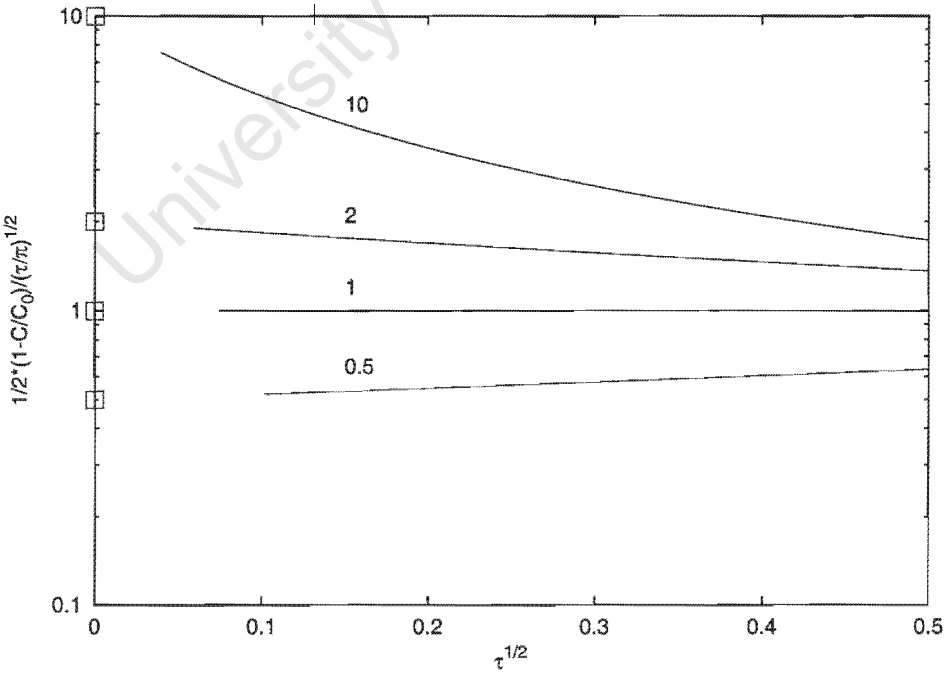

Figure 2.6: ZLC desorption curves showing the proposed method of extracting the diffusion parameters according to Eq. 2.30 for various values of L as indicated.

approximation Equation 2.27 would systematically overpredict the diffusion coefficient, while the long time method would tend to underpredict it.

Thus Han et al. (1999) suggest a fuller time approach (previously used in, e.g. (Micke et al., 1993) and (Brandani and Ruthven, 1995)), in which one considers all points along the desorption curve and minimises the objective function

$$\text{Objective function} = \sum_i \left(\frac{C(t_i)}{C_0} - F(t_i) \right)^2 \tag{2.31}$$

i.e. a simple least squares regression. This method does not weight the short or long time regions as the respective approximate methods would do. It is claimed this would help counteract the deviations incorrect experimental baselining would have on the long time method, as well as problems caused to the short time method (Equation 2.27) by uncertainties in the point of zero time due to dead volume contributions in the apparatus. It was also proposed that it is preferable to use the data in the mid-time region for a sorbent sample with a wide crystal size distribution, since this is the region in which the response of the average sized crystals (i.e. the size most likely to be considered when calculating D) is best represented.

2.3.4 Moments analysis

The method of moments is a commonly used technique for the extraction of kinetic parameters from chromatographic experiments (Ruthven, 1984). Differences in the results obtained from the long and short time analysis methods in the work of Hufton and Ruthven (1993) prompted Brandani and Ruthven (1996b) to derive the relevant equations for analysing ZLC desorption curves using the moments approach.

Considering the following integrals:

$$\begin{aligned} I &= \int_0^\infty \frac{C}{C_0}\, dt \\ \mu &= \frac{\int_0^\infty Ct\, dt}{\int_0^\infty C\, dt} \\ \sigma^2 &= \frac{\int_0^\infty Ct^2\, dt}{\int_0^\infty C\, dt} - \mu^2 \end{aligned} \tag{2.32}$$

where I is the area under the desorption curve, μ is the mean (first moment) and σ^2 is the variance (second moment), it is possible to derive the relevant equations from the standard ZLC model (Equation 2.16):

$$\begin{aligned} I &= \frac{1}{3L}\frac{R^2}{D} \\ \mu &= \frac{1}{15}\frac{R^2}{D}\frac{5+L}{L} \\ \sigma^2 &= \frac{1}{225}\left(\frac{R^2}{D}\right)^2\left(\frac{25}{L^2}+\frac{10}{L}+\frac{13}{7}\right) \end{aligned} \tag{2.33}$$

along with the ratios

$$\begin{aligned} \frac{\mu}{I} &= 1+\frac{L}{5} \\ \frac{\sigma^2}{\mu^2} &= 1+\frac{6}{7}\left(\frac{L}{L+5}\right)^2 \end{aligned} \tag{2.34}$$

There are clearly several combinations of equations one can use to extract the desired parameters, providing a built-in check for the validity of the analysis.

2.4 Systems with external mass transfer

If external film resistance is significant, one can no longer assume instantaneous thermodynamic equilibrium at the external surface of the adsorbent particle. Instead, one must consider a finite transport rate across the film of the form

$$\text{Flux} = k_{\text{m}}\left(q|_R - KC\right) \tag{2.35}$$

where k_{m} is the first order external mass transfer coefficient. The definition of L must then be modified to the form (Eic and Ruthven, 1989)

$$\frac{1}{L_{\text{m}}} = \frac{3V_{\text{s}}KD}{FR^2} + \frac{2KD}{N_{\text{Sh}}D_{\text{m}}} \tag{2.36}$$

The desorption curve then takes the form

$$\frac{C}{C_0} = \frac{2L_{\text{m}}}{L\frac{2KD}{N_{\text{Sh}}D_{\text{m}}}+1}\sum_{n=1}^{\infty}\frac{\exp\left(-\beta_n^2\tau\right)}{\beta_n^2+L_{\text{m}}(L_{\text{m}}-1)} \tag{2.37}$$

where L is defined as in Equation 2.15 and the eigenvalues are obtained from Equation 2.17 using L_{m} in place of L. The shape of the desorption curve is practically indistinguishable from that for pure intracrystalline diffusion. The model eigenvalues are affected, however, if L_{m} is substantially different to L, indirectly affecting the measured diffusion constant.

For a measurement that is unaffected by external mass transfer effects is is necessary that the second term in Equation 2.36 be insignificant with respect to the first. Taking $N_{\text{Sh}} = 2$, the usual conservative approximation, it is thus required that

$$\frac{FR^2}{3V_{\text{s}}} \ll D_{\text{m}} \tag{2.38}$$

Eic and Ruthven (1988) suggest the condition $D_{\text{m}}/KD \gg 5$.

2.5 External heat transfer effects

Nonisothermal desorption in a ZLC system has been studied by Brandani et al. (1998) and Silva et al. (2001) to yield a criterion for which heat effects may be neglected. The former analysis was performed for the case of a system with a linear adsorption isotherm, the Henry constant varying with a van't Hoff temperature dependence. It was assumed that the fluid phase is isothermal, and external mass transfer effects were neglected. The energy balance takes the form

$$C_s \frac{dT}{dt} = \frac{d\bar{q}}{dt}(-\Delta T) + ha(T_0 - T) \tag{2.39}$$

where h is the external heat transfer coefficient, T_0 is the temperature of the carrier phase and T is the temperature of the sorbent. Most of the analysis was for the case of negligible intracrystalline diffusion resistances, but a limited analysis was performed solving the energy balance simultaneously with the diffusion equation (Equation 2.3), but with the assumption that D does not vary with temperature. This is the case considered here.

Numerical solution of the equations showed that, for strong external heat transfer resistance, the characteristic linear tail of the ZLC desorption curve shows an inflection point and a large (negative) slope compared to the isothermal case. This is physically reasonable, since desorption is an endothermic process and, in the latter stages of the experiment, the catalyst would be at low loading and thus little energy would be consumed by the desorption process. The transfer of heat into the particle from the carrier fluid would therefore begin to dominate and the particle would heat up, decreasing the strength of adsorption and causing a more rapid purging.

A similar effect should be observed if the temperature dependence of the diffusivity were considered: since the slope of the long time region determines its slope, if the temperature of the particle were to increase with time, causing the diffusion coefficient to increase and thus causing an increase in the long time slope (i.e. it would become more negative).

The criterion developed for isothermal operation (below the line shown in Figure 2.7) showed the surprising result that neither the particle size nor the purge flow rate were significant factors. This is a counterintuitive result, probably arising from several of the assumptions in the analysis. Firstly, it was assumed that the external heat transfer coefficient is constant; it is, however, strongly affected by both flow rate and particle size. Secondly, neglecting the strong temperature dependence of the intracrystalline diffusivity is likely a large source of error, diffusional activation energies often being similar in magnitude to the corresponding heats of adsorption, implying that it is common for the temperature dependence of D to be as strong as that of K and is thus likely to have a similarly significant effect.

The results of this study should not be dismissed, however, as the criterion they provide can be used to at least qualitatively assess the likelihood of the intrusion of external heat transfer resistances.

The analysis of Silva et al. (2001) is somewhat different in that an analytical model was derived for the microporous sorbent case; this work also uses the assumptions of a linear adsorption isotherm and temperature-independent diffusion coefficient. It was found that, for isothermal operation, it is

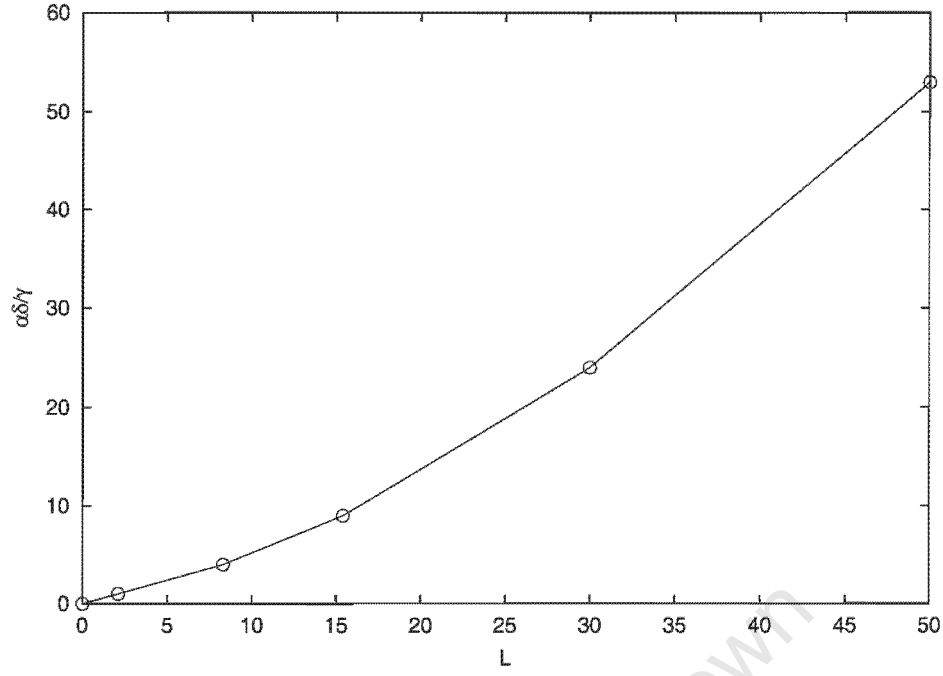

Figure 2.7: Criterion for negligible thermal effects as a function of diffusion resistance, reproduced from Brandani et al. (1998). The ordinate is given by $(\alpha\delta/\gamma) = \left(\frac{\Delta H}{R_g T_0}\right)^2 \cdot \frac{C_0 F R}{h a V_s}$.

required that

$$\frac{3L\beta}{\alpha} < 0.1 \tag{2.40}$$

where

$$\alpha = \frac{ha}{C_p}\frac{R^2}{D} \tag{2.41}$$

and

$$\beta = \frac{\Delta H_a}{C_p}\left.\frac{\partial q}{\partial T}\right|_{C_0,T_0} \tag{2.42}$$

Assuming a van't Hoff temperature dependence for K, it is easy to show that

$$\frac{3L\beta}{\alpha} = C_0\frac{F}{V_s}\frac{(\Delta H_a)^2}{R_g T_0^2 ha} \tag{2.43}$$

Analysis of Equation 2.43 shows that external heat transfer effects can be minimised by changing various parameters in the following ways:

1. decreasing the initial concentration, C_0;

2. decreasing the space velocity (F/V_s) in the cell; or

3. decreasing the particle size in order to increase a.

2.6 Model for liquid systems

The liquid phase counter-diffusion measurements of Ruthven and Stapleton (1993) showed that these systems do not conform to the simple ZLC model described above. This lead to the later development of an analytical model for liquid systems (Brandani and Ruthven, 1995). In this case, accumulation of sorbate in the carrier phase is not neglected; thus we require all the terms in Equation 2.6. We also again assume a linear adsorption isotherm.

The solution for the effluent concentration as a function of time is then

$$\frac{C}{C_0} = 2L \sum_{n=1}^{\infty} \frac{\exp(-\beta_n^2 \tau)}{\beta_n^2 + (1 - L + \gamma\beta_n^2)^2 + L - 1 + \gamma\beta_n^2} \tag{2.44}$$

where L is defined as in Equation 2.15, the eigenvalues are calculated using

$$\beta_n \cot \beta_n + L - 1 - \gamma\beta_n^2 = 0 \tag{2.45}$$

and the dimensionless parameter γ is defined as

$$\gamma = \frac{V_\mathrm{f}}{3KV_\mathrm{s}} \tag{2.46}$$

Inspection of this definition shows that γ represents the ratio of the fluid capacity for the sorbate to that of the sorbent. Representative desorption curves are shown in Figure 2.8 for a range of values of γ.

It is clear that Equation 2.44 reduces to the standard model (Equation 2.16) for the case $\gamma = 0$. The two models are effectively identical for $\gamma < 0.1$ (Brandani and Ruthven, 1995), as can be seen in Figure 2.8. It may be seen that the value of γ does not have a great influence on the slope of the long time asymptote.

Liquid phase systems tend to have adsorption coefficients (K) of approximately unity (since the liquid and adsorbed phase densities are generally of the same order of magnitude), while K values for vapour systems are of the order of hundreds or thousands. Thus the parameter γ may generally be neglected for gaseous systems and the simpler Equation 2.16 may be used for analysing the experimental desorption curves.

The effect of γ is mostly evident in the initial part of the desorption curve, where it causes a slower decrease in concentration due to the extra resistance (washout) to the sorbate exiting the reactor. The short time approximation to Equation 2.44 is (Brandani and Ruthven, 1995)

$$\frac{C}{C_0} = \exp\left(-\frac{F}{V_\mathrm{f}} t\right) \tag{2.47}$$

from which it is seen that the initial slope of the desorption curve (on semilogarithmic axes) is proportional to the purge flow rate, as is the case with any mixed flow reactor. The long time region of the curve is unaffected, although a large value of γ would indirectly affect the long time slope by

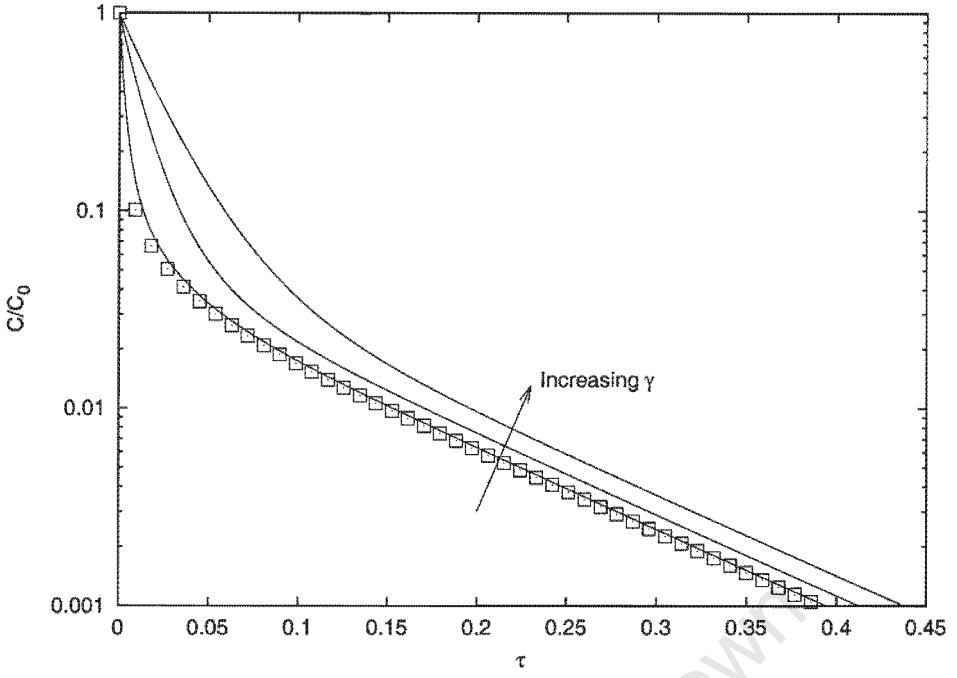

Figure 2.8: Representative desorption curves generated with the liquid phase ZLC model (Eq. 2.44) for $L = 50$ and $\gamma = 0.1$, 0.5 and 1. The standard model (Eq. 2.16, points) is shown for reference.

modifying the value of β_1 by Equation 2.45.

2.7 Model for nonlinear systems

One of the fundamental assumptions in the derivation of the standard (and most other) ZLC models is that of isotherm linearity. In practice, however, it is not always easy or convenient to achieve concentrations low enough to approach the linear region of the adsorption isotherm. It is thus important to assess the accuracy of the standard model in the case of isotherm nonlinearity.

Two models have been proposed in the literature for this purpose: those of Micke et al. (1993) and Micke et al. (1994b) and of Brandani (1998). The former work used a Volterra integral equation with numerical solution approach for the general case of an arbitrary adsorption isotherm. It was shown that the shape of the adsorption isotherm dramatically influenced the shape of the desorption curve, including the limiting slope of the long time region. It appeared that a highly favourable isotherm would cause a slow initial drop in concentration, but would then decay more rapidly than in the linear isotherm case. Thus, neither the long or short time methods based on the standard model could be used for the analysis of such data. It should be noted that the behaviour in the initial region of the presented curves was complicated by the inclusion of significant interstitial holdup.

The later work presents the numerical solution of the differential equations for the case of a Langmuir type isotherm. This paper provides an intuitively more correct result, i.e. that the low concentration region of the desorption curve is similar to that for a linear isotherm system and the zero loading diffusivity may still be found using the long time method. One would expect the Henry

law limit to be attained in that region. In addition, it was shown that increasing the initial loading of the sorbent tends to increase L, thus decreasing the integral of the normalised curve, i.e. decreasing the mass balance compared to that for the linear isotherm case. This is again intuitively correct, as one would find less material adsorbed close to the saturation limit of the sorbent that would be calculated by a simple extrapolation of the Henry isotherm to high concentrations.

It is thus believed that the earlier work was in error, while the latter is more feasible. Experimental verification of the later work has since shown its validity (Brandani et al., 2000b). The shape of the desorption curve largely retains that of the standard model, except that the intercept of the long time region tends to decrease with initial loading, as does the time required for the long time asymptote to be attained.

The model for ZLC systems with a Langmuir type isotherm does not have an analytical solution (see Brandani (1998) for numerical solutions), but a number of approximations provide important insight. Note that the model was evaluated using the Darken correction factor to account for the concentration dependence of the diffusion coefficient; below, D shall refer only to the zero-loading diffusivity.

The Langmuir adsorption isotherm has the form (in dimensionless variables)

$$Q = \frac{Y}{1-\lambda+\lambda Y} \tag{2.48}$$

where

$$\lambda = \frac{q_0}{q_s} \tag{2.49}$$

is the initial fractional loading of the adsorbent. The long time asymptote of the desorption curve under conditions of diffusion control may be approximated as

$$\ln\frac{C}{C_0} = \frac{1}{2}\left[\ln(1-\lambda) - \lambda + \ln\left\{\frac{2L_T}{\beta_T^2 + L_T(L_T-1)}\right\} + \ln\left\{\frac{2L}{\beta_1^2 + L(L-1)}\right\}\right] - \beta_1^2\tau \tag{2.50}$$

where $L_T = L/(1-\lambda)$ and β_T is the first root of Equation 2.17 with L replaced by L_T. It is clear from the above equation that, using the long time solution method for the standard model, it is possible to obtain the value of D at infinite dilution even though the linear isotherm assumption does not hold.

For the equilibrium controlled case, the desorption curve is given by

$$3L\tau = 1 - \lambda + \ln(1-\lambda) - \frac{1-\lambda}{1-\lambda+\lambda Y} - \ln Y + \ln\left(1 + \frac{\lambda}{1-\lambda}Y\right) \tag{2.51}$$

which, for long times, reduces to

$$\begin{aligned}\ln\frac{C}{C_0} &= \ln(1-\lambda) - \lambda - 3L\tau \\ &= \ln(1-\lambda) - \lambda - \frac{F}{KV_s}t\end{aligned} \tag{2.52}$$

Qualitatively, this equilibrium controlled curve has the same shape as the standard, diffusion controlled ZLC model. A reasonable experimental check for equilibrium control would be to vary the flow rate: the long time slope of the desorption curve would be proportional to F, while that for the diffusion controlled case should be independent of F for large enough L. Alternatively, one could plot $\ln(C/C_0)$ versus Ft (Brandani et al., 2000b). Under conditions of equilibrium control all curves will collapse to a single curve, while for kinetic control the curves will diverge.

2.8 Incomplete initial equilibration

The initial stage of a ZLC experiment involves the equilibration of the sorbent sample with a stream of given sorbate concentration, giving the initial condition Equation 2.4. With the measured variable being fluid phase concentration, it is difficult to discern when the sorbent sample is completely equilibrated, since the fluid phase concentration will stabilise along with that of the sorbent surface. For systems with slow diffusion, however, the interior of the crystal may still contain a significant concentration gradient.

In order to elucidate the effect of this partial saturation case, Brandani and Ruthven (1996a) derived a model for which the initial condition was given by the solution of the uptake curve for an equilibration time t_s. If the corresponding dimensionless time is $\tau_s = Dt_s/R^2$, the desorption curve is given by

$$\frac{C}{C_0} = \frac{\sum_{n=1}^{\infty} \frac{2L}{\beta_n^2+L(L-1)} \left[1-\exp\left(-\beta_n^2\tau_s\right)\right] \exp\left(-\beta_n^2\tau\right)}{1-\sum_{n=1}^{\infty} \frac{2L}{\beta_n^2+L(L-1)} \exp\left(-\beta_n^2\tau_s\right)} \tag{2.53}$$

which has the approximate long time solution

$$\frac{C}{C_0} \simeq \frac{\frac{2L}{\beta_1^2+L(L-1)} \left[1-\exp\left(-\beta_1^2\tau_s\right)\right]}{1-\sum_{n=1}^{\infty} \frac{2L}{\beta_1^2+L(L-1)} \exp\left(-\beta_1^2\tau_s\right)} \exp\left(-\beta_1^2\tau\right) \tag{2.54}$$

which should be compared to Equation 2.18.

It is clear that the largest error will be in the determination of L from the intercept of the desorption curve tail. The intercept will be lower than for the standard case, causing L to be overestimated. The effect on D/R^2 will likely be small since β_1 is always approximately π for large L. This was confirmed by generating desorption curves with the partial saturation model and then fitting the standard model to them. It was found that the error in the diffusional time constant was less than 1% for a wide range of conditions, while L was far more sensitive. The large error in L is intuitively correct, since the mass balance would indicate an initial adsorbed amount smaller than the equilibrium value, leading to the adsorption constant being underestimated.

A similar exercise was carried out using the short time solution method, for which the approximate solution is

$$\frac{C}{C_0} \simeq \frac{1}{L}\left[\sqrt{\frac{R^2}{\pi Dt}} - \frac{1+(L-1)\sum_{n=1}^{\infty} \frac{2L}{\beta_n^2+L(L-1)} \exp\left(-\beta_n^2\tau_s\right)}{1-\sum_{n=1}^{\infty} \frac{2L}{\beta_n^2+L(L-1)} \exp\left(-\beta_n^2\tau_s\right)}\right] \tag{2.55}$$

which should be compared to Equation 2.27. It was found that the deviation in L is inversely

proportional to L, while that in the diffusional time constant is proportional to L^2. The errors were significantly worse than for the long time solution method.

Comparison of Equation 2.53 to the standard model (Equation 2.16) reveals that is it not feasible to detect partial saturation by inspection of the shape of the experimental desorption curve.

Analysis of the uptake equation shows that, for large L, complete equilibration (defined as $\bar{q}$ being 99% of the equilibrium value) requires a saturation time of approximately $0.416R^2/D$.

2.9 Evaluation of analysis methods

The great majority of ZLC work in the literature has used the long time method for analysing the desorption curves. In all the cases above that deviate from the assumptions of the standard model it can be seen that the short time region of the curve is more strongly affected than the slope of the long time asymptote. Short time analysis methods are thus more vulnerable to inaccuracies due to the intrusion of extraneous effects.

The moments analysis approach (Brandani and Ruthven, 1996b) and the long time approach in conjunction with partial saturation experiments (Brandani and Ruthven, 1996a) are claimed to be able to distinguish surface barrier control from diffusion control. It should be noted, however, that both approaches are only able to recognise complete surface barrier control. A combined transport mechanism involving both a surface barrier resistance and the standard intracrystalline diffusion resistance would only be identified as not being surface barrier controlled.

While analysis by the method of moments has the advantage of being the only approximate method to use all the data on the desorption curve to obtain the sorption parameters, deviations from the assumptions of the model would not be easy to explain. One would only be able to state that the experimental system does not conform to the model and a comparison of the theoretical and experimental desorption curves would be required to attempt to identify the source of the deviation. This again requires a method of plotting the curves: the standard semilogarithmic plot is the easiest to interpret and lends itself naturally to the use of the long time analysis method.

Simply put, the ZLC desorption curve tends to show the 'correct' long time asymptote under a range of conditions and may often be analysed using the simple ZLC model (Equation 2.16) even though the system under study does not conform to the assumptions of the model. The long time approach is very robust for obtaining intracrystalline diffusivities.

The alternative analysis methods have been suggested largely to address the concern that the linear asymptote is obtained at very low concentrations and may be adversely affected by erroneous baselining as well as the accuracy of the instrument. It is felt, however, that these problems may be overcome by careful experimental design and operation.

Chapter 3

A 'Zero Length' Criterion

The development of ZLC theory assumes that the adsorber is well mixed (a CSTR), i.e. mathematically (if not physically) identical to a differential plug flow reactor, leading to the standard (Equation 2.16) and liquid (Equation 2.44) models. This treatment leads to significant mathematical simplification. It may well be justifiable when thin sorbent layers (Eic and Ruthven, 1988) and small particles (Ruthven, 1984) are used. The equally simple case of differential operation is, as in reaction engineering, not only a function of bed length, but also depends on flow rate, diffusivity and the adsorption equilibrium constant. This characteristic may be exploited in, for example, reaction studies, where longer beds would be used, to investigate *in-situ* diffusion behaviour.

This chapter will aim to analyse the zero length assumption theoretically and develop a simple criterion which will ensure that differential operation is always achieved and the diffusivity is accurately measured. Axial dispersion and plug flow models are developed and used to establish the deviation from the CSTR approximation as a function of diffusivity and adsorption equilibrium constant.

3.1 Development of the models

[Detailed derivations may be found in Appendix A.]

As described in Section 2.1, Fick's Second Law in spherical coordinates is used for the sorbate mass balance in the micro-particles:

$$\frac{\partial q}{\partial t} = D\left(\frac{\partial^2 q}{\partial r^2} + \frac{2}{r}\frac{\partial q}{\partial r}\right) \tag{3.1}$$

with the initial condition

$$q(r, t = 0) = KC_0 \tag{3.2}$$

and the boundary conditions

$$q(r = R, t) = KC \tag{3.3}$$

$$\frac{\partial q}{\partial r}(r = 0, t) = 0 \tag{3.4}$$

For disperse flow, the fluid phase mass balance may be written as (Ruthven, 1984)

$$-D_{\mathrm{L}}\frac{\partial^2 C}{\partial z^2}+v\frac{\partial C}{\partial z}+\frac{\partial C}{\partial t}+\left(\frac{1-\varepsilon}{\varepsilon}\right)\frac{\partial \bar{q}}{\partial t}=0 \tag{3.5}$$

with the initial condition

$$C(z,t=0)=C_0 \tag{3.6}$$

and the Dankwerts boundary conditions (Ruthven, 1984)

$$\frac{\partial C}{\partial z}(z=L_{\mathrm{bed}},t)=0 \tag{3.7}$$

$$\frac{\partial C}{\partial z}(z=0,t)=\frac{v}{D_{\mathrm{L}}}\left[C(z=0^+,t)-C(z=0^-,t)\right] \tag{3.8}$$

in which, for a perfect step, it was assumed that

$$C(z=0^-,t)=0 \tag{3.9}$$

For the case of pure plug flow, $D_{\mathrm{L}}=0$ and so the first term of Equation 3.5 may be ignored and the single boundary condition

$$C(z=0,t)=0 \tag{3.10}$$

may be used.

These equations were solved in the Laplace domain and inverted into the time domain using the fast Fourier transform algorithm. This approach proved more efficient than the integral solutions given in Ruthven (1984, p. 237).

For the general disperse flow case the solution for the diffusion controlled ZLC desorption curve may be written as

$$\frac{\hat{C}}{C_0}=\frac{1}{s}\left[1+\frac{2He^{\frac{1}{2}(N_{\mathrm{Pe}}+H)}}{(N_{\mathrm{Pe}}+2G-H)-(N_{\mathrm{Pe}}+2G+H)\,e^{H}}\right] \tag{3.11}$$

where

$$G=\tau_{\mathrm{f}}s+\frac{1}{L}\left(\sqrt{s}\coth\sqrt{s}-1\right) \tag{3.12}$$

$$H=\sqrt{N_{\mathrm{Pe}}^2+4GN_{\mathrm{Pe}}} \tag{3.13}$$

$$L=\frac{FR^2}{3V_{\mathrm{s}}KD} \tag{3.14}$$

$$N_{\mathrm{Pe}}=\frac{vL_{\mathrm{bed}}}{D_{\mathrm{L}}} \tag{3.15}$$

$$\tau_{\mathrm{f}}=\frac{V_{\mathrm{f}}D}{FR^2}=\frac{L_{\mathrm{bed}}D}{vR^2}=\frac{\gamma}{L} \tag{3.16}$$

N_{Pe} is the vessel Peclet number and L and γ are defined as in Equations 2.15 and 2.46 respectively; s is the Laplace parameters with respect to τ.

The Laplace domain expression for the effluent concentration in the case of plug flow (i.e. $N_{\mathrm{Pe}} = 0$) is

$$\frac{\hat{C}}{C_0} = \frac{1}{s}\left[1 - e^{-\tau_{\mathrm{f}} s - \frac{1}{L}\left(\sqrt{s}\coth\sqrt{s} - 1\right)}\right] \tag{3.17}$$

The standard ZLC model solution has the Laplace domain form

$$\frac{\hat{C}}{C_0} = \frac{1}{s}\frac{\tau_{\mathrm{f}} s + \frac{1}{L}\left(\sqrt{s}\coth\sqrt{s} - 1\right)}{1 + \tau_{\mathrm{f}} s + \frac{1}{L}\left(\sqrt{s}\coth\sqrt{s} - 1\right)} \tag{3.18}$$

It is easy to show that the equilibrium controlled counterparts to these models are, for disperse flow,

$$\frac{\hat{C}}{C_0} = \frac{1}{p}\left[1 + \frac{2Ie^{\frac{1}{2}(N_{\mathrm{Pe}} + I)}}{(N_{\mathrm{Pe}} + 2p - I) - (N_{\mathrm{Pe}} + 2p + I)\, e^{I}}\right] \tag{3.19}$$

where

$$I = \sqrt{N_{\mathrm{Pe}}^2 + 4pN_{\mathrm{Pe}}} \tag{3.20}$$

for plug flow

$$\frac{\hat{C}}{C_0} = \frac{1}{p}\left[1 - e^{-p}\right] \tag{3.21}$$

and for mixed flow

$$\frac{C}{C_0} = e^{-\tau_{\mathrm{e}}} \tag{3.22}$$

The variable p is the Laplace parameter with respect to τ_{e} and

$$\tau_{\mathrm{e}} = \frac{F}{V_{\mathrm{s}}K + V_{\mathrm{f}}}t \tag{3.23}$$

3.2 Results and discussion

τ_{f} represents the residence time of the carrier fluid in the void space of the sorbent bed. Inspection of Equation 3.17 and Figure 3.1 reveals that, for the plug flow case, it is a time delay term that has no effect on the shape of the curve, but only on its horizontal position. However, for the case of mixed flow behaviour (CSTR), increasing the relative amount of interstitial fluid (i.e. γ or τ_{f}) causes the initial steep drop of the standard ZLC curve to become exponential, as shown in Figure 3.1, reflecting the purging of fluid from a well mixed reactor with exponential short time behaviour as given by Equation 2.47. The disperse flow curve with $N_{\mathrm{Pe}} = 3$ shows the expected intermediate behaviour between the plug flow and CSTR cases.

Figure 3.1 shows that none of the models are able to reproduce the steep drop observed in the standard model. The most striking feature of Figure 3.1 is that all the desorption curves show similar exponential decay in the diffusion controlled long time region, regardless of the degree of axial mixing or interstitial fluid.

When diffusion is rapid and the system is in the equilibrium control region, the adsorbent behaves as an additional fluid volume, scaled by the adsorption constant K. Figure 3.2 shows the expected

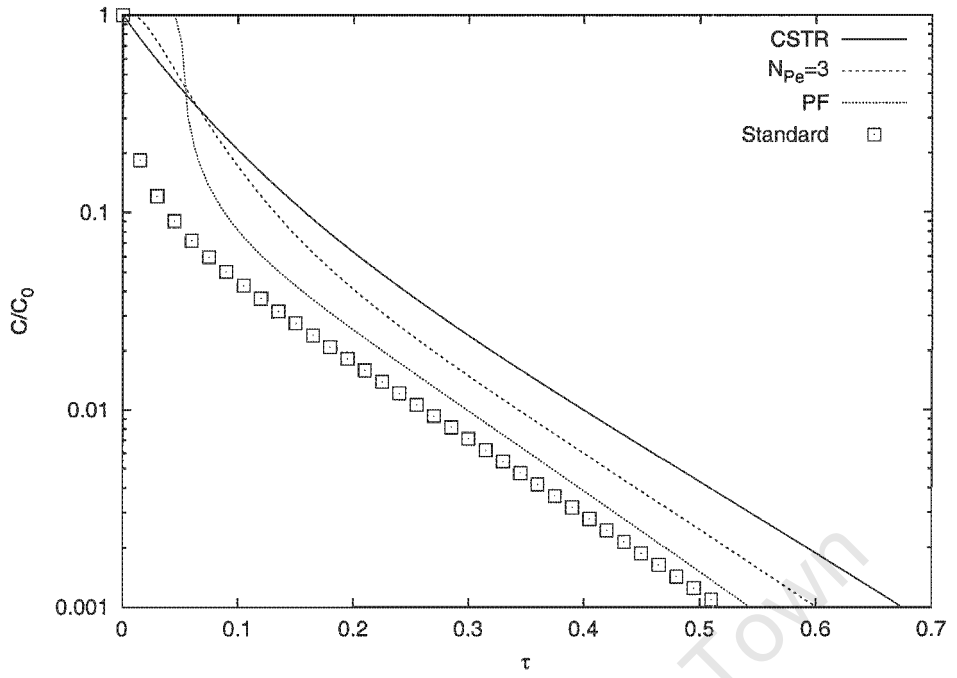

Figure 3.1: Plot of desorption curves using the plug flow (Eq. 3.17), liquid (Eq. 2.44) and disperse flow (Eq. 3.11) models for $L = 20$ and $\gamma = 1$. The standard model (Eq. 2.16) is shown for reference.

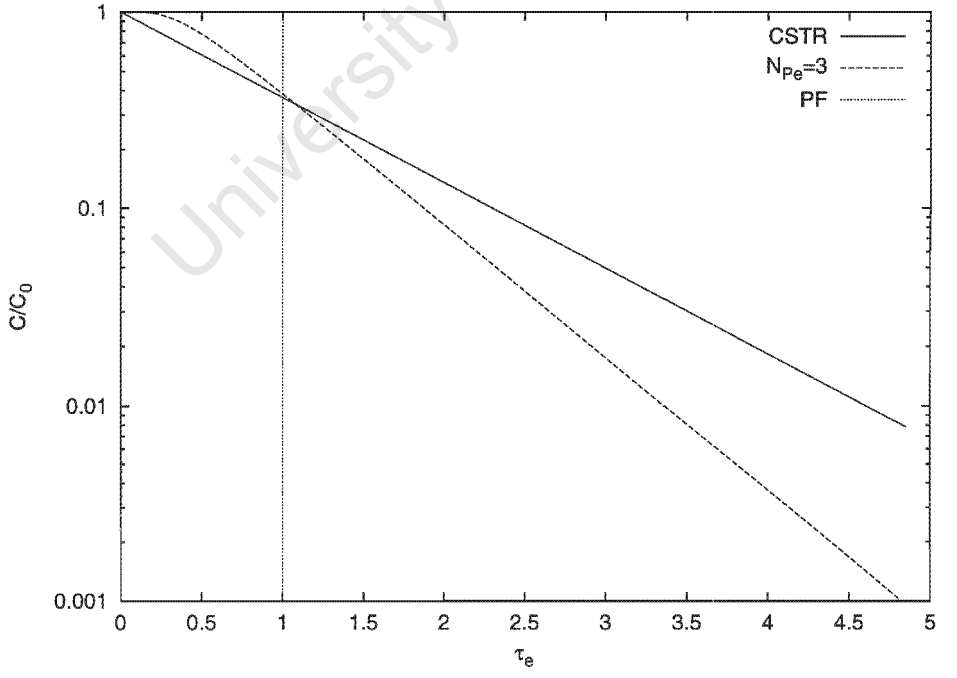

Figure 3.2: Plot of equilibrium controlled desorption curves using the plug flow (Eq. 3.21), CSTR (Eq. 3.22) and disperse flow (Eq. 3.19, $N_{\mathrm{Pe}} = 3$) models.

behaviour for the three cases under consideration: exponential decay for the mixed flow system, a delayed step for the plug flow model (both of which are clear from the respective equations) and intermediate behaviour for the case of finite dispersion. In the latter case, equilibrium control is easily detected experimentally as the slope of the tail of the desorption curve will be a (nonlinear) function of purge flow rate, similar to the mixed flow case. In addition, the curve would not show an inflection point which indicates transition into the diffusion controlled regime.

3.2.1 Comparison of the plug flow and standard models

It would be instructive to note the conditions under which the standard treatment of ZLC curves could be used regardless of the axial flow pattern. The issue of interstitial fluid has been treated in Section 2.6, so that only the case $\gamma = 0$ (i.e. negligible interstitial hold-up) was considered. To this end the two extreme cases, the plug flow and standard models (Eqs. 3.17 and 2.16) were compared with the assumption being that the finite dispersion case should lie between the two.

For large values of L (and $\gamma = 0$) the denominator of Equation 3.18 tends toward unity and it may be approximated as

$$\frac{\hat{C}}{C_0} = \frac{1}{sL}\left(\sqrt{s}\coth\sqrt{s} - 1\right) \tag{3.24}$$

Similarly, the exponential in Equation 3.17 may be approximated by the first two terms of a Taylor series expansion, leading to an identical result. Now Equation 3.24 may be easily inverted into the time domain (using the method of residues) to give

$$\frac{C}{C_0} = \frac{2}{L}\sum_{n=1}^{\infty} e^{-n^2\pi^2\tau} \tag{3.25}$$

which is exactly the approximation that can be obtained from Equation 2.16 for large L. It is thus seen that, at large L, the standard and plug flow models converge. It should be noted that this approximation does not hold for short times since many terms are needed for the summation to converge but Equation 3.25 requires that $n^2\pi^2 \ll L^2$, and in fact breaks down completely at zero time. It is the first term in this expression that was presented as the long time asymptote of the standard model (Equation 2.19) for large L (Eic and Ruthven, 1988).

The full model comparison was accomplished by using the plug flow model (Equation 3.17) to generate desorption curves for a range of L (between 5 and 150), then fitting the standard model to them by minimising the objective function

$$\text{Objective function} = \sum_{i=1}^{N}\left[\ln\left(\frac{C}{C_0}\right)_{\text{PF},i} - \ln\left(\frac{C}{C_0}\right)_{\text{Standard},i}\right]^2 \tag{3.26}$$

where N is the number of points used in the regression. All values between a normalised concentration of 1 and 10^{-3} were used in the curve fit. The error was then quantified in terms of the deviation of the apparent parameters, found from the regression procedure, from the values used to generate the original curve.

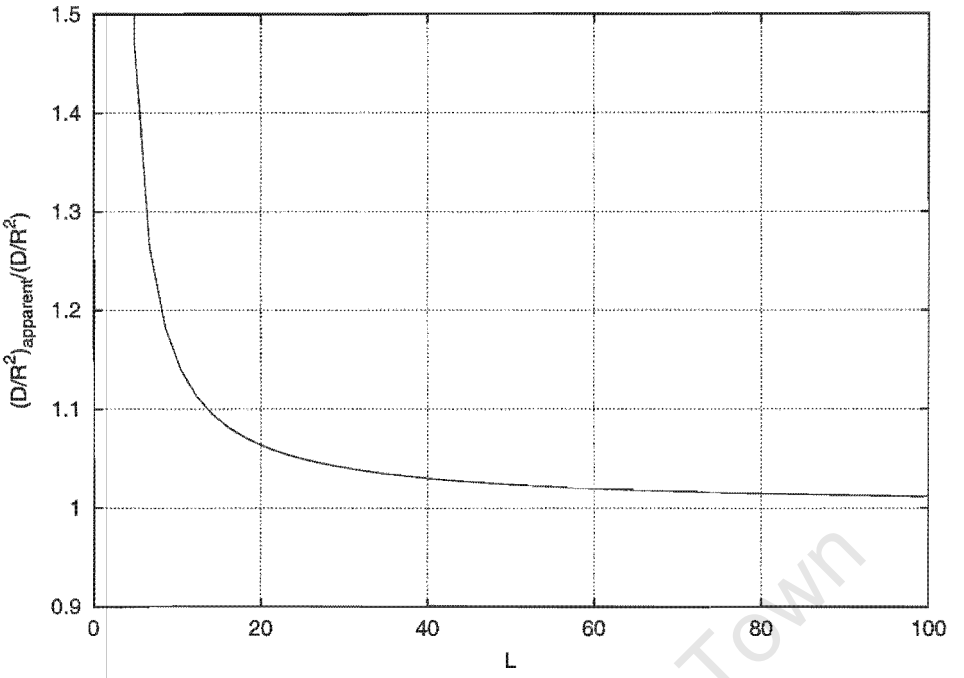

Figure 3.3: Deviation in the apparent value of D/R^2 when fitting the standard ZLC model (Eq. 2.16) to the plug flow model (Eq. 3.17).

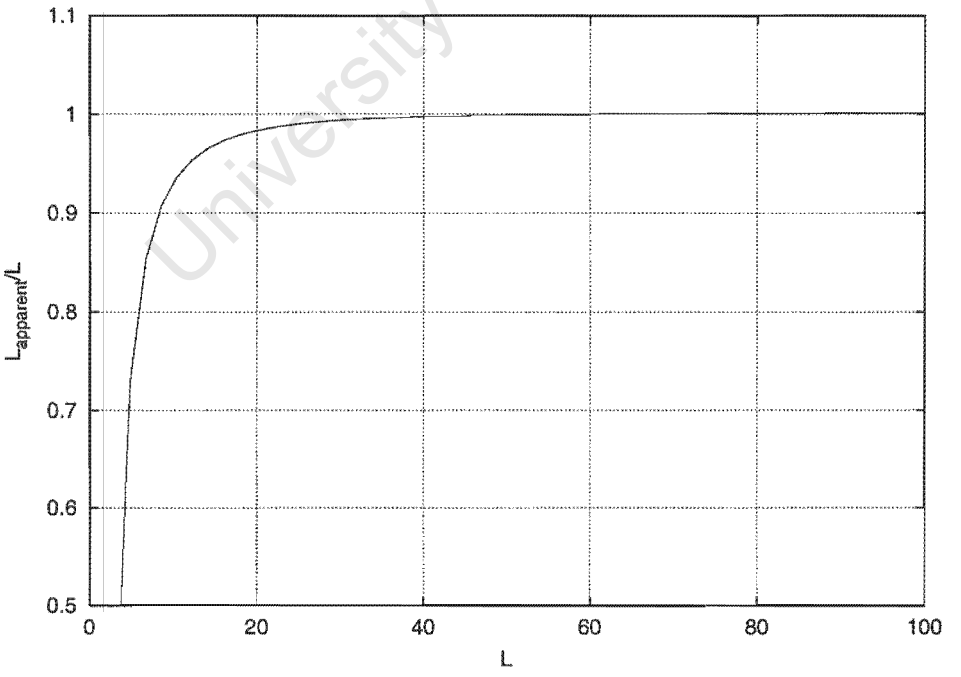

Figure 3.4: Deviation in the apparent value of L when fitting the standard ZLC model (Eq. 2.16) to the plug flow model (Eq. 3.17).

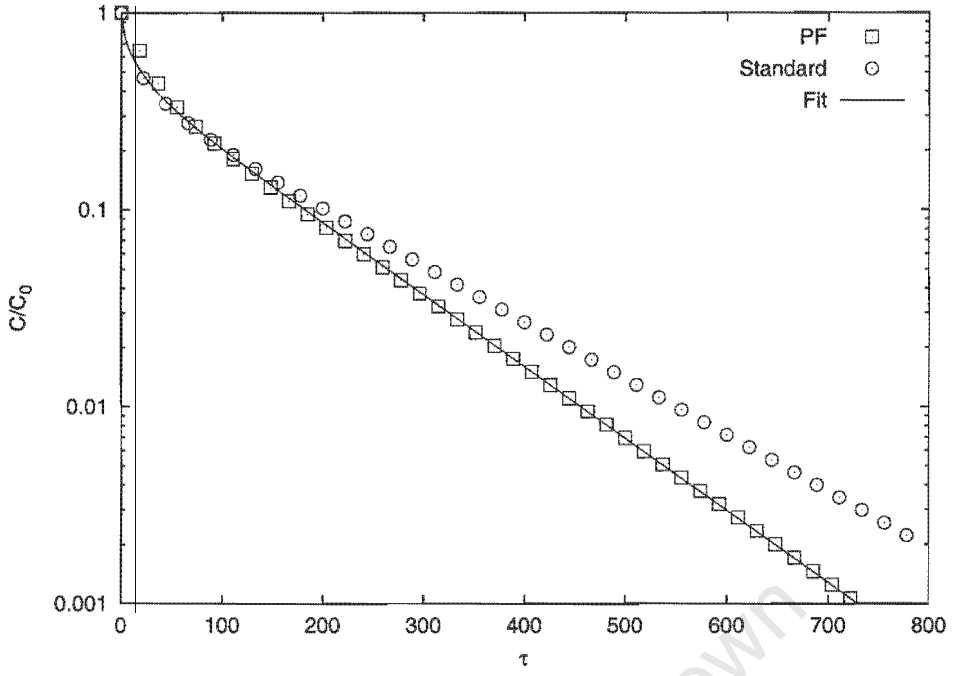

Figure 3.5: Desorption curves plotted with the plug flow model (Eq. 3.17) and the standard model (Eq. 2.16) for $L = 5$ and $\gamma = 0$, with the standard model fitted to the plug flow model having parameters $(D/R^2)_{\text{apparent}} = 1.45(D/R^2)$ and $L_{\text{apparent}} = 3.73$.

Figures 3.3 and 3.4 indicate good agreement between the two models for large values of L. This is consistent with the physical interpretation of the parameter, in that the models are similar when diffusion effects dominate over removal of material by convection. It can be seen that, for an error of less that 10% in D/R^2, it is necessary to operate such that $L > 14$, while the restriction for a similar error in L is less stringent at $L > 8$. For values of L smaller than this lower bound the diffusivity is overestimated and L itself is underestimated.

Figure 3.5 shows the desorption curves for the two models for $L = 5$, when the deviation is expected to be severe, as is indeed seen to be the case in both the short and long time regions. The plug flow curve shows a slower initial drop than even the standard curve that is fitted to it. This is a manifestation of the plug flow system's ability to purge faster than a mixed flow vessel, causing a greater mass of sorbate to exit the bed in the region where convective transport plays a large role. The plug flow curve then drops below the standard curve in the diffusion controlled long time region, which is simply a mass balance phenomenon. Figure 3.6 shows the desorption curves for large L, and it is seen that the two models are practically identical.

3.3 Conclusions on zero length behaviour

It has been shown by Brandani and Ruthven (1995) (Section 2.6) that the interstitial fluid hold-up in a well mixed sorbent bed may be neglected if the adsorption constant of the system is large enough that $\gamma < 0.1$. The work presented in this chapter shows that, if this condition is met, the flow pattern

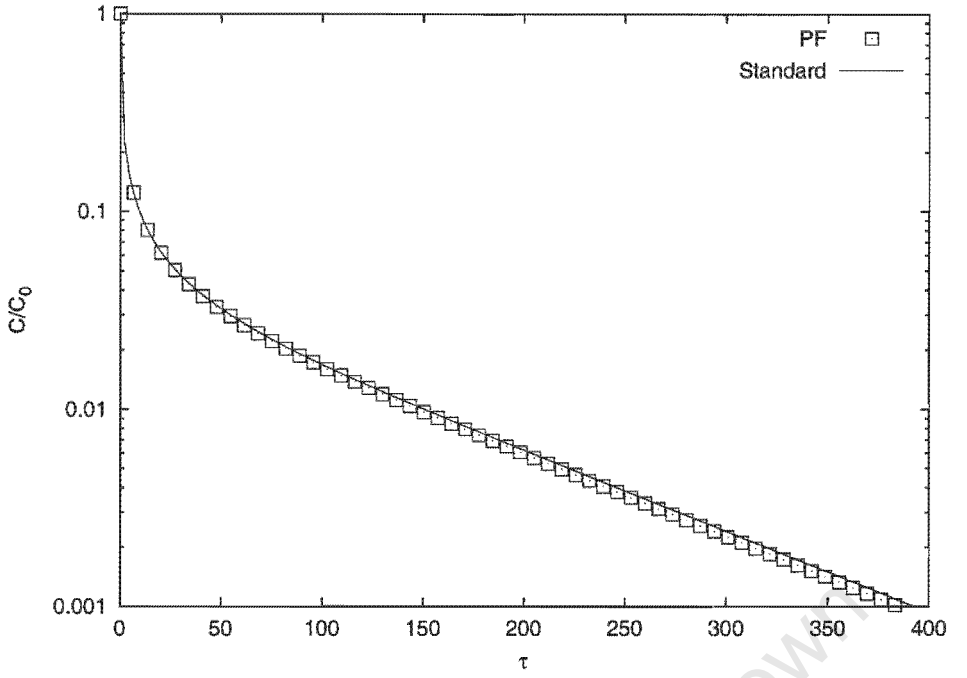

Figure 3.6: Desorption curves plotted with the plug flow model (Eq. 3.17) and the standard model (Eq. 2.16) for $L = 50$ and $\gamma = 0$.

within the bed may be disregarded if $L > 15$, i.e. if diffusive transport is sufficiently dominant over convective transport. Operating below this bound could result in overestimation of the diffusion time constant and underestimation of L. These criteria define 'zero length' behaviour for any adsorbent bed, regardless of its physical length and degree of mixing.

Chapter 4

The Effect of a Crystal Size Distribution

The long time analysis method of ZLC desorption curves, used in this work, comprises fitting a straight line to the linear tail to extract the relevant transport parameters. There are, however, several examples of data in the literature in which the long time region of the curve is not convincingly linear, but shows a 'tailing' effect (i.e. it is convex to the time axis) (Voogd et al., 1991; Hufton and Ruthven, 1993; Brandani et al., 2000a; Loos et al., 2000); see also the desorption curves in Chapter 6. The only theoretical work to attempt to describe this behaviour is that incorporating the effect of a distribution of discrete sorbent particle sizes (Loos et al., 2000), although the effect is not readily apparent as the authors of that work chose a logarithmic time scale when plotting their desorption curves. Analogous behaviour has been shown for the jet loop reactor (Möller and O'Connor, 1996).

The work in this chapter quantifies the effect of a crystal size distribution on the ZLC desorption curve using the standard long time approach. This is done by comparing the standard model (Equation 2.16) to a model incorporating a continuous, log-normal size distribution. A second model, for possible use when experimental size distribution data are available, is also developed. Finally, a mean particle size is defined in such a way as to reduce the error in calculating diffusivity when using the standard model to analyse a sorbent sample showing a size distribution.

4.1 Development of the models

Detailed derivations may be found in Appendix A.

4.1.1 Continuous size distribution model

As described in Section 2.1, Fick's Second Law spherical coordinates is used for the sorbate mass balance in the micro-particles:

$$\frac{\partial q}{\partial t} = D\left(\frac{\partial^2 q}{\partial r^2} + \frac{2}{r}\frac{\partial q}{\partial r}\right) \tag{4.1}$$

with the initial condition

$$q(r, t = 0) = KC_0 \tag{4.2}$$

and the boundary conditions

$$q(r = R, t) = KC \tag{4.3}$$

$$\frac{\partial q}{\partial r}(r = 0, t) = 0 \tag{4.4}$$

The sorbent particles are assumed to follow a log-normal size distribution, which is common for zeolite crystals (Hsu and Haynes, 1981):

$$P(\ln R) = R\,P(R) = \frac{1}{\sqrt{2\pi}\sigma} \exp\left(-\frac{(\ln R - \mu)^2}{2\sigma^2}\right) \tag{4.5}$$

where μ represents the number mean of the normal distribution of the logarithm of particle size and σ its standard deviation.

The fluid phase mass balance, neglecting interstitial sorbate accumulation (Brandani and Ruthven, 1995), takes the form

$$-\frac{4\pi V_s \int_0^\infty R^2 \left.\frac{\partial q}{\partial r}\right|_{r=R} P(R)\,dR}{\frac{4}{3}\int_0^\infty R^3\,P(R)\,dR} = FC \tag{4.6}$$

These equations were solved in dimensionless form in the Laplace domain, making use of the following substitutions:

$$R = e^{\mu+\sqrt{2}\sigma\zeta} \tag{4.7}$$

$$X_m = \frac{r}{R_m} \tag{4.8}$$

$$\tau_m = \frac{D}{R_m^2}t \tag{4.9}$$

$$R_m = e^{\mu} \tag{4.10}$$

It should be noted that $R_m \neq \bar{R}$, i.e. the former is not the number mean particle radius, which is instead given by

$$\begin{aligned} \bar{R} &= \int_0^\infty R\,P(R)\,dR \\ &= e^{\mu+0.5\sigma^2} \\ &= R_m e^{0.5\sigma^2} \end{aligned} \tag{4.11}$$

The solution for the desorption curve in the Laplace domain is

$$\frac{\hat{C}}{C_0} = \frac{1}{s}\frac{\int_{-\infty}^{\infty}\left[\left(e^{\sqrt{2}\sigma\zeta}\sqrt{s}\right)\coth\left(e^{\sqrt{2}\sigma\zeta}\sqrt{s}\right) - 1\right] e^{\sqrt{2}\sigma\zeta-\zeta^2}\,d\zeta}{\sqrt{\pi}L_m e^{4.5\sigma^2} + \int_{-\infty}^{\infty}\left[\left(e^{\sqrt{2}\sigma\zeta}\sqrt{s}\right)\coth\left(e^{\sqrt{2}\sigma\zeta}\sqrt{s}\right) - 1\right] e^{\sqrt{2}\sigma\zeta-\zeta^2}\,d\zeta} \tag{4.12}$$

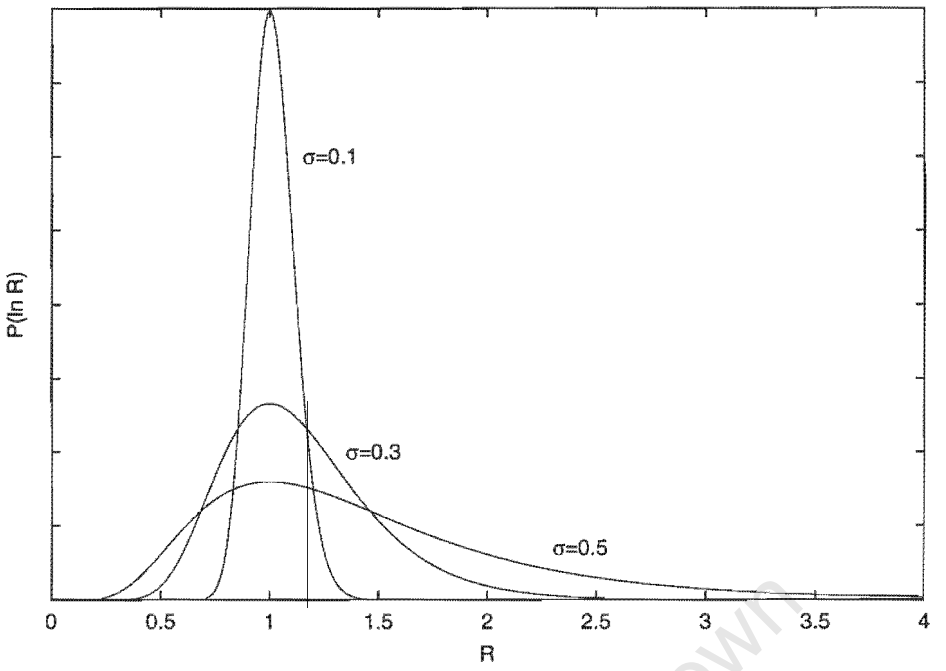

Figure 4.1: Particle size distribution plot in arbitrary units for $\mu = 0$ and values of σ as indicated.

where

$$L_{\mathrm{m}} = \frac{FR_{\mathrm{m}}^2}{3V_{\mathrm{s}}KD} \tag{4.13}$$

This may be compared to the solution of the standard model (i.e. $\sigma = 0$) in the Laplace domain (Brandani and Ruthven, 1996a) :

$$\frac{\hat{C}}{C_0} = \frac{1}{s}\frac{\sqrt{s}\coth\sqrt{s} - 1}{L + \sqrt{s}\coth\sqrt{s} - 1} \tag{4.14}$$

Equation 4.12 may be solved numerically using the Fast Fourier Transform algorithm, with the indicated integral being evaluated by Gauss-Hermite quadrature. Since a dimensionless time scale is used, the model has two independent parameters, namely L_{m}, which is similar to L in the standard model, and σ, which defines the width of the particle size distribution. The usual third experimental parameter, D/R^2, defines the real time length of the experiment and has no effect on the shape of the desorption curve.

Size distributions are shown in Figure 4.1 for various values of σ at constant μ (i.e. constant R_{m}). It may be seen that increasing σ not only increases the width of the distribution, but also skews it toward the larger particles.

Figure 4.2 shows desorption curves generated using Equation 4.12. For $\sigma = 0$ the curve corresponds to that of the standard model (Equation 2.16), as would be expected. when the width of the size distribution is increased, the normally linear tail becomes increasingly curved. The slope of the tail is, of course, dependent on the diffusional time constant D/R^2; since multiple values of R exist, as described by the size distribution, the slope cannot be constant. The large increase in experimental

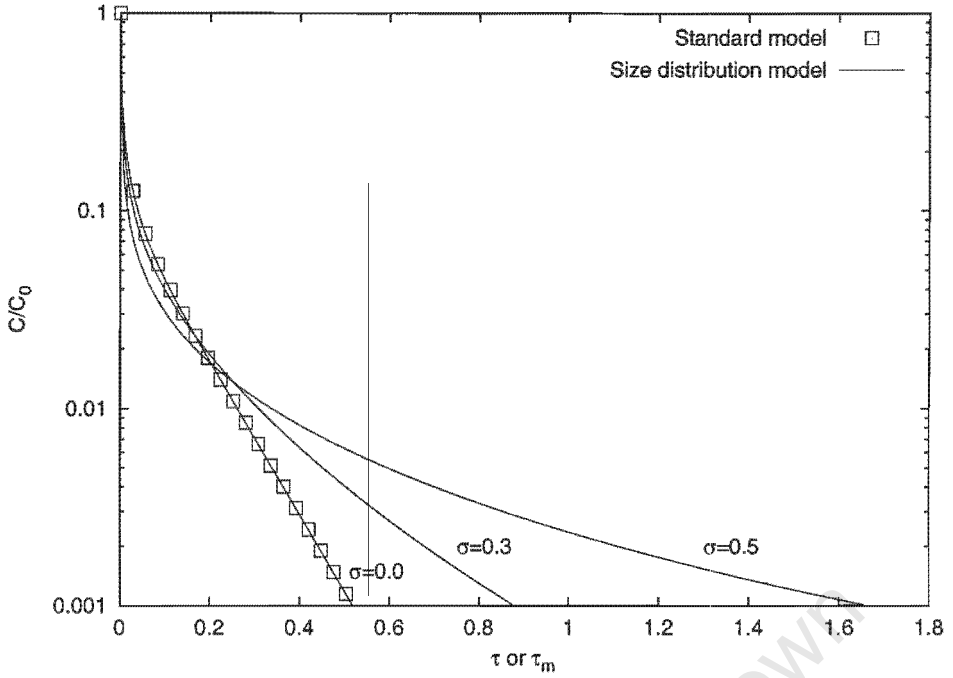

Figure 4.2: Desorption curves generated using the size distributions model (Eq. 4.12) for $L = 20$ and various values of σ as shown. The standard ZLC model (Eq. 2.16) is shown for verification.

duration is due to the chosen distribution model being skewed towards the larger particles for large σ.

4.1.2 Discrete size distribution model

One may write the fluid phase mass balance in the form

$$FC = -V_s \frac{d\bar{q}}{dt} \tag{4.15}$$

where $\bar{q}$ is the space-averaged adsorbed phase concentration. Considering N discrete sorbent size fractions, this may be rewritten as

$$FC = -\sum_{i=1}^{N} V_{si} \frac{d\bar{q}_i}{dt} \tag{4.16}$$

where V_{si} is the volume of sorbent in fraction i. It can then be seen that the overall desorption curve is given by the sum of the desorption curves for the individual size fractions, i.e.

$$\frac{C}{C_0} = \sum_i v_i \frac{C}{C_0}(\tau_i, L_i) \tag{4.17}$$

with

$$L_i = \frac{FR_i^2}{3V_s KD} \tag{4.18}$$

$$\tau_i = \frac{D}{R_i^2} t \tag{4.19}$$

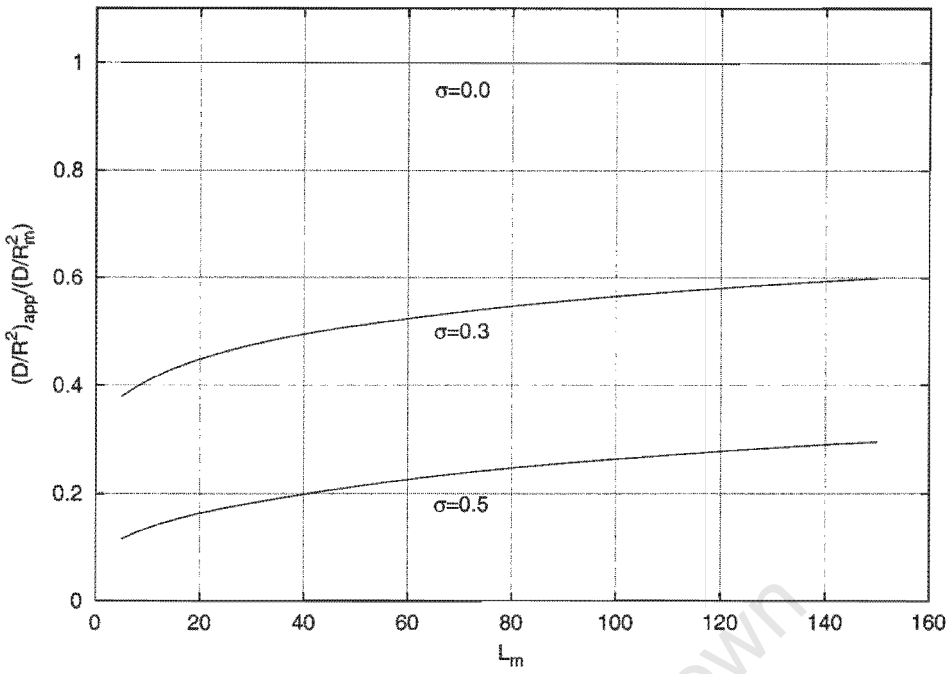

Figure 4.3: Apparent deviation in diffusional time constant when fitting the standard ZLC model to that with a crystal size distribution, for various distribution widths.

and

$$v_i = \frac{V_{si}}{V_s} \tag{4.20}$$

where R_i is the representative radius of size fraction i and $C/C_0(\tau_i, L_i)$ is calculated by Equation 2.16. Note that the definition of L_i here is an approximation only, in that it has been assumed that the solution for the desorption curve of each fraction is linear with respect to L. This is only valid for the case of large L and long times, where the analogue of Equation 2.19 may be written as

$$\frac{C}{C_0} = \sum_{i=1}^{N} v_i \frac{2}{L_i} e^{-\pi^2 \tau_i} \tag{4.21}$$

4.2 Results and discussion

4.2.1 Comparison of size distribution and standard models

In order to quantify the deviation from the standard ZLC model caused by non-monosized sorbent particles, desorption curves were generated with Equation 4.12 and Equation 2.16 was then fit to them. The comparison is based on the apparent values of L and D/R^2 obtained from the regression compared to the values used to generate the original curves. All points in the range $0.001 \leq C/C_0 \leq 1$ were considered. The results are shown in Figures 4.3 and 4.4.

Examples of the model fits obtained by this procedure are shown for various L and σ in Figures 4.5 and 4.6. The curvature in the desorption curve tail is most evident for the low L value. At high L most of the tail is below the observed concentration range, so it is possible to obtain a 'good' model

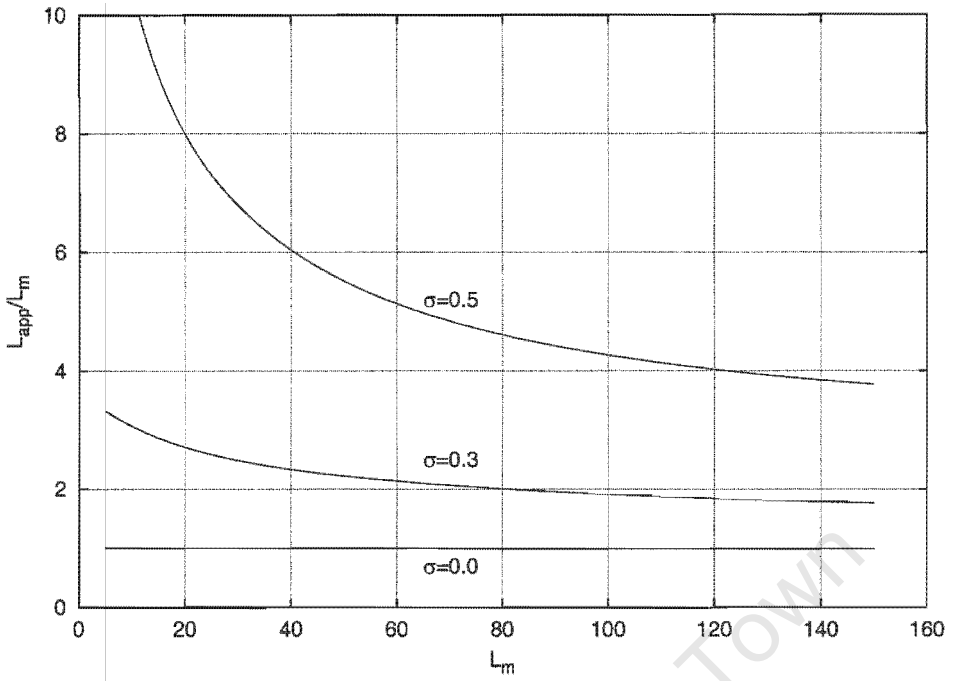

Figure 4.4: Apparent deviation in L when fitting the standard ZLC model to that with a crystal size distribution, for various distribution widths.

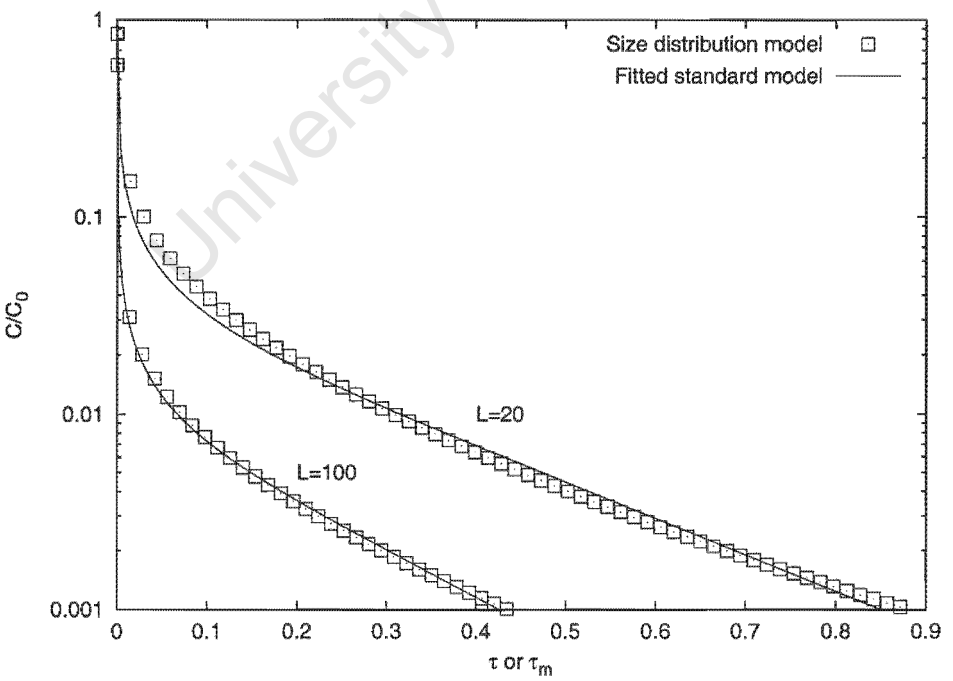

Figure 4.5: Model comparison for the standard model fitted to the crystal size distribution model when $\sigma = 0.3$ for L as shown.

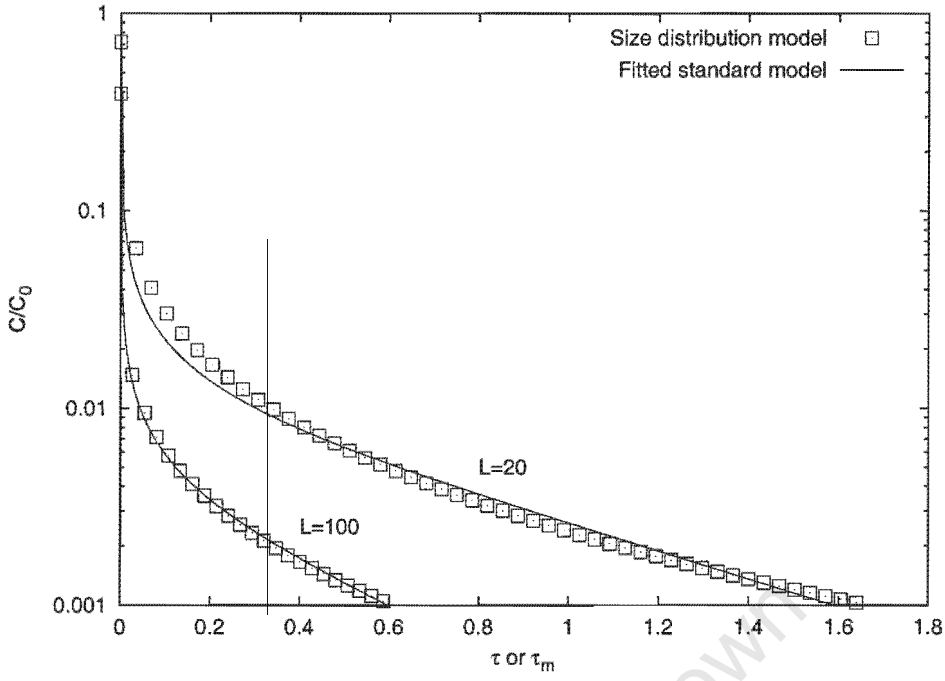

Figure 4.6: Model comparison for the standard model fitted to the crystal size distribution model when $\sigma = 0.5$ for L as shown.

fit in this regime although, as may be seen in Figures 4.3 and 4.4, the parameters one obtains from the fit may be subject to a substantial error since the contribution of the larger particles is below the measured threshold. The problem would be practically impossible to identify in an experiment, a reason for excessively large L to be avoided experimentally.

One should note that, although the errors introduced in this manner are relatively small (generally less than a factor three), they are systematic and additive to the random error inherent in any experimental work.

It is evident from Figures 4.3 and 4.4 that, for a series of experiments at constant temperature and varying flow rate, a plot of L versus flow rate would tend to rise sharply, then flatten off somewhat into a linear region (Figure 4.7). D/R^2 would appear to increase with flow rate, the dependency becoming decreasingly marked at increasing flow rate, as in Figure 4.3.

4.2.2 Description of experimental data with the size distribution model

It is tempting to fit Equation 4.12 to experimental data. However, it is important to note the quality of the information this is likely to produce. It is inevitable that the model will fit the experimental curves better: it has an extra parameter that can provide curvature. This will be true regardless of the physical meaning of the third parameter. It is important to check the consistency of the parameters over several experiments rather than assuming that the model is more accurate because it provides a better fit.

Figure 4.8 shows an example of how Equation 4.12 is able to fit an experimental desorption curve (all data are for Sample B, discussed in Chapter 6) far better than the standard model (Equation

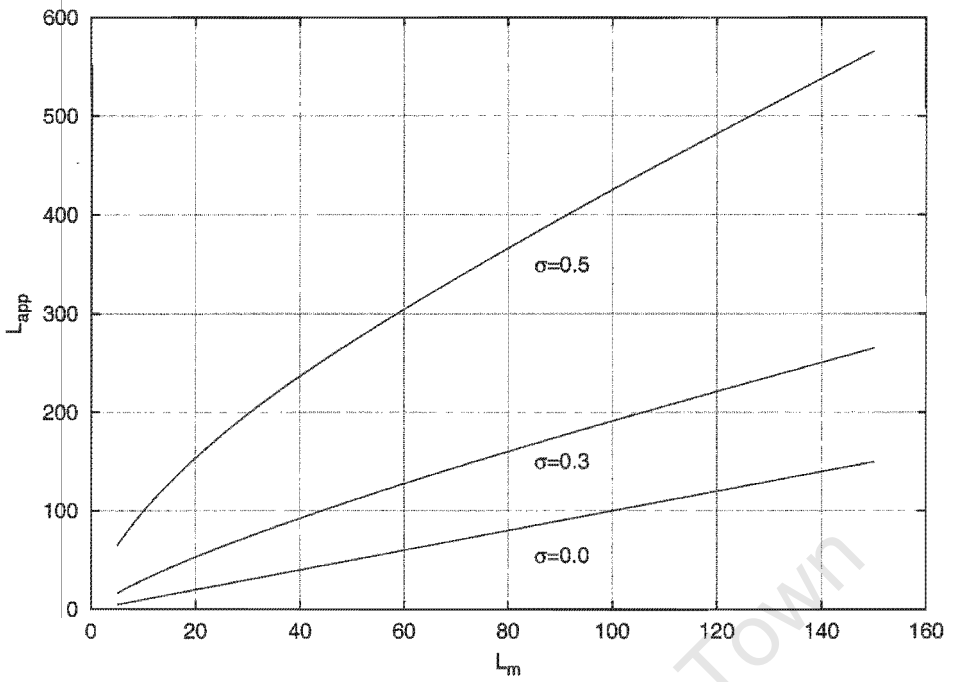

Figure 4.7: Dependence of measured L on flow rate ($L_m \propto F$) when fitting the standard ZLC model to that with a crystal size distribution, for various distribution widths.

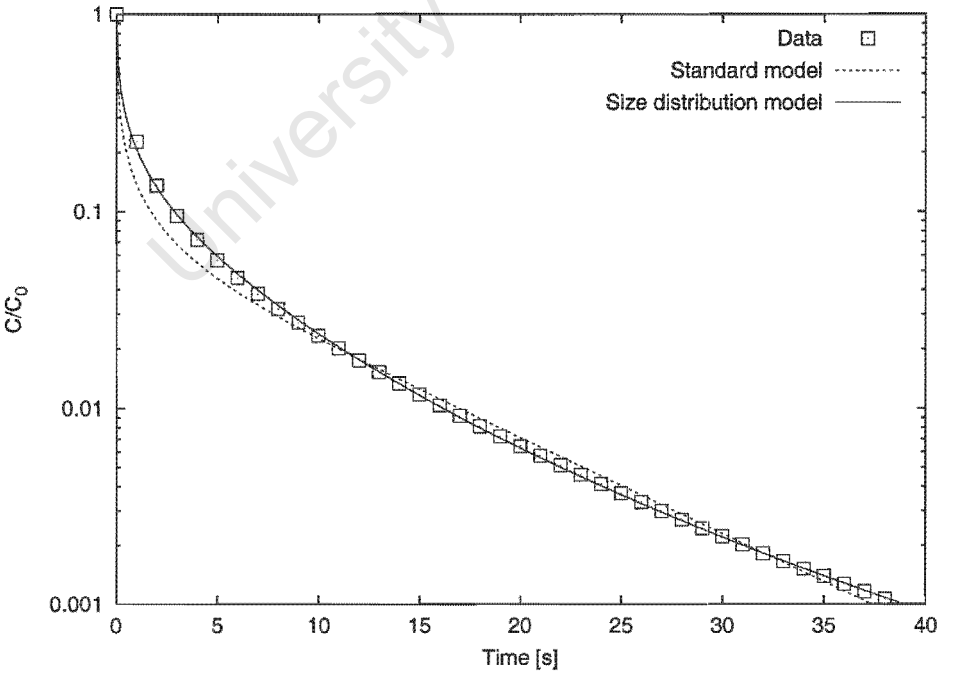

Figure 4.8: Example of model fit for the standard and size distribution models to an experimental desorption curve ($T = 200$℃, $F = 41.6\,\mathrm{ml/min}$, $m_s = 2\,\mathrm{mg}$, $D/R^2 = 1.22 \times 10^{-2}\,\mathrm{cm^2/s}$, $L = 30.3$).

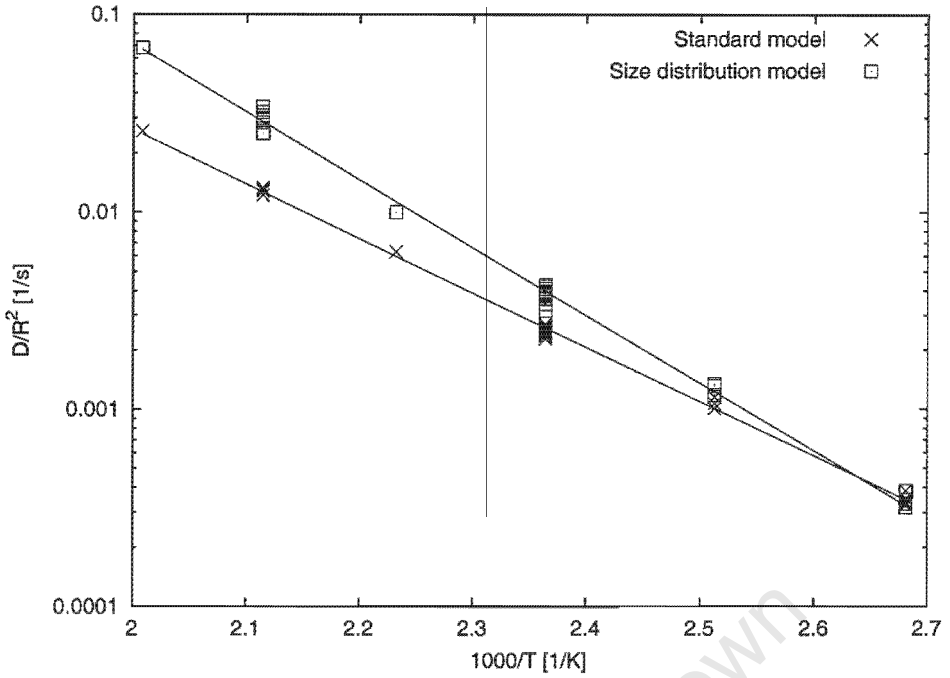

Figure 4.9: Temperature dependence of the diffusional time constant as determined by both the standard and size distribution models.

2.16). The Arrhenius plot in Figure 4.9 confirms that the former tends to give larger values for the diffusional time constant, as was indicated in Figure 4.3, but it is also apparent that some scatter is introduced into the data. The activation energy given by the standard model is 52.8 kJ/mol, while the size distribution model indicates a value of 65.8 kJ/mol, a significant increase.

Most significant, however, is the wide range of σ obtained for the data, as shown in Figure 4.10. As would be expected if the size distribution was not the same shape as assumed, or if the curvature in the desorption curve was caused by a different effect, σ decreases with increasing L as less of the tail is visible, masking the contribution of the larger members of the distribution. The scatter is not likely to be caused by model insensitivity to the adjustable parameters: several of the regression runs were repeated with different initial guesses, all resulting in similar solutions. On the other hand, increasing the number of adjustable parameters in the curve fit (to three from the usual two) would tend to increase the variance of the estimates.

If one were to assume that the values of σ obtained for the curves where L is small are most likely to be correct, since more of the curvature in the tail that is caused by the size distribution is seen, Figure 4.10 shows that $\sigma \simeq 0.3$. It may then be possible to obtain a more accurate value of D/R^2 (smaller variance since we now have only two adjustable variables) while still accounting for the size distribution.

Figure 4.11 shows the temperature dependence of the diffusional time constants thus obtained. The diffusional activation energy ($E_a = 57.8$ kJ/mol) is closer to that obtained for the standard model than when σ was fitted, while D/R^2 is consistently higher. The data are also less scattered than when three adjustable parameters were used, but there is still more spread than for the case of

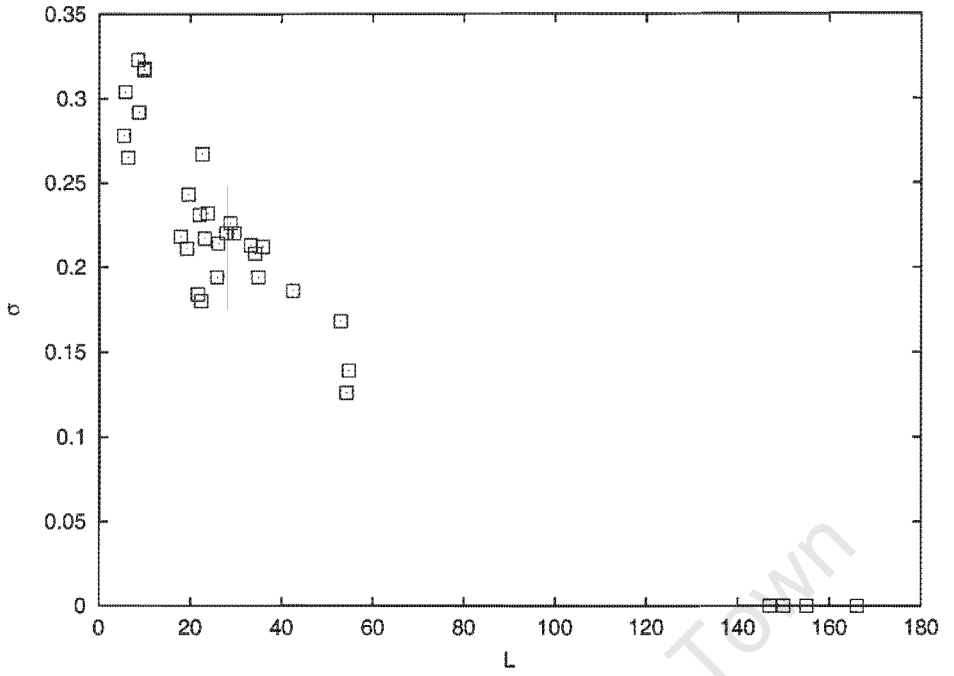

Figure 4.10: Crystal size distribution width as a function of L for all points shown in Figure 4.9.

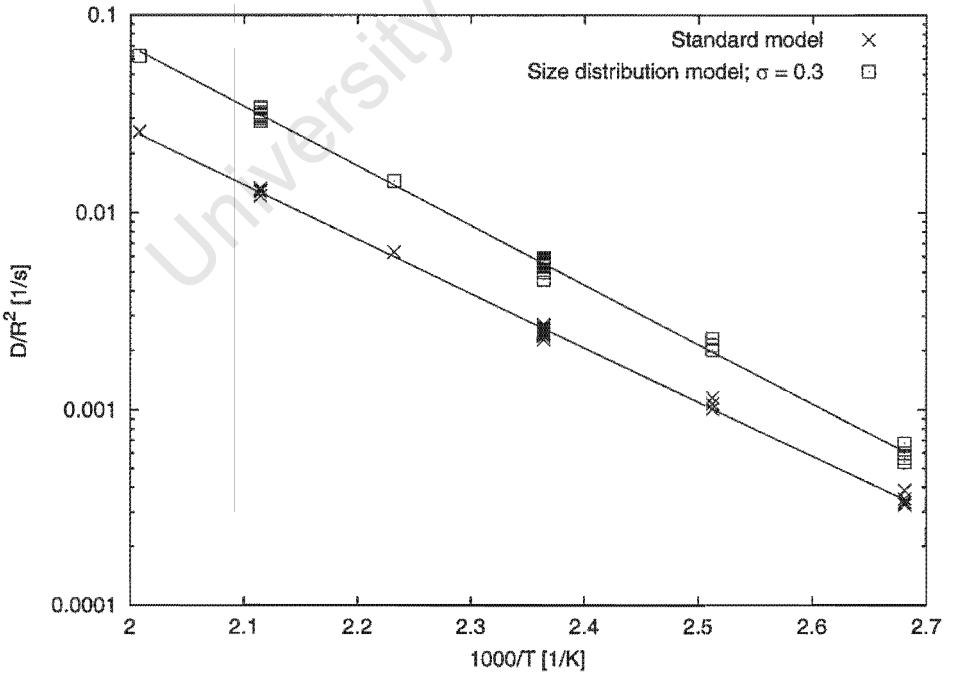

Figure 4.11: Temperature dependence of the diffusional time constant as determined by both the standard and size distribution models with fixed $\sigma = 0.3$.

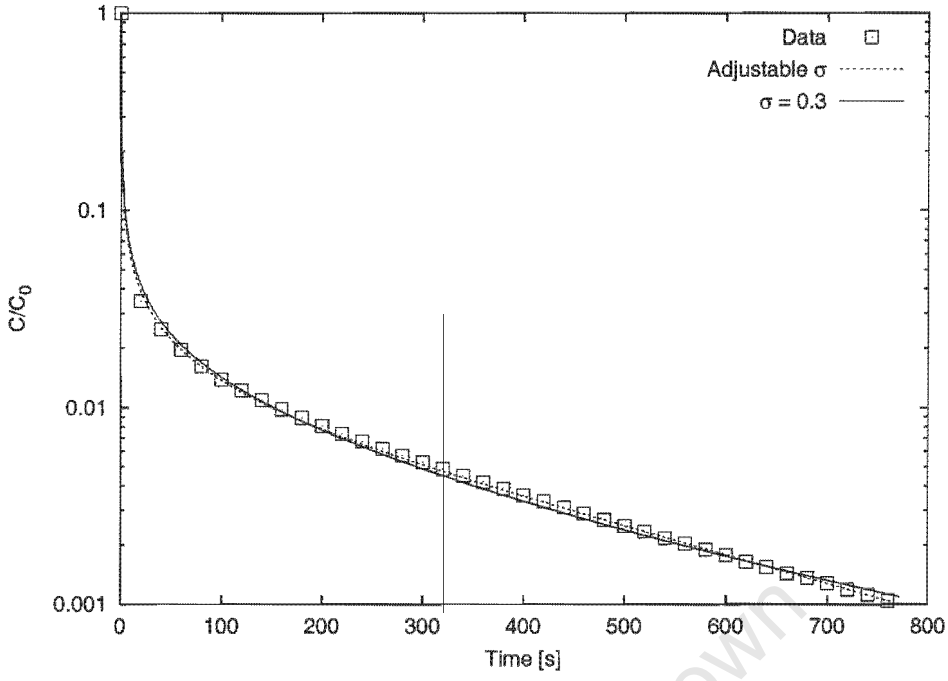

Figure 4.12: Example model fits using the size distribution model for two and three adjustable parameters, for desorption curve with large L (standard model fit gives $D/R^2 = 3.50 \times 10^{-4}\,\mathrm{cm}^2/\mathrm{s}$, $L = 146$).

the standard model.

If the basic premise leading to the $\sigma = 0.3$ assumption is correct, then the model fit should be good even for large L. Such curves are shown in Figure 4.12, where it may be seen that the fit is not good when σ is held constant; the tail of the model curve is too curved, while that of the data is nearly linear, as predicted by the standard model.

Quite clearly, Equation 4.12 does not adequately describe the experimental data presented here, probably simply due to the shape of the crystal size distribution. The data did not show any significant trends in σ with temperature, flow rate or initial sorbate concentration.

4.2.3 Approximate models to account for a particle size distribution

An approximate method of evaluating the desorption curve for a non-monosized sorbent has been suggested by Loos et al. (2000): one simply adds the normalised responses of each (discrete) size fraction. The fractions are weighted according to the fraction a_i of the total surface area of the sample that each one contains. Each size fraction is represented by its largest dimension, which defines its diffusional time constant and value of L. The desorption curve is then given by

$$\frac{C}{C_0} = \sum_i a_i \frac{C}{C_0}(\tau_i, L_i) \tag{4.22}$$

analogously to Equation 4.17.

To compare this approximate approach and the volume fraction based method developed above to the full solution (Equation 4.12), ten size fractions were defined as shown in Table 4.1, each having

Table 4.1: Division of a continuous size distribution into discrete fraction such that all fractions have equal surface area or volume; $\mu = 0$.

	$a_i = 0.1$		$v_i = 0.1$	
σ	Size range	Area in fraction	Size range	Volume in fraction
0.3	0.20 – 0.81	1.45	0.20 – 0.89	0.620
	0.81 – 0.93	1.56	0.89 – 1.02	0.649
	0.93 – 1.02	1.46	1.02 – 1.12	0.619
	1.02 – 1.11	1.56	1.12 – 1.21	0.596
	1.11 – 1.20	1.54	1.21 – 1.31	0.656
	1.20 – 1.29	1.43	1.31 – 1.41	0.608
	1.29 – 1.40	1.52	1.41 – 1.53	0.633
	1.40 – 1.54	1.51	1.53 – 1.68	0.621
	1.54 – 1.76	1.52	1.68 – 1.91	0.622
	1.76 – 4.00	1.50	1.91 – 6.00	0.654
	$4\pi\overline{R^2} = 15.04$	$\sum = 15.05$	$\frac{4}{3}\pi\overline{R^3} = 6.280$	$\sum = 6.278$
0.5	0.10 – 0.87	2.08	0.10 – 1.10	1.23
	0.87 – 1.08	2.04	1.10 – 1.38	1.30
	1.08 – 1.27	2.12	1.38 – 1.62	1.29
	1.27 – 1.45	2.03	1.62 – 1.86	1.31
	1.45 – 1.65	2.11	1.86 – 2.11	1.28
	1.65 – 1.87	2.05	2.11 – 2.40	1.31
	1.87 – 2.14	2.06	2.40 – 2.75	1.30
	2.14 – 2.51	2.09	2.75 – 3.22	1.29
	2.51 – 3.12	2.06	3.22 – 4.01	1.29
	3.12 – 12.00	2.08	4.01 – 12.00	1.30
	$4\pi\overline{R^2} = 20.72$	$\sum = 20.72$	$\frac{4}{3}\pi\overline{R^3} = 12.90$	$\sum = 12.90$

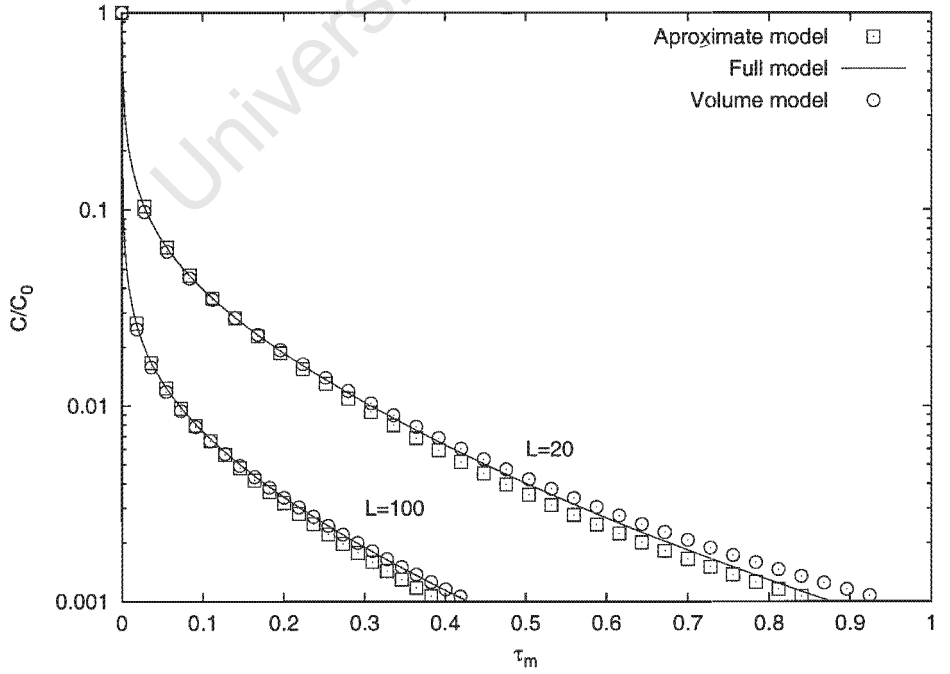

Figure 4.13: Desorption curves plotted using the full and approximate size distribution models for $\sigma = 0.3$ and L as indicated.

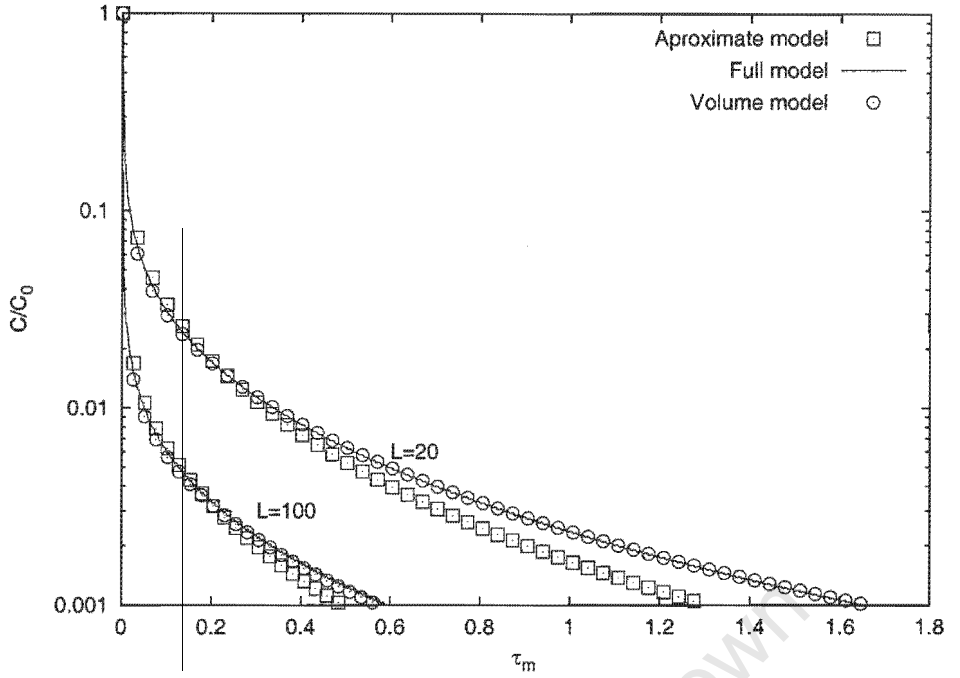

Figure 4.14: Desorption curves plotted using the full and approximate size distribution models for $\sigma = 0.5$ and L as indicated.

an approximately equal surface area or volume ($a_i = v_i = 0.1$). The resulting desorption curves are shown in Figures 4.13 and 4.14.

It can be seen that the volume based approximation generally corresponds to the full model better than does the area based model. This is unsurprising since it has been shown above to be exact for large L and long times. Curves with large L show very good agreement between the exact and approximate models for both indicated distribution widths, as does the example for small L and wider distribution. The exception is the curve for $L = 20$ and $\sigma = 0.3$; this is likely the result of L not being quite large enough that the approximations in Equation 4.18 hold.

The obvious advantage to this sort of approach is that it is not tied to a specific shape of size distribution. This makes it a superior choice in practical terms over the analytical sort of approach leading to Equation 4.12. In fact, it is possible that one may introduce more scope for error by trying to describe the real distribution with a simple analytical one and using an 'exact' model than simply using this semi-empirical approach.

4.2.4 Definition of mean particle size

While Equation 4.10 is the mathematically most elegant way to define the mean particle radius, it is certainly not the most intuitive value to use when dealing with experimental size distribution data. It is also useless if the sorbent does not have the type of size distribution that has been assumed here. Inspection of Equations 4.12 and 4.14 suggests that a starting point for a practically more useful definition would be

$$R_{\text{mean}} = e^{\mu + 2.25\sigma^2} \tag{4.23}$$

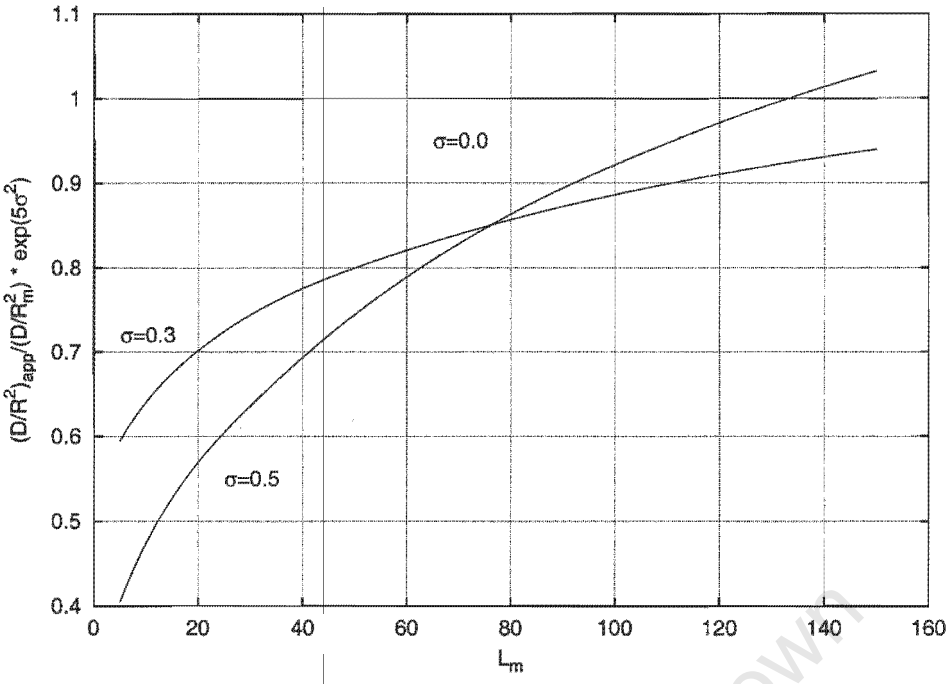

Figure 4.15: Deviation in apparent diffusional time constant when fitting the standard ZLC model to that with a crystal size distribution, for various widths, including the correction factor indicated by Equation 4.26.

By analogy with Equation 4.11, the volume and area based mean radii may be found from the relations

$$\bar{R}^3 = e^{3\mu+4.5\sigma^2} \tag{4.24}$$

$$\bar{R}^2 = e^{2\mu+2\sigma^2} \tag{4.25}$$

and it is easy to see that

$$\frac{\bar{R}^3}{\bar{R}^2} = e^{\mu+2.5\sigma^2} \simeq e^{\mu+2.25\sigma^2} \tag{4.26}$$

Thus the common engineering approximation, taking the representative dimension as essentially the ratio of volume to surface area, would be reasonable in this case, and probably for other distributions as well.

This definition of mean size is useful for the case when insufficient particle size data are available to use, for example, Equation 4.17 and makes it feasible to use the standard model (Equation 2.16). The effect of this choice may be observed by comparing Figures 4.15 and 4.16 to Figures 4.3 and 4.4 respectively: the apparent model parameters become less severely over- or underpredicted, although the flow rate dependence is exaggerated.

4.2.5 Some practical considerations

When packing the amounts of sorbent generally used in ZLC work, i.e. a couple of milligrams, it is very difficult to obtain a representative sample. Thus, even when size distribution data are available, they

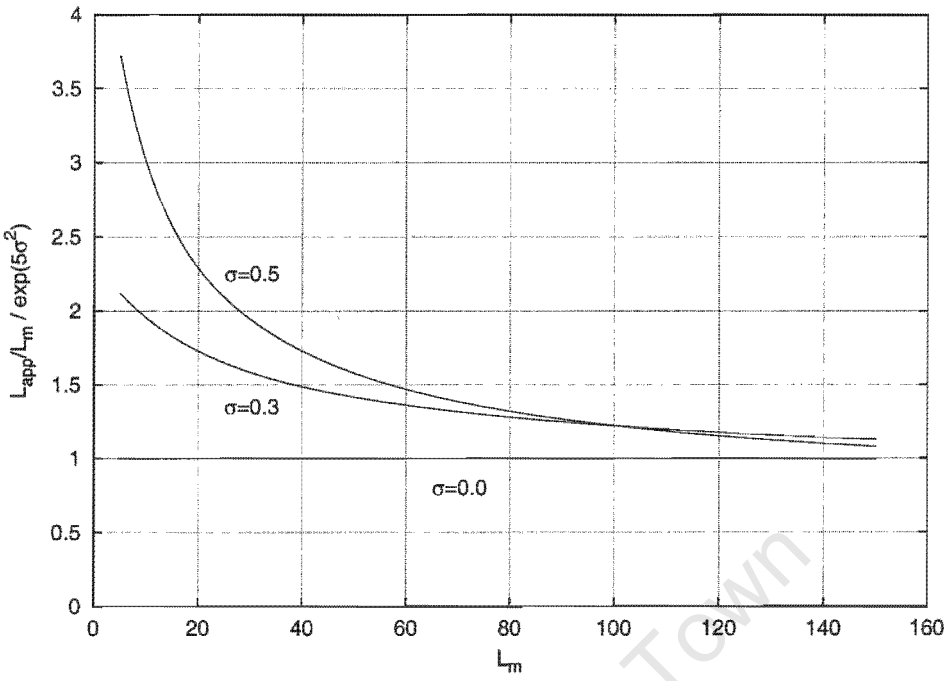

Figure 4.16: Deviation in apparent L when fitting the standard ZLC model to that with a crystal size distribution, for various widths, including the correction factor indicated by Equation 4.26.

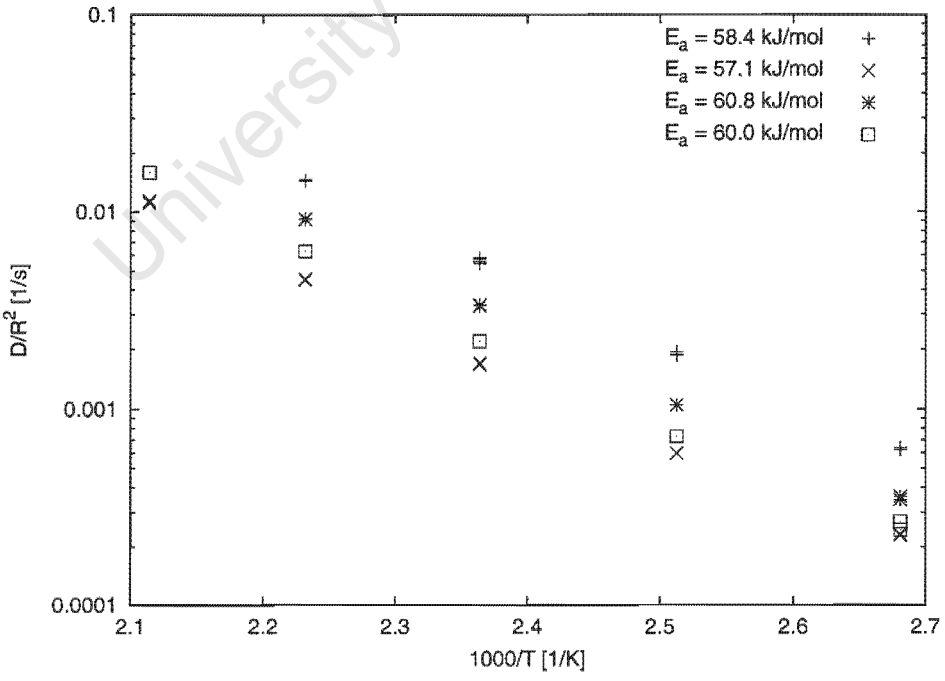

Figure 4.17: Arrhenius plot showing series of experiments where the sorbent was allowed to settle (lower two data sets) or was agitated (upper data) before packing.

are not necessarily useful. This may be simply demonstrated by the cyclohexane/ZSM-5 experiments shown in Figure 4.17; D/R^2 was obtained by fitting the standard model. (These data are for sample Z-L-0.5/W as in Chapter 7.) For the lower two sets of data, the sorbent was allowed to settle for a day on a vibrating surface and then the material at the top of the sample container packed in an attempt to obtain a narrow distribution of the largest material. For the upper two sets, the container was shaken before packing to get the widest distribution possible.

The measured diffusional time constants for the similarly packed samples differ by approximately a factor two, agreeing with the accuracy previously proposed for the ZLC technique (Brandani, 1998). There was no notable difference, visually, in the quality of the model fit between the settled and agitated samples. As can be seen by the data provided on the figure, the diffusional activation energies are in good agreement.

A further consideration is the source of the distribution, which will probably be well defined and relatively easy to measure for spherical particles (provided they may be considered isotropic) and well-formed single crystals (e.g. perfect ZSM-5 particles). Twinned zeolite crystals, however, would be more difficult to describe from this perspective, as indeed would any anisotropic sorbent particles, when the definition of the characteristic dimension in unclear (see Section 6.1.4), although an attempt has been made to elucidate effective geometry through the consideration of a shape factor (Loos et al., 2000).

4.3 Conclusions

Using an analytical model, the effect of a sorbent particle size distribution on the ZLC desorption curve has been demonstrated. A non-monosized sorbent introduces curvature into the normally linear long time asymptote (when plotted on a semilogarithmic scale). This is expected, as the slope of this linear region is given by the diffusional time constant, D/R^2. A size distribution introduces a range of values of R, and thus a varying slope.

When the standard model is used to interpret data obtained from a non-monosized sorbent sample, D/R^2 tends to be underpredicted while L is overpredicted. This systematic error increases with the distribution width and decreases with increasing L.

The model incorporating the size distribution is unsuited to modelling experimental data as it assumes a log-normal distribution. It is more advisable to use a sum of the standard model responses for each size fraction, weighted by volume fraction. If size distribution data are not available, the systematic error in D when using the standard model may be decreased by defining the average particle radius as the ratio of the volume of the sample to its surface area.

Chapter 5

Experimental Procedures and Apparatus

5.1 Unmodified sorbents

This section refers to the unmodified ZSM-5 samples as discussed in Chapter 6.

Characterisation data for sample A are available in the literature (Chen et al., 1988). The crystals are twinned and uniform in size and shape, with an average size of $9 \times 10 \times 12\,\mu$m, as shown by scanning electron microscopy (SEM). The size and shape were verified for this work using a light microscope. The equivalent spherical diameter of these particles is $12\,\mu$m, defined as being the diameter of a sphere with an identical volume to surface area ratio. The silicon to aluminium (Si/Al) ratio (on a molar basis) from the synthesis reagents was 51. This sample was provided by Professor Lovat V. C. Rees of Edinburgh University.

The crystals of sample B (Figure 5.1) were manufactured within the Catalysis Research Unit by Mrs Leslie Petrik. They are twinned and spherulitic in shape, with a mean size of $3\,\mu$m as given by SEM analysis. The micrographs indicate that the crystals are not monosized; the distributions were not quantified. The Si/Al ratio was approximately 100 for this catalyst.

Sample C was manufactured by Dr Rein Weber for his PhD thesis (Weber, 1998) with an Si/Al

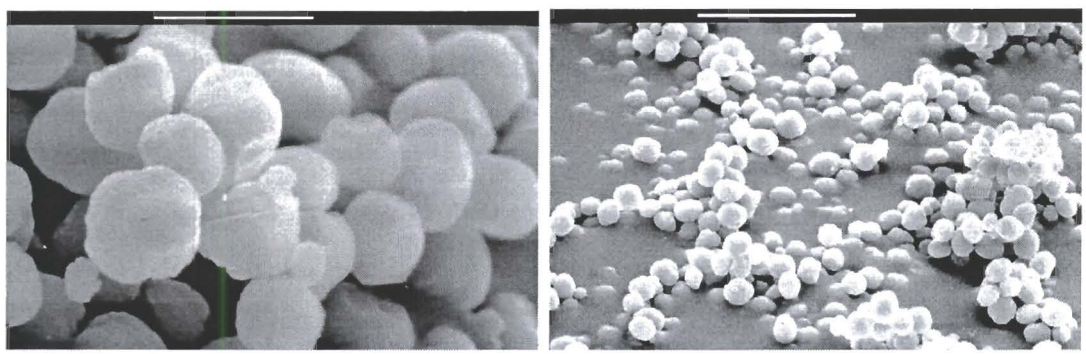

Figure 5.1: Scanning electron micrographs of sample B.

Table 5.1: Naming convention of silanised ZSM-5 samples used in this work.

Sample	Diluent	TEOS concentration (vol %)
Z-L-5/E	ethanol	5%
Z-L-5/H	*n*-hexane	5%
Z-L-5/W	water	5%
Z-L-0.5/W	water	0.5%
Z-L-100/-	–	100%
Z-L-100/-(60h)[a]	–	100%

[a](Exposed for 60 h rather than 21 h)

ratio of 34 as determined by atomic absorption analysis. Malvern particle size analysis showed two peaks on the size distribution plot at 2 and 4 μm; the former peak was the more significant however, and so the characteristic size was chosen to be 2 μm. No significant amounts of material were found smaller than 1 μm or larger than 10 μm. SEM shows the crystals to be of uneven shape; some agglomeration is evident. No significant deposits of amorphous material were observed on either the SEM's or the X-ray diffraction data (Weber, 1998).

All catalyst samples were used in the hydrogen ion-exchanged form.

5.2 Silanised sorbents

This section refers to the modified ZSM-5 samples as discussed in Chapter 7. This work will use the same naming convention as Weber (1998) for the different catalyst samples, as shown in Table 5.1.

5.2.1 Silanisation procedure

The liquid phase silanised ZSM-5 samples of Weber (1998) were used in this study, as was the parent sample of that work. Each modified sample was produced by contacting 2.5 g of the dry H form of the parent catalyst (sample C, described above) with tetraethoxy silane (TEOS) at ambient conditions. A total of 20 ml of TEOS mixed with water, ethanol or *n*-hexane, in varying concentrations, was used for the deposition. The mixture was stirred for 21 hours, then washed with water and dried.

5.3 Apparatus and experimental procedure

A schematic diagram of the ZLC apparatus is shown in Figure 5.2. The carrier gas is introduced as two streams: a high flow rate stream passing through mass flow controller (MFC) 1 and a low flow rate stream through another MFC (2). A bleed stream is controlled by a third MFC (7), the flow rate of which is set lower than that of 2. During the equilibration stage the three way valve (3) diverts the flow through 5 and the saturator. Some of this flow is bled off via 7, while a small amount mixes with the main stream, the dilution allowing very low concentrations.

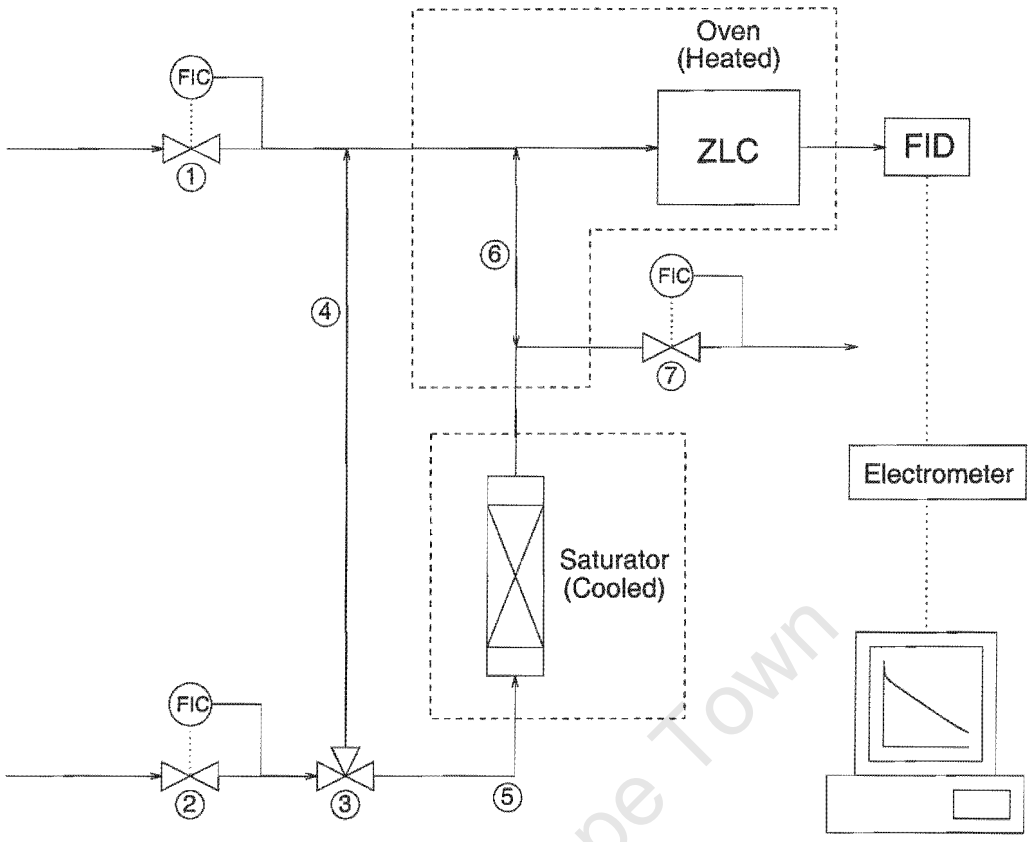

Figure 5.2: Flow sheet of the ZLC apparatus used in this work.

During the desorption stage of the experiment, the flow from 2 bypasses the saturator via 4 and the flow in 6 is reversed. This arrangement ensures that no residual sorbate can enter the carrier gas stream from 6 during the desorption. Care was taken to ensure that the equilibration times were greater than $0.5R^2/D$ to eliminate partial saturation effects (Brandani and Ruthven, 1996a) and that $L > 20$ to ensure zero length behaviour (see Chapter 3).

The saturator consisted of a jacketed glass tube containing chromosorb, which was saturated with cyclohexane. The cooling water temperature was monitored by means of a thermocouple placed directly into the water exiting the saturator jacket. Initial concentrations were inferred by assuming that the stream exiting the saturator was completely equilibrated, i.e. the cyclohexane partial pressure was equal to its vapour pressure (Daubert and Danner, 1991) at the temperature of the cooling water. A number of experiments were performed using a jacketed bubbling type saturator, which gave similar (within 15%) signals for the same settings of flow rate and coolant temperature.

The zeolite samples were packed into either a 1/8 in. o.d. (1.6 mm i.d.) or a 1/4 in. o.d. (4.6 mm i.d.) stainless steel tube approximately 45 mm in length. The large amounts of sample A needed to obtain a measurable response necessitated the wider tube for pressure drop reasons. The crystals were placed on a glass wool plug at the bottom of the tube, which was mounted vertically in a gas chromatograph (GC) oven with ca. 15 cm of 1/8 in. tubing leading directly to the flame ionisation detector (FID). The 1/4 in. tube contained a 25 μm frit at the entrance to counteract 'jet stream' behaviour.

The more usual packing method, i.e. placing the sorbent between two frits within a Swagelock union, was not used because of concerns about the flow pattern in the bed. It is very difficult to pack a homogeneous monolayer of powder and easy to introduce channeling. The second frit is inconvenient to seat without crushing the crystals while sealing the edges to prevent bypassing without blocking any of the flow area.

Approximately 2 mg of catalyst was used when working with samples B and C, while about 20 mg was required for sample A in order that L be small enough that the very important desorption curve tail not lie at too low a concentration to be reasonably measurable. Various masses of samples A and B were measured with consistent results. In addition, sample B was tested in the 1/4 in. tube, with and without a bed of inert quartz particles preceding the sorbent bed, in order to check that the method of packing did not have a significant effect on the results. For all of the sample B experiments, the measured diffusivities were within the factor 2 accuracy limit that has been suggested for the ZLC method (Brandani, 1998).

No particular precautions were taken to ensure that pressure drop through the catalyst bed was insignificant. Consistent experimental behaviour for various packing configurations and masses of sorbent were taken as an indirect indication that the fluid phase could be treated as being incompressible. Gauge pressure upstream of the mass flow controllers was kept constant at 1.5 bar.

The FID response data were collected on a PC using an APC50 data acquisition board (from Intelec Systems) with a high resolution (24 bit) analogue to digital converter. Between 400 and 4000 data points were collected per run at frequencies of 1–10 samples per second, depending on the length of the experiment. Approximately 10 seconds of data was collected for each run prior to commencing the desorption and averaged in order to determine the initial concentration. The baseline was determined prior to each run, and care was taken to ensure that the signal returned to this value at the end of the experiment.

Sample blank experiments, using cyclohexane as the sorbent, are shown in Figure 5.3 at a range of temperatures; the data collection for obtaining the initial signal are shown as well. It may be seen that the normalised concentration drops the first two orders of magnitude very rapidly (within two seconds), while the subsequent decrease to $C/C_0 = 10^{-3}$ requires about 5 seconds more. This is a result of extraneous adsorption on the metal tubing and some dead zones, but the effect is negligible. The results are somewhat better at the higher temperatures (since adsorption effects are minimised), but this effect is again negligible.

5.4 Data analysis

The standard ZLC model in spherical coordinates (Equation 2.16) was used to analyse the experimental desorption curves. All points in the concentration range $0.001 \leq C/C_0 \leq 1$ were considered in the curve fitting routine. The objective function for minimisation

$$\text{Objective function} = \sum_{n=1}^{N} \left[\ln\left(\frac{C}{C_0}\right)_{i,\text{data}} - \ln\left(\frac{C}{C_0}\right)_{i,\text{model}} \right]^2 \left[1 + \frac{9i}{N}\right] \tag{5.1}$$

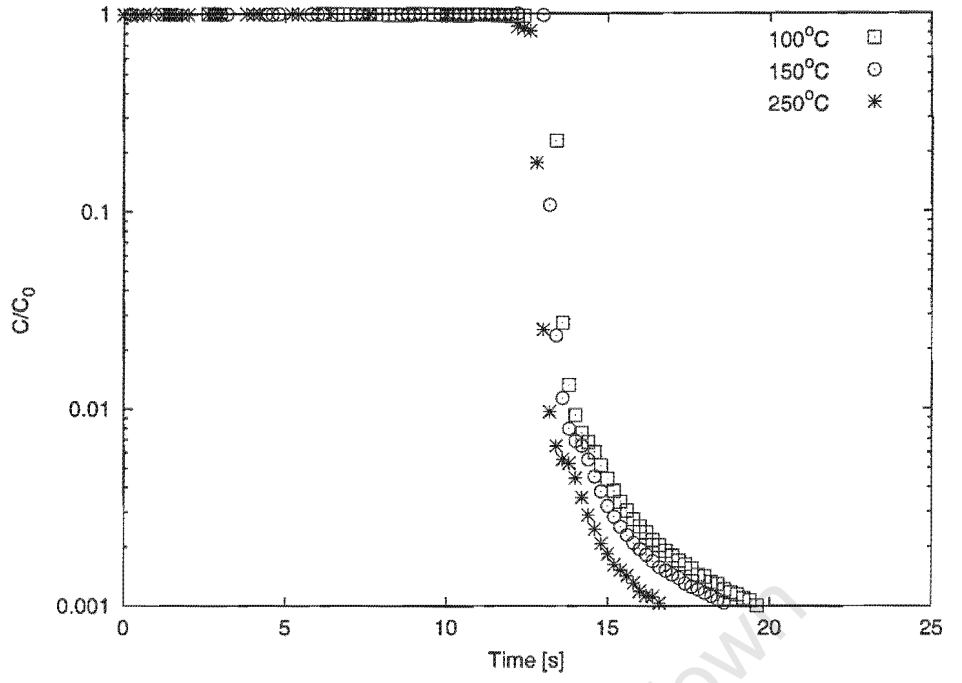

Figure 5.3: Blank experiments (i.e. in the absence of sorbent) performed using an 1/8" diameter reactor at various temperatures as shown.

was chosen to simulate the long time solution method (see Section 2.3.1) by weighting the long time region of the curve. It should be remembered that the long time method involves fitting a straight line to the tail of the desorption curve as plotted on semilogarithmic axes. The use of logarithms in the objective function serves to simulate these axes, while the weighting factor biases the fit to the latter part of the experiment.

The fitting routine was implemented in Fortran77. The programme code, as well as a sample data file and tables of experimental results are shown in Appendices B and C.

Chapter 6

The Diffusion of Cyclohexane in Unmodified ZSM-5

This chapter presents the results of an experimental program examining the intracrystalline diffusion of cyclohexane in three samples of ZSM-5 of varying size and morphology. In the course of the work, some apparent deviations of the data from the standard model were observed, which were influenced by the initial sorbate concentration during the equilibration stage of the experiment. The sorption equilibrium for the system can be described with a Langmuir adsorption isotherm (Cavalcante and Ruthven, 1995a). An attempt is made to explain these deviations from the simple theory, which do not appear to have severely affected the accuracy or validity of the measured diffusion coefficients.

6.1 Results and discussion

It is seen from Figure 6.1 that the diffusion coefficients for the three samples (summarised in Table 6.1) compare well with one another and also with previously published data. The temperature dependence of the data sets are well described by the Arrhenius model, as seen in Figure 6.2. The activation energies differ by about 5%, with acceptable experimental error; these values are consistent with literature data.

It would appear that the data fall into two distinct groups: this work and the results of Cavalcante and Ruthven (1995b) are about an order of magnitude greater than the diffusivities obtained by Chon and Park (1988) and Xiao and Wei (1992). There is better agreement in the activation energies. This separation is not a result of the experimental technique used (Cavalcante and Ruthven (1995b) used gravimetric uptake and confirmed the data using ZLC, while Chon and Park (1988) used a volumetric uptake method) nor is it a consequence of aluminium content, as can be seen in Table 6.1. Chon and Park (1988), in fact, used three sorbent samples of different Al content and report consistent results.

Figures 6.3–6.5 show typical desorption curves for the different sorbents. The blank run (i.e. in the absence of sorbent) shown in Figure 6 indicates that extraneous adsorption and dead volume effects were minimal. The model (Equation 2.16) fits the experimental data well, particularly in the case of the well-defined crystals of sample A.

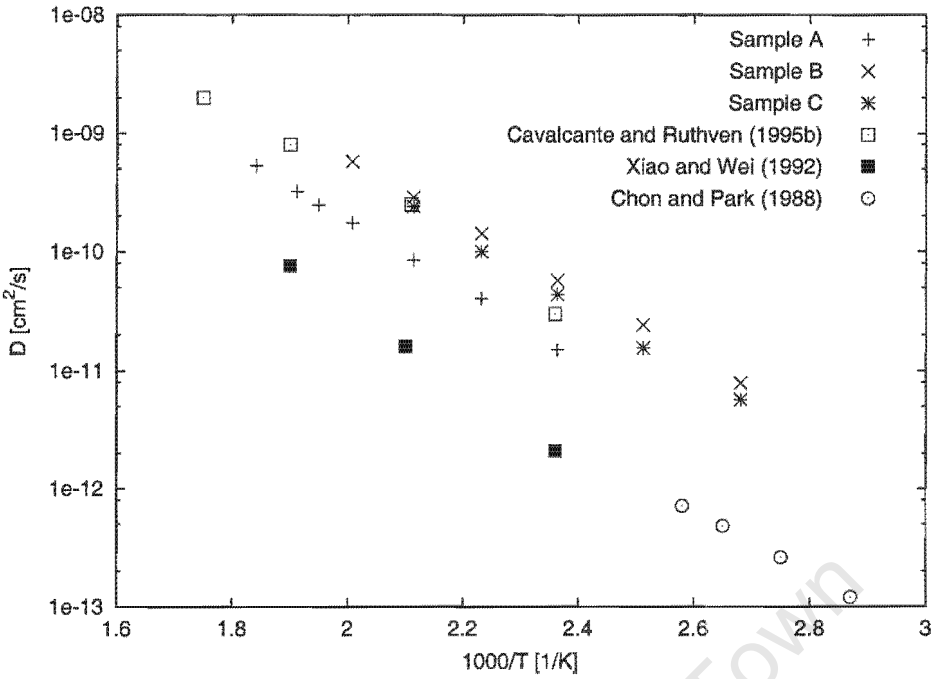

Figure 6.1: Temperature dependence of the diffusivity of cyclohexane in ZSM-5 with literature data shown for reference. Experimental data at the same temperatures have been averaged.

Table 6.1: Summary of measured diffusivities and diffusional activation energies.

Sample	Si/Al	Temp [°C]	D [cm^2/s]	E_a [kJ/mol]
A ($R = 12\,\mu$m)	51	150	1.49×10^{-11}	55.7
		175	4.03×10^{-11}	
		200	8.48×10^{-11}	
		225	1.74×10^{-10}	
		240	2.47×10^{-10}	
		250	3.22×10^{-10}	
		270	5.29×10^{-10}	
B ($R = 3\,\mu$m)	100	100	7.88×10^{-12}	52.8
		125	2.42×10^{-11}	
		150	5.71×10^{-11}	
		175	1.42×10^{-10}	
		200	2.88×10^{-10}	
		225	5.76×10^{-10}	
C ($R = 2\,\mu$m)	34	100	5.68×10^{-12}	54.9
		125	1.55×10^{-11}	
		150	4.37×10^{-11}	
		175	9.97×10^{-11}	
		200	2.40×10^{-10}	
Cavalcante and Ruthven (1995b)	silicalite			53.6
Xiao and Wei (1992)	110			64.9
Chon and Park (1988)	106–403			50.6

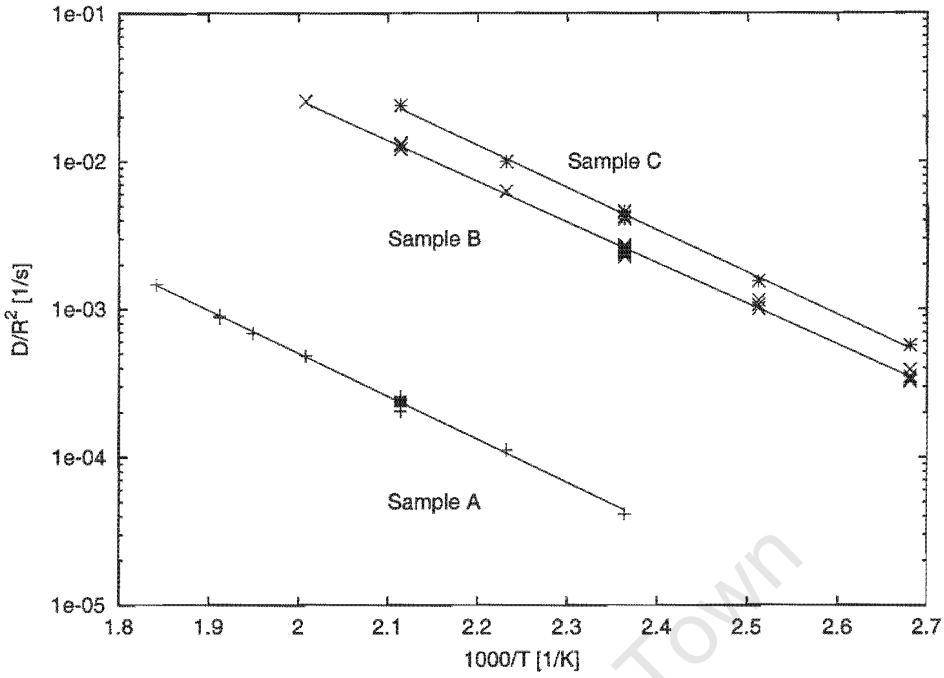

Figure 6.2: Arrhenius plots of the diffusional time constants measured for the three samples with best-fit lines. Full data sets are shown.

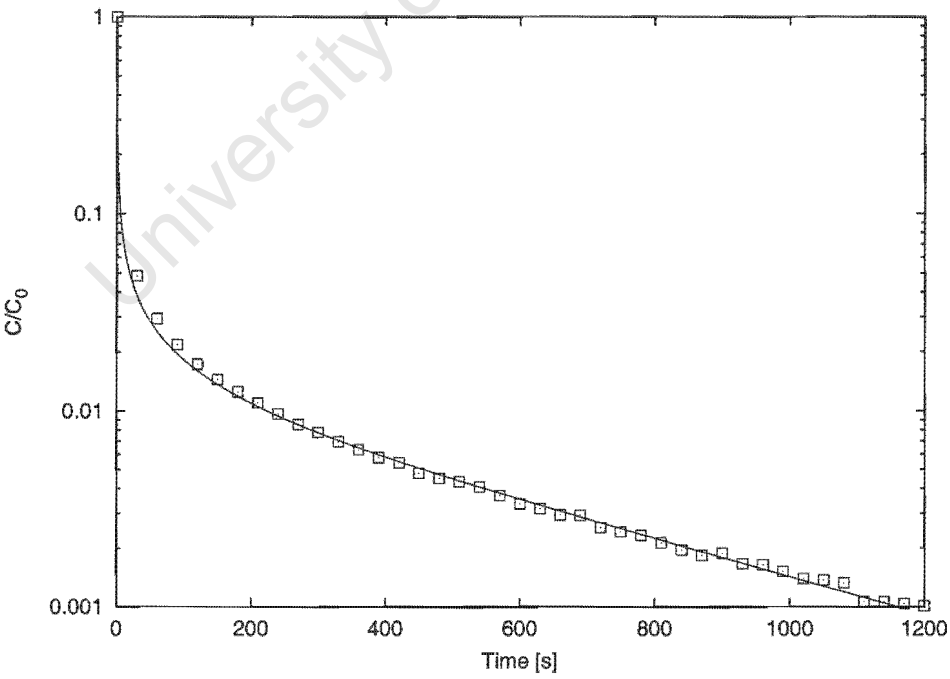

Figure 6.3: Representative desorption curve for sample A with model fit. Experimental conditions: $T = 200$℃, $F = 34.7\,\mathrm{ml/min}$, $C_0 = 395\,\mathrm{Pa}$, $m_s = 22\,\mathrm{mg}$. Fitted model parameters: $D/R^2 = 2.31 \times 10^{-4}\,/\mathrm{s}$, $L = 150$.

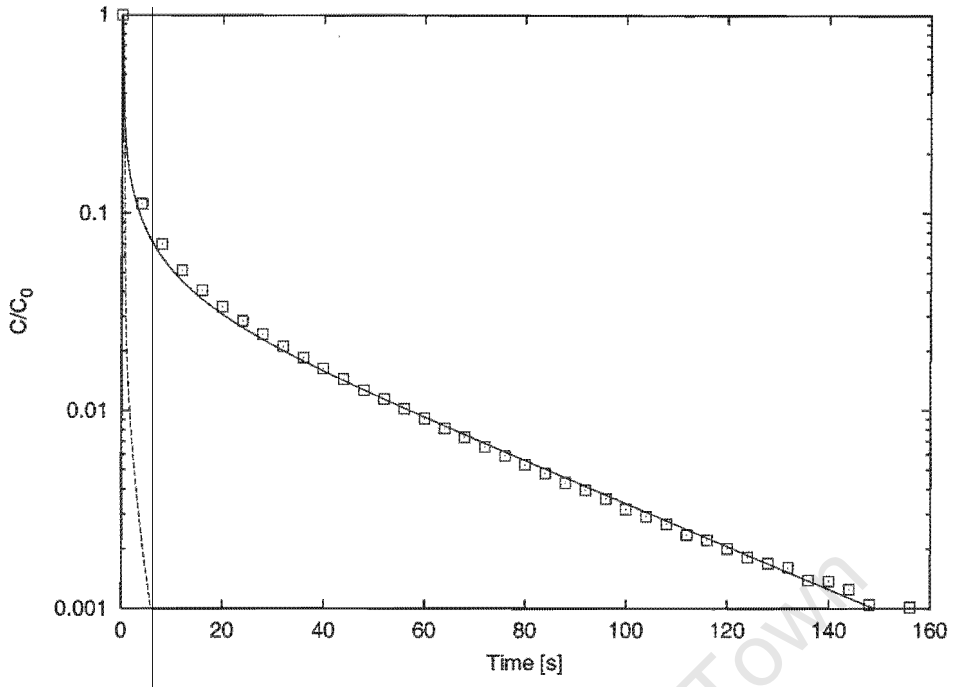

Figure 6.4: Representative desorption curve for sample B with model fit. Experimental conditions: $T = 150℃$, $F = 68.2\,\mathrm{ml/min}$, $C_0 = 495\,\mathrm{Pa}$, $m_s = 2\,\mathrm{mg}$. Fitted model parameters: $D/R^2 = 2.61 \times 10^{-3}\,/\mathrm{s}$, $L = 50.4$. The dashed line indicates a blank run (i.e. in the absence of sorbent) performed at similar conditions.

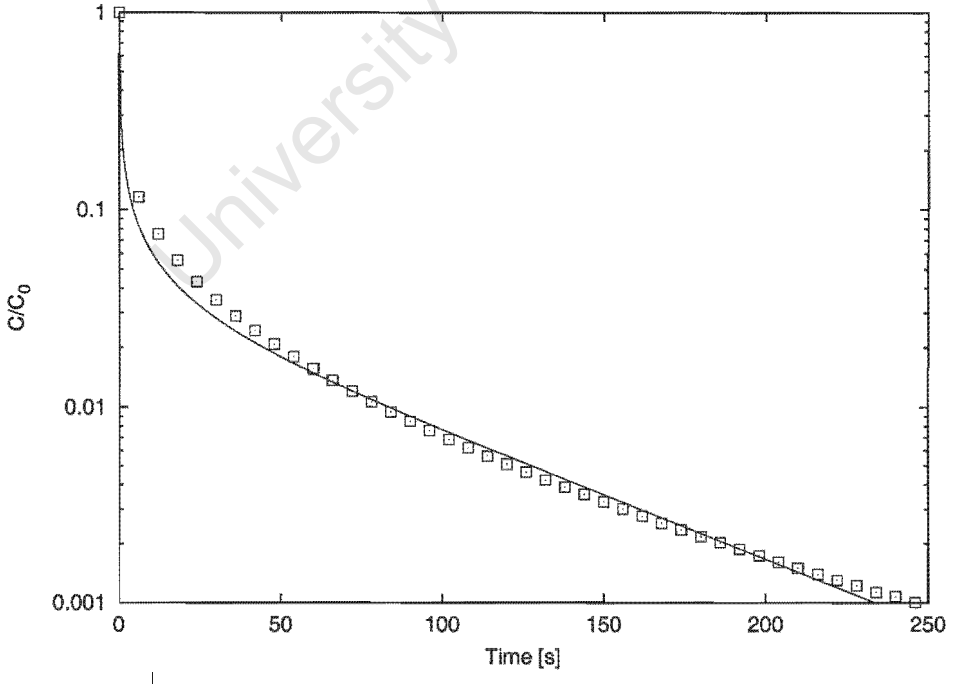

Figure 6.5: Representative desorption curve for sample C with model fit. Experimental conditions: $T = 125℃$, $F = 87.5\,\mathrm{ml/min}$, $C_0 = 191\,\mathrm{Pa}$, $m_s = 2\,\mathrm{mg}$. Fitted model parameters: $D/R^2 = 1.55 \times 10^{-3}\,/\mathrm{s}$, $L = 61.0$.

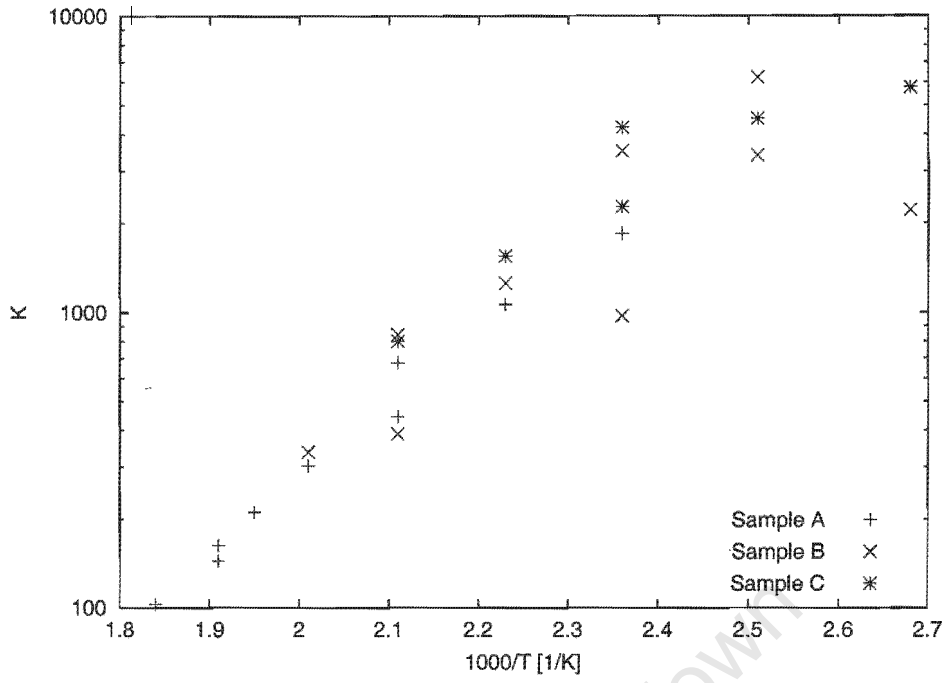

Figure 6.6: Temperature dependence of the Henry adsorption constant for cyclohexane on ZSM-5 as measured for the three different samples. Pairs of points show the upper and lower limits of the data.

Figure 6.6 shows a van't Hoff plot for the dimensionless Henry adsorption constants. While the data show, qualitatively, consistency and the correct temperature dependence, there is large scatter, especially in the case of sample B and the van't Hoff plot is not linear. It has been shown in Chapter 2 that several factors, while having only a small influence on the measured diffusional time constant, have a far greater effect on the determination of L, and thus K.

The enthalpy change on adsorption was calculated from the van't Hoff equation (Ruthven, 1984) using the less scattered data of sample A, seen in Figure 6.7. When the two lowest temperature points are disregarded, on the admittedly questionable basis that they are the most likely to be underpredicted because of isotherm nonlinearity effects (Brandani, 1998), one obtains $-\Delta H_a = 57.3\,\mathrm{kJ/mol}$. This value is in reasonable agreement with previous gravimetric data (Cavalcante and Ruthven, 1995a): $-\Delta H_a = 63.2\,\mathrm{kJ/mol}$. It should be noted, however, that the adsorption constants reported in that work, using a more accurate technique, are significantly greater than those measured here.

According to Equation 2.15, a plot of L versus flow rate should be linear, passing through the origin, if all other variables are held constant. Figures 6.8 and 6.9, however, show that this is not the case at the lower temperature, while the high temperature graph also seems to indicate a plateauing at the higher flow rates, although not nearly so marked. Similar incorrect behaviour has been measured for the sorption of n-hexane in silicalite-1 and ferrierite (Voogd et al., 1991), although insufficient data are presented in that work to draw any meaningful comparison on this point.

There is also a concentration effect at the lower temperature (L tends to be higher at the same flow rate as concentration increases), which is less marked at 200°C. Figure 6.10 shows an apparent

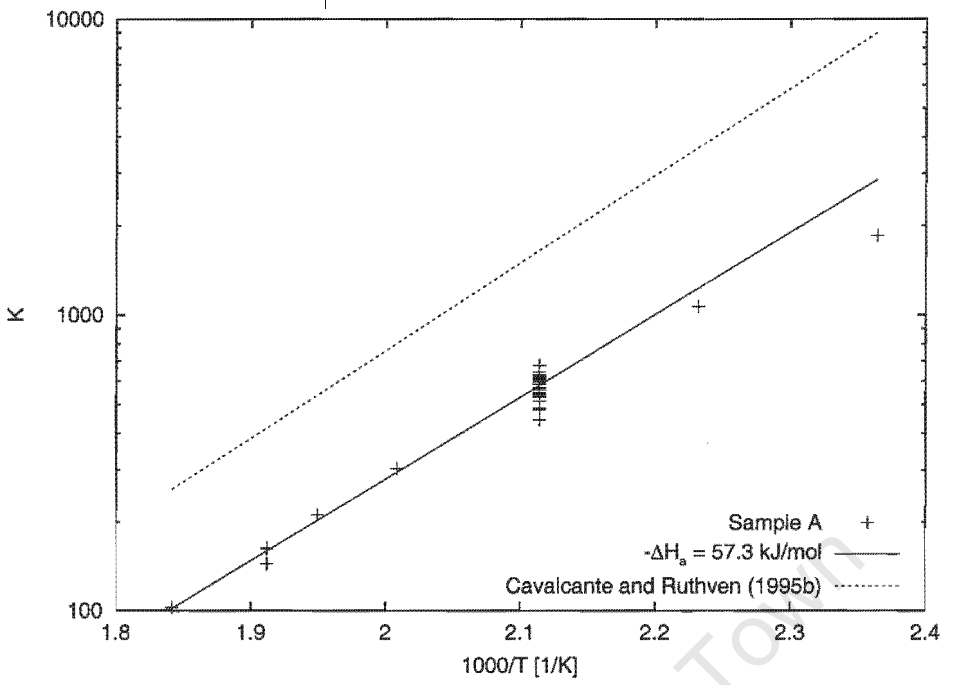

Figure 6.7: Adsorption constants measured for sample A, with the van't Hoff equation fitted to all but the two lower temperature points. The full data set is shown. Literature data are shown for comparison.

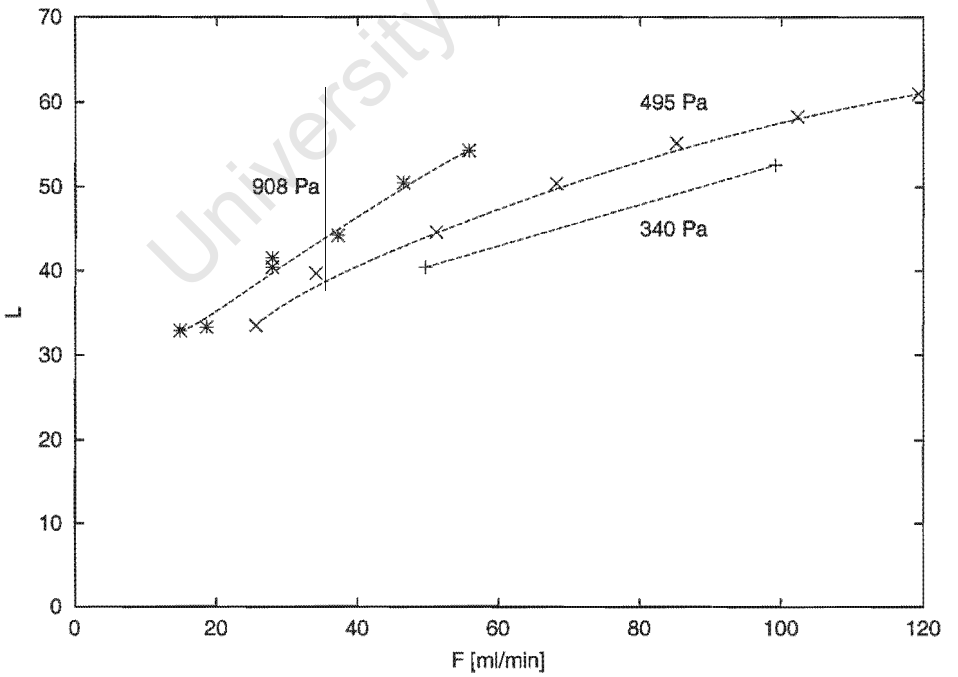

Figure 6.8: Dependence of L on flow rate for sample B at 150°C, measured at different initial sorbate concentration as indicated, in a 1/8 in. tube. Lines are to aid the eye.

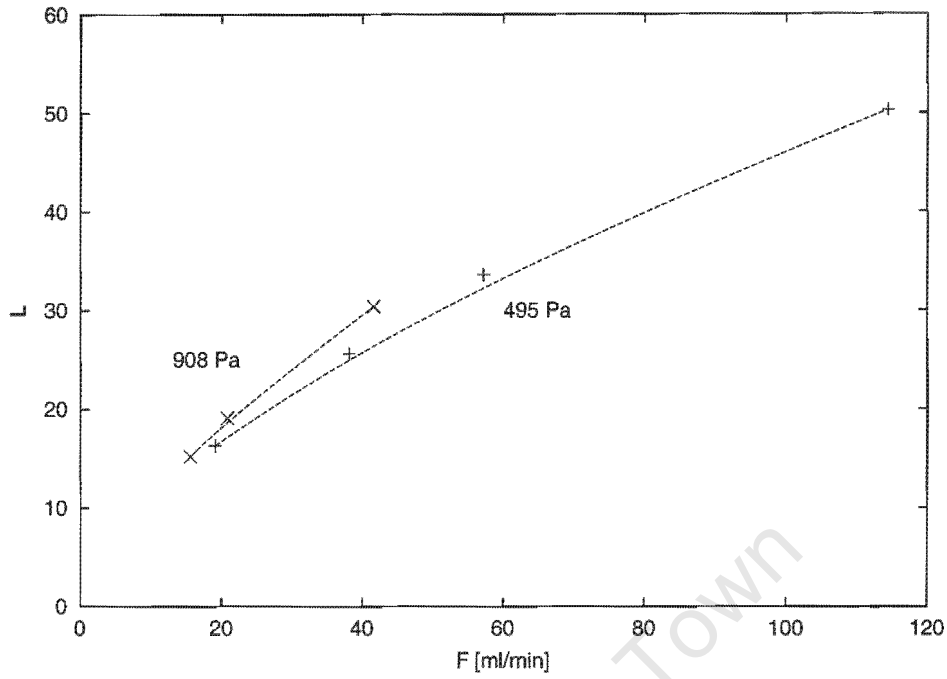

Figure 6.9: Dependence of L on flow rate for sample B at 200℃, measured at different initial sorbate concentration as indicated, in a 1/8 in. tube. Lines are to aid the eye.

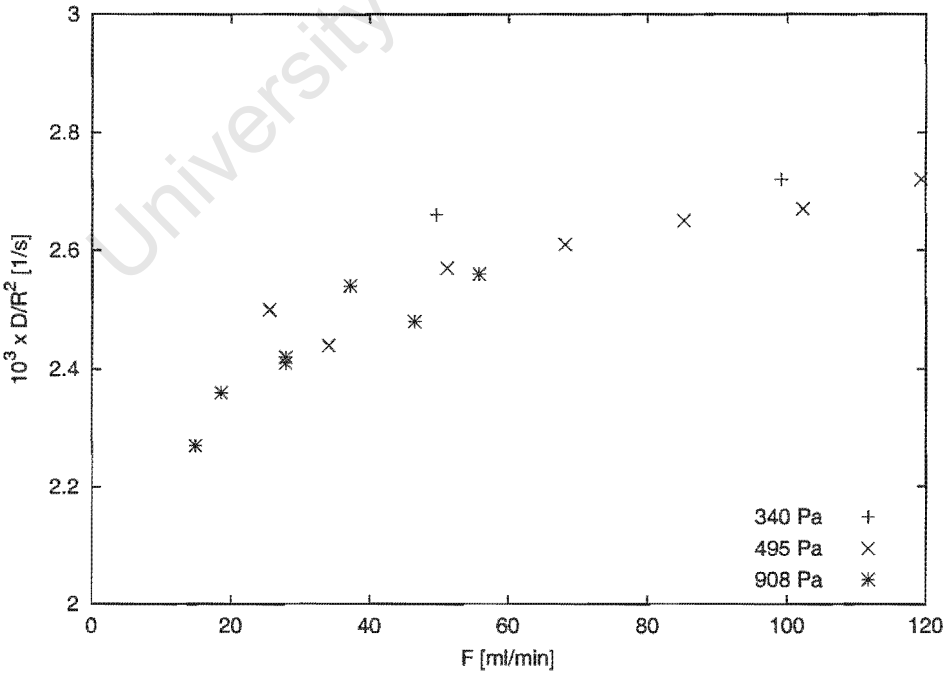

Figure 6.10: Dependence of D/R^2 on flow rate for sample B at 150℃, measured at different initial sorbate concentrations, as indicated, in a 1/8 in. tube.

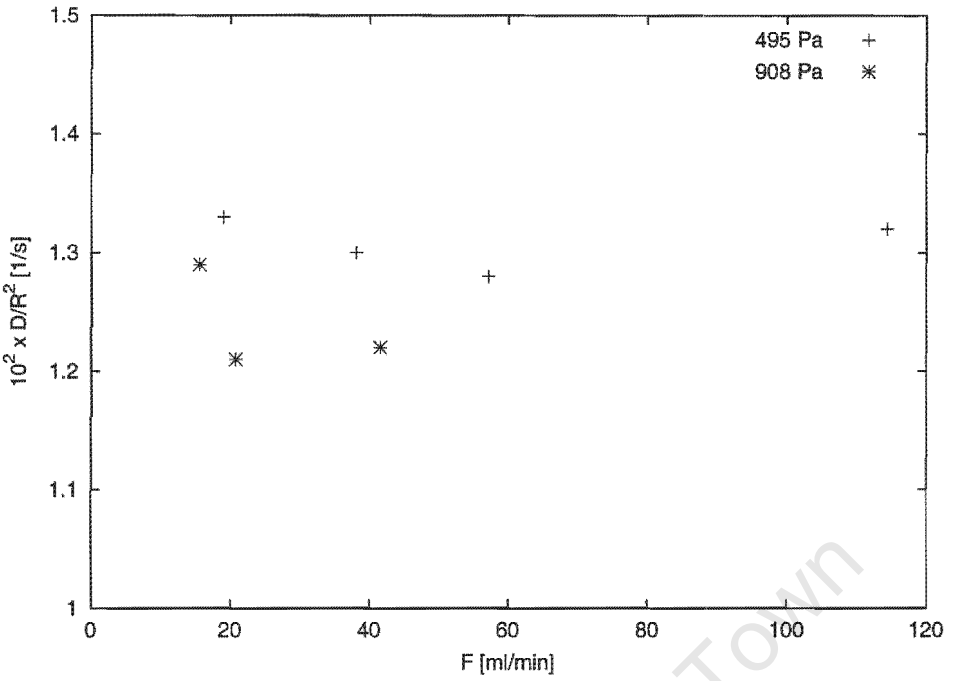

Figure 6.11: Dependence of D/R^2 on flow rate for sample B at 200℃, measured at different initial sorbate concentrations, as indicated, in a 1/8 in. tube.

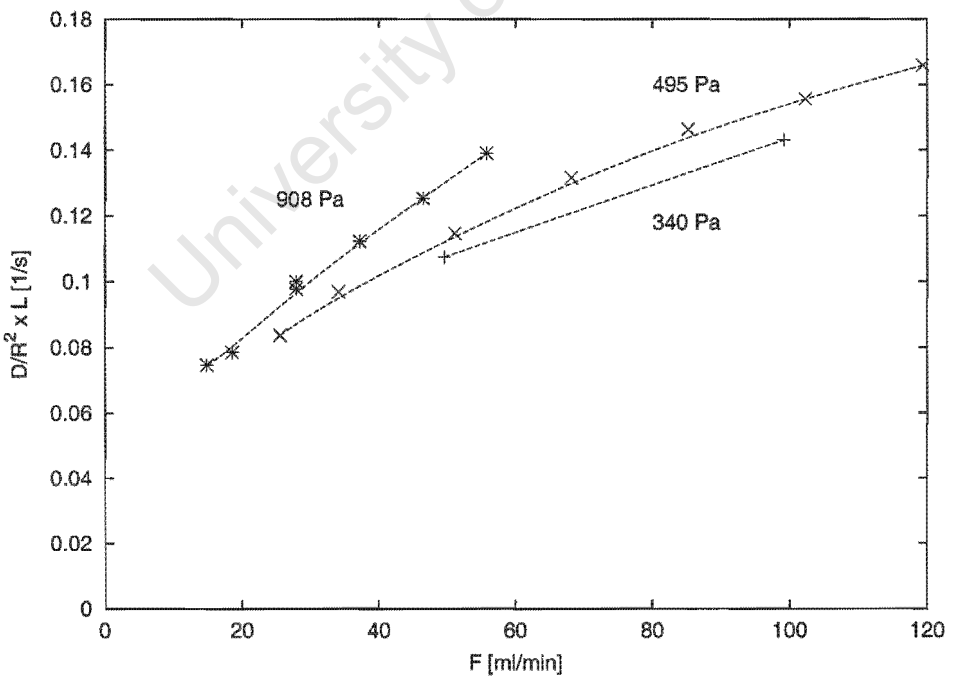

Figure 6.12: Dependence of $D/R^2 \times L$ on flow rate for sample B at 150℃for the same data as shown in Figures 6.8 and 6.10 to show the apparent dependence of K on flow rate. Lines are to aid the eye.

increase in the diffusional time constant with flow rate at 150°C, which is not seen at 200°C(Figure 6.11). This latter effect cannot, however, account for the nonlinear behaviour of L with flow rate, as can be seen in Figure 6.12. Here, the flow rate dependence of the diffusional time constant has been accounted for, and the graph still clearly shows the incorrect behaviour that implies that the adsorption constant K is a function of the purge rate.

This behaviour in L and D/R^2 naturally calls the applicability of the diffusion model into question, and further analysis is therefore merited. There are two phenomena that must be investigated, *viz.* the effects of flow rate (external mass transfer) and initial concentration (the effect of a nonlinear adsorption isotherm). The presence of external film heat transfer is an additional possibility, because the measured diffusivity would probably appear to increase with flow rate as a result of the improved thermal transport (desorption being an endothermic process). However, both it and an inhomogeneous flow pattern within the bed were considered unlikely because of the agreement in the diffusivities for the experiments performed in different sized tubes and with a preceding bed of quartz particles. In the former case, the inert packing should act as a heat source and in the latter as a flow disperser. It has been shown by Brandani et al. (1998) and Silva et al. (2001) that the intrusion of external heat transfer effects for systems with small particles like zeolite crystals is highly unlikely; the effect should only manifest itself for larger particles (i.e. pellets).

6.1.1 External mass transfer

Intuitively, one may expect the measured diffusivity to vary with flow rate if external mass transfer were significant. The desorption rate would increase as an increasing flow rate decreased the thickness of the stagnant boundary layer. It has been shown in Section 2.4, however, that the shape of the desorption curve is practically indistinguishable from that for pure intracrystalline diffusion. The modified definition of L may result in an initial eigenvalue lower than would appear to be the case if using the standard model, thus causing the diffusion coefficient to be underestimated as a result of the overestimation of β_1. The dependence of this effect on flow rate would, however, be nontrivial and the phenomenon would be difficult to detect.

For a ZLC experiment that is unaffected by external mass transfer effects, it is necessary that

$$\frac{FR^2}{3V_s} \ll D_m \tag{6.1}$$

Using the Fuller-Schettler-Giddings correlation (Perry et al., 1997), D_m was estimated to be approximately 0.4–0.8 cm^2/s for the range of conditions used, while the left-hand term was of the order 10^{-7}–10^{-8} cm^2/s. These results indicate that the effect of external mass transfer may be neglected for the experiments presented here.

6.1.2 Particle size distribution effects

The dependencies on flow rate shown in Figures 6.8 and 6.10 bear a resemblance to those shown in Figures 4.7 and 4.3, which indicate the behaviour of L and D/R^2 if a sample showing a size

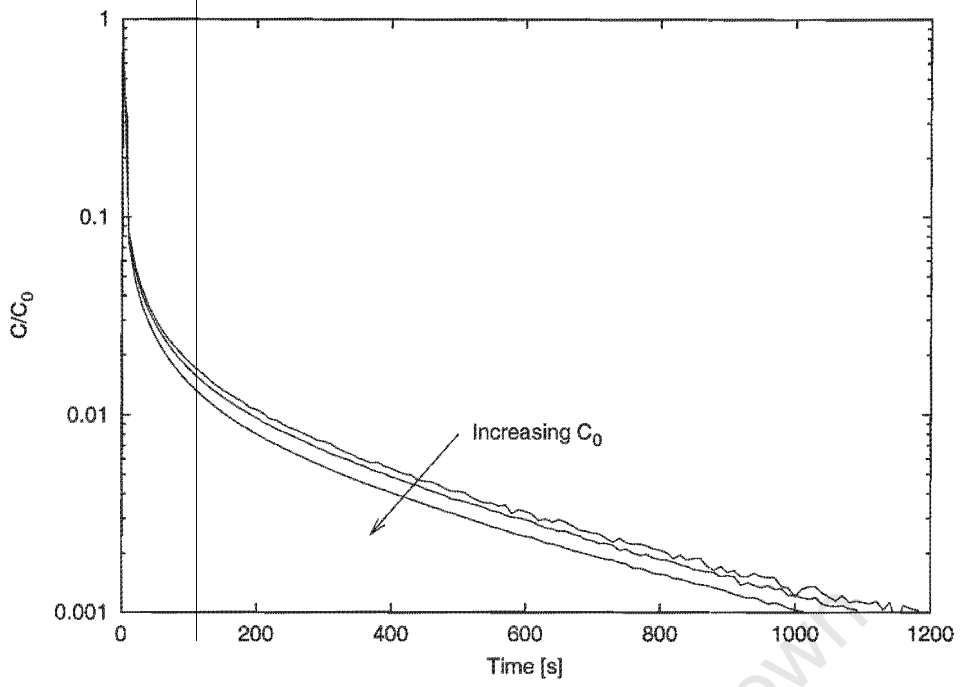

Figure 6.13: Desorption curves for sample A at different initial concentrations ($C_0 = 263$, 1468 and 2855 Pa). Other experimental conditions: $T = 150$℃, $F = 52.0$ ml/min, $m_s = 22$ mg.

distribution were analysed using the standard model. This may indicate that the catalyst samples used here are not monosized and the effect is indeed being seen. Inspection of the desorption curves (Figures 6.3, 6.4 and 6.5) shows that, certainly in the case of Sample C, the curvature of the long time region appears to confirm the presence of a significant size distribution. The effect is not obvious for sample A, but experiments for this sample were generally performed at large values of L, in which case most of the curvature will be below the considered concentration threshold of $C/C_0 = 10^{-3}$.

6.1.3 Nonlinear adsorption isotherm effects

If the adsorption behaviour of the system may be described by a Langmuir isotherm, the resulting ZLC desorption curve largely retains the shape of that for a Henry isotherm, except that L tends to increase with initial loading, as does the time required for the characteristic long time linear asymptote to be attained (Brandani, 1998), as described in detail in Section 2.7. At least the former effect may be seen in Figure 6.13; the latter is unlikely to be readily apparent in experimental curves.

Equation 2.50 has been proposed for the long time asymptote of the desorption curve for Langmuir systems (Brandani, 1998). Making the large L approximation and letting L_{app} be the apparent value of L obtained by fitting the linear isotherm model (Equation 2.19) to the nonlinear case, one obtains

$$\ln L_{app} = L - \ln(1-\lambda) + \frac{\lambda}{2} \tag{6.2}$$

This approximation is quite accurate for $L > 10$, even for initial loadings as high as 80% of the sorbent's saturation capacity, as may be seen by inspecting the sample desorption curves given in

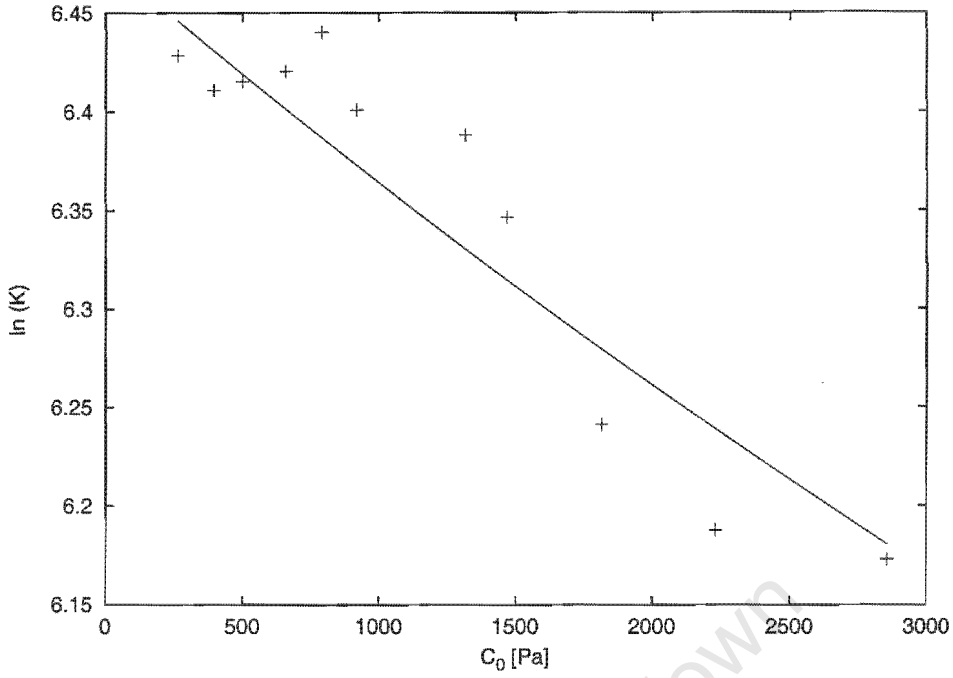

Figure 6.14: Plot to extract Langmuir isotherm parameters from apparent Henry constants. Data are for 22 mg of sample A at 200°C and 52 ml/min.

Brandani (1998).

Equation 6.2 may be rewritten to give, for the apparent adsorption constant K_{app} in terms of the initial gas phase concentration, assuming all other variables are constant, that

$$\ln K_{app} = \ln K - \ln(1 + bC_0) - \frac{1}{2}\left(\frac{bC_0}{1 + bC_0}\right) \tag{6.3}$$

which suggests it is possible to obtain the 'true' Henry constant as well as the adsorption capacity ($q_s = K/b$) by comparing this equation to the variation in the measured adsorption constant with the initial concentration.

This exercise has been performed using a set of data for sample A, with all parameters other than the initial concentration held constant, as seen in Figure 6.14. Qualitatively, the data show the correct behaviour, but the fit is not convincing and gives the saturation capacity as 9.1%(g/g), compared to the previously reported value of 5.6%(g/g) (Cavalcante and Ruthven, 1995a). The limiting Henry constant is 662, as compared with the corresponding literature value of 1240 ($bq_s = 0.20\%$(g/g)/Torr).

Figure 6.15 plots the diffusional time constants versus initial concentration for the same experiments referred to above and shows no discernible trend with concentration. This supports the idea that the low concentration tail of the desorption curve, from which the diffusion data are obtained, generally falls within the linear region of the adsorption isotherm, in which the Darken correction factor approaches unity. Numerical analysis has confirmed that desorption curves for various initial loadings tail with the same slope (Brandani, 1998).

The same numerical analysis has also shown that, if the initial sorbate loading is high, the

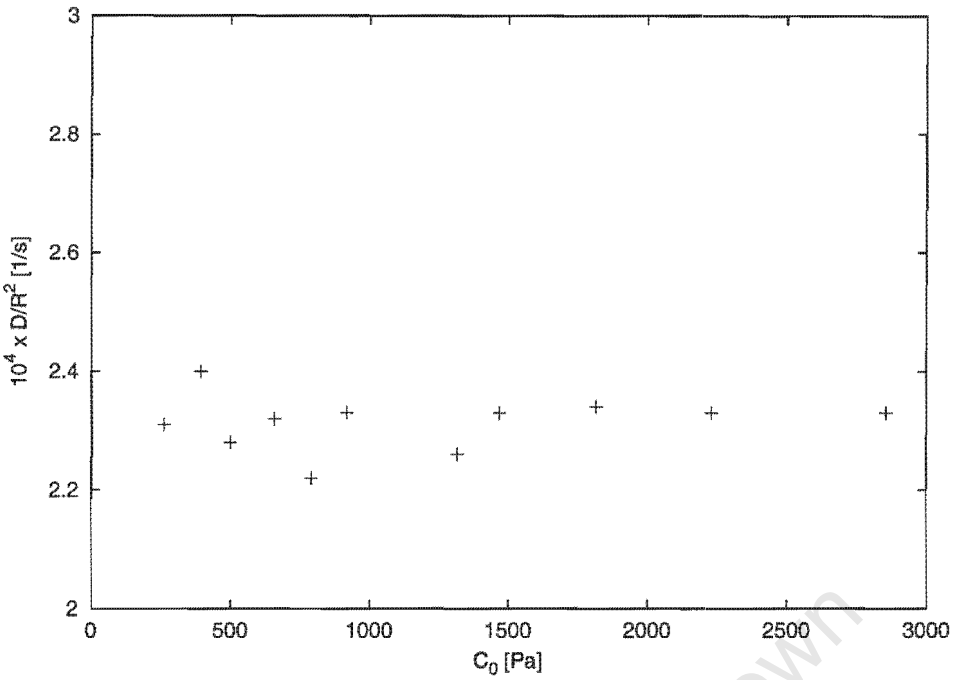

Figure 6.15: Diffusional time constant as a function of the initial concentration for the same experiments as those shown in Figure 6.14. Data are for 22 mg of sample A at 200℃ and 52 ml/min.

desorption curve takes longer to approach the linear asymptote that in the Henry's Law case. It is thus possible to overestimate D/R^2 and underestimate L by mistakenly applying the long time solution method to the incorrect region of the curve. In this work, with the model being applied to data between $0.001 \leq C/C_0 \leq 1$, it is plausible that, especially when working with large L, too little of the true linear region is 'seen' by the curve-fitting routine. This would therefore have a similar effect, which would provide a reasonable explanation of both the nonlinear behaviour of L with respect to flow rate, especially at low temperatures, and the apparent dependence of D/R^2 on flow rate at low temperature. The understimation of L for large L provides a reasonable qualitative explanation for the plateauing of the paramater at high flow rates

It is thus clear that the standard ZLC model does not adequately describe the system, which appears to be somewhat better described by an analysis incorporating the presence of a Langmuir-shaped adsorption isotherm. Even this, however, does not explain all the deviations from the simple theory. There is enough consistency in the diffusivity data, however, to conclude that these are probably correct.

6.1.4 Lack of variation of diffusivity with crystal size

The agreement in the diffusion coefficients measured in this work using sorbent samples of different size and morphology is perhaps somewhat surprising. Previous work has suggested, as with other systems, that the diffusion of cyclohexane in small ZSM-5 crystals is slower than that in larger particles (Cavalcante and Ruthven, 1995b). In some systems, e.g. CO_2/4A, the discrepancy can be two or three orders of magnitude (Kärger and Ruthven, 1992). The agreement between the activation

energies is a far more common and reassuring result.

While the small particles may be well described by a diffusion model with spherical symmetry, this is highly unlikely for the larger crystals. It is well established that diffusion in ZSM-5 occurs mainly through the straight channels (Cavalcante and Ruthven, 1995b; Chon and Park, 1988; Voogd et al., 1991; Haag et al., 1982), particularly in the case of large sorbate molecules (Rees, 1994). The orientation of these channels in an intergrowth, however, remains unclear although it has been suggested that, in twinned crystals, the straight and sinusoidal channels probably alternate (Voogd et al., 1991). Even for spherical crystals, the physical geometry may bear little relation to the symmetry of the diffusion process because of anisotropy effects. An imperfect pore system may create dead-ends and shortcuts within the crystal, changing the effective geometry as well as the diffusive path length. These latter variations in intracrystalline tortuosity between samples will cause significant differences because macroscopic experiments can measure only the diffusional time constant D/R^2, from which the diffusivity is inferred by assuming a path length; any error in the path length is magnified by the square term.

On the other hand, the small crystals usually referred to in the literature are of a commercial origin. These particles are generally subjected to severe hydrothermal treatment and it is indeed this treatment which is used as the basis for explaining the difference between these are the larger, laboratory synthesised samples. The results presented here could support that view, because both the smaller zeolite samples used in this work were laboratory synthesised with no such hydrothermal treatment.

6.2 Conclusions

The sorption behaviour of cyclohexane has been investigated in three samples of ZSM-5, differing in both size and morphology: fairly large, uniform and twinned crystals and small spherical and irregular particles. In spite of uncertainty over the correct geometry and diffusive path length, as well as apparent model inconsistency, the samples give very similar results that agree well with previously published data. Flow rate and initial concentration did not significantly affect the measured diffusivities. The inconsistency in the adsorption related parameter L obtained from the standard linear adsorption isotherm diffusion model can be at least partly explained by the presence of a Langmuir type isotherm and a distribution of crystal sizes.

Chapter 7

Diffusion in Silanised ZSM-5

The deposition of alkoxysilanes to increase the shape selectivity of zeolite catalysts has been extensively studied (Hibino et al., 1989, 1993; Kim et al., 1996; Čejka et al., 1996; Röger et al., 1998; Weber et al., 2000). While many authors believe that the predominant reason for this change in shape selectivity is a transport rate reduction due to narrowing of the pore entrances (Kim et al., 1996), some believe that blockage of the pore mouths is a factor (Weber et al., 2000; Röger et al., 2001). Some rudimentary diffusion studies have been carried out on these silanised catalysts, but not in sufficient quantitative detail to draw any other conclusion than that the transport rate had indeed decreased after silanisation (Čejka et al., 1996). Theoretical studies using stochastic models on finite grids have also been performed to determine the behaviour of a sorbate with surface modifications (Theodorou and Wei, 1983), but the two dimensional nature of the theoretical systems causes quantitative extrapolation to experimental systems to be questionable.

This chapter presents the results of a detailed study into the diffusion characteristics of cyclohexane in ZSM-5 modified by the liquid phase deposition of tetraethoxy silane (TEOS). (These results may be compared to those presented in Chapter 6 for unmodified ZSM-5. The parent sample of this section is Sample C of that chapter.) Mathematical models speculating the system behaviour are developed, indicating possible trends that are looked for in the experimental data.

Cyclohexane should be a good choice to detect pore mouth narrowing effects, since its size is similar to that of the ZSM-5 pores, yet it is flexible and should thus be able to enter the pore mouths if they are narrowed. The distortion required to pass through a narrowed pore mouth should reveal itself as a surface barrier type phenomenon.

7.1 Surface barrier analysis for the ZLC

Pore mouth narrowing effects are represented by using a surface barrier model (Kärger and Ruthven, 1992), i.e. we assume a first order desorption rate process at the surface of the catalyst particle:

$$\text{rate} = k_s(\text{area})(q|_R - KC) \tag{7.1}$$

The barrier rate constant k_s is the ratio of the effective diffusivity of the solid surface 'film' and its thickness (Kärger and Ruthven, 1992).

The boundary condition for Fick's Law at the particle surface is then

$$FC = \frac{3k_s V_s}{R}\left(q|_R - KC\right) \tag{7.2}$$

or, in dimensionless form,

$$\left(\frac{D}{k_s R} + \frac{1}{L}\right)\left.\frac{\partial U}{\partial X}\right|_1 + U|_1 = 0 \tag{7.3}$$

This may be compared to the corresponding condition for the standard ZLC model, i.e.

$$\frac{1}{L}\left.\frac{\partial U}{\partial X}\right|_1 + U|_1 = 0 \tag{7.4}$$

from which it is clear that the characteristic parameter in the surface barrier model (Equation 7.3) is L_s, where

$$\frac{1}{L_s} = \frac{1}{L} + \frac{D}{k_s R} \tag{7.5}$$

which is analogous to L in the standard model. The solution for the desorption curve is

$$\frac{C}{C_0} = 2L_s\frac{L_s}{L}\sum_{n=1}^{\infty}\frac{\exp\left(-\beta_{sn}^2\tau\right)}{\beta_{sn}^2 + L_s\left(L_s - 1\right)} \tag{7.6}$$

where β_{sn} are calculated as in Equation 2.17 with L replaced by L_s:

$$\beta_{sn}\cot\beta_{sn} + L_s - 1 = 0 \tag{7.7}$$

For complete surface barrier control, the desorption curve is given by a simple exponential decay (Kärger and Ruthven, 1992)

$$\frac{C}{C_0} = \exp\left(-\frac{3k_s t}{R}\right) \tag{7.8}$$

This condition may be easily detected by the fact that the shape of the desorption curve does not vary with changing purge flow rate.

Sample desorption curves calculated from Equation 7.6 are shown in Figure 7.1. Note that Equation 7.6 gives an initial value < 1 for $D/(k_s R) > 0$. This is an artifact of assuming the film has an insignificant sorbate capacity. There is thus no volume to purge which creating the concentration gradient across the surface barrier, resulting in an instantaneous drop in effluent concentration. This also causes incorrect behaviour in the limit of complete surface barrier control, in that the model does not tend toward the required exponential decay.

It is clear from Figure 7.1 that the surface barrier has a significant effect on the linear tail of the curve, from which the diffusivity is normally obtained by the long time method. The slope of the tail decreases with increasing surface barrier resistance. This is a result of the eigenvalues being calculated using L_s: although L is large ($L = 100$), the significant value of $D/(k_s R)$ causes that L_s

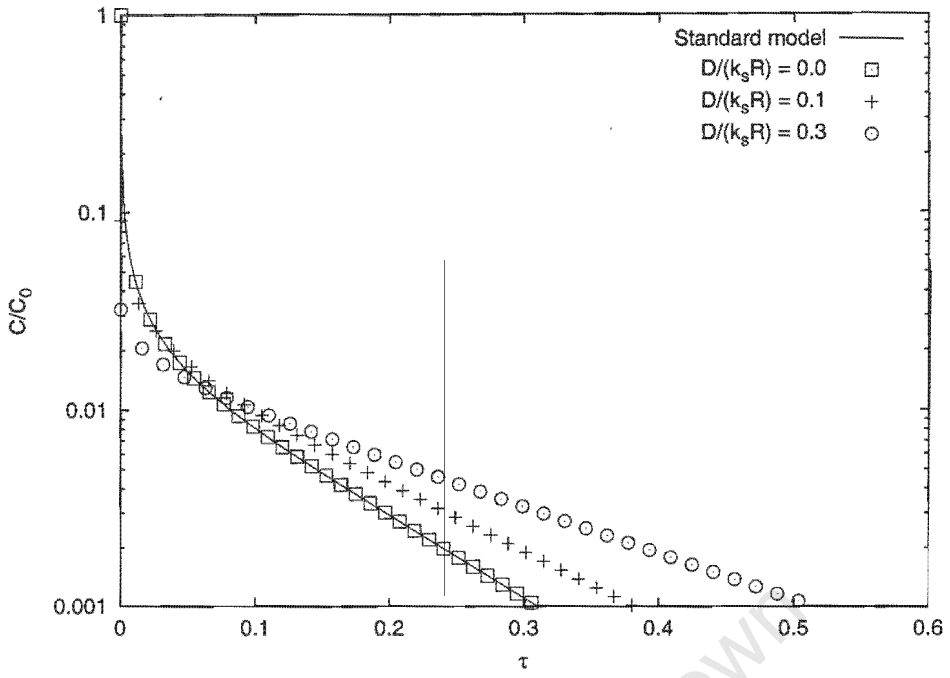

Figure 7.1: Desorption curves for the surface barrier model for various $D/(k_sR)$ as shown and $L = 100$. The standard model is shown for verification.

is not large enough that $\beta_{s1} \simeq \pi$, although it would appear that way from the intercept of the linear region of the desorption curve if the standard approach were being used. For example, for the case $D/(k_sR) = 0.1$ and $L = 100$, it is found that $L_s = 5$ and so $\beta_{s1} \simeq 2.57$. If the curve were analysed using the standard long time method with the assumption $\beta_1 = \pi$, the diffusional time constant would be calculated at 67% of its 'true' value, while the apparent value of L would be 106.

Figure 7.2 shows that the only visible difference between the desorption curves of the two models is that the surface barrier case undergoes a more rapid initial concentration decrease. It is unlikely that this effect would be experimentally noticeable, particularly considering that the effect is exaggerated as outlined above. The true short time behaviour is likely to be an exponential decay, similar to the liquid phase model (Equation 2.44).

7.1.1 Behaviour of the intercept with flow rate

The long time approximation to Equation 7.6, for the case of non-large L_s, is

$$\ln \frac{C}{C_0} = \ln \left[\frac{2L_s}{\beta_{s1}^2 + L_s(L_s - 1)} \cdot \frac{L_s}{L} \right] - \beta_{s1}^2 \tau \tag{7.9}$$

For large values of L (at high flow rates, for example), $L_s \simeq k_sR/D$, which is constant with respect to flow rate, implying that β_{s1} is constant with F. Thus, at high flow rates

$$\ln \frac{C}{C_0} = \ln \frac{\eta}{L} - \beta_{s1}^2 \tau \tag{7.10}$$

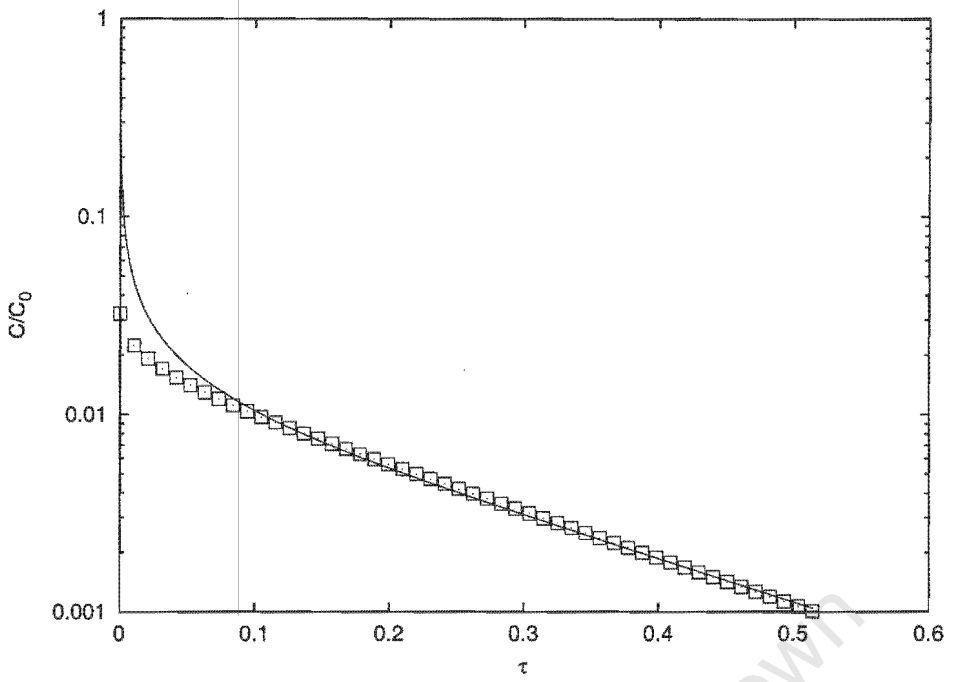

Figure 7.2: Fit of the standard model (lines) to the surface barrier model (points) for $D/(k_s R) = 0.3$ and $L = 100$.

where

$$\eta = \frac{2L_s^2}{\beta_{s1}^2 + L_s(L_s - 1)} \tag{7.11}$$

which does not change with purge rate. This is the same form as the standard large L, long time approximation (Equation 2.19).

Thus, when a system with a significant surface barrier resistance is analysed using the standard model and the long time solution method, an apparent L is obtained that is linear with flow rate (passing through the origin) at large flow rates, but has more complex behaviour at low flow rates. This behaviour would likely be very difficult to detect experimentally.

7.1.2 The effect of a surface barrier on activation energy

Intuitively, it may be expected for the presence of an additional, series resistance to diffusive transport to increase the apparent diffusional activation energy. The above analysis shows, however, that such a conclusion is far from obvious. To investigate any such effect, the temperature dependence of β_{s1}, which is the parameter the surface barrier truly affects, must be considered.

The limiting value of $\beta_1 = \pi$ occurs at high values of L (high flow rates). The analogous limiting value of β_{s1} similarly occurs at large values of L, such that $L_s \simeq k_s R/D$ and β_{s1} is independent of purge rate. The eigenvalues of the model are then given by the roots of

$$\beta_{sn} \cot \beta_{sn} + \frac{k_s R}{D} - 1 = 0 \tag{7.12}$$

It is reasonable to assume that transport across the surface barrier is an activated process, so k_s

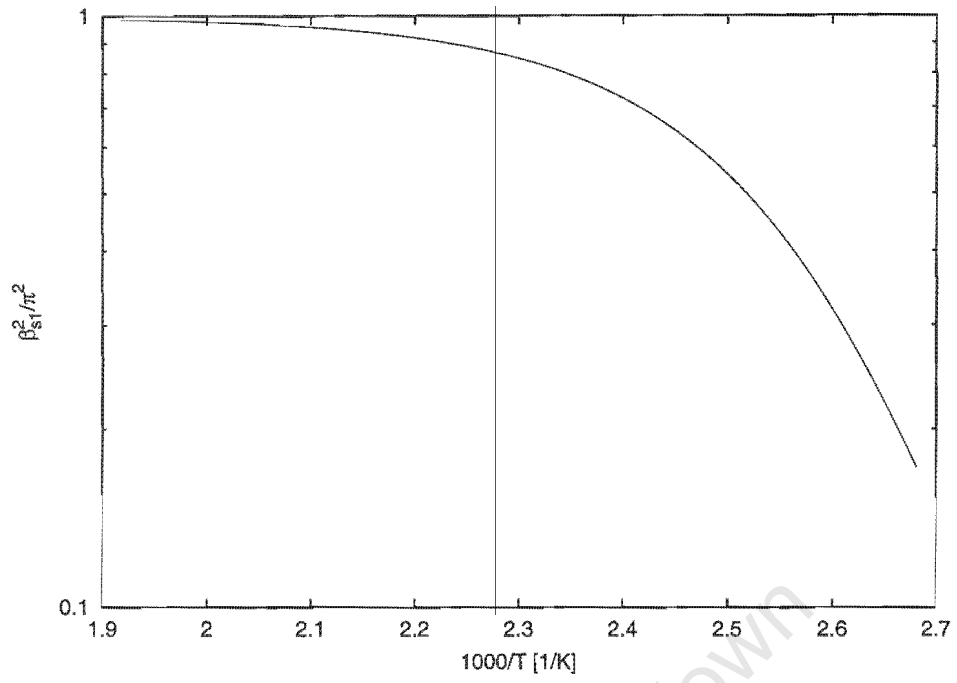

Figure 7.3: Variation of the initial eigenvalue of the surface barrier model with temperature for $E_a - E_{as} = -55\,\mathrm{kJ/mol}$ and $k_s R/D = 10^8$.

follows an Arrhenius temperature dependency:

$$k_s = k_{s\infty} e^{-\frac{E_{as}}{R_g T}} \tag{7.13}$$

where E_{as} is the activation energy for penetrating the barrier. Additionally expressing the diffusion coefficient as an explicit function of temperature, one may write Equation 7.12 as

$$\beta_{sn} \cot \beta_{sn} + \frac{k_{s\infty} R}{D_\infty} e^{\frac{E_a - E_{as}}{R_g T}} - 1 = 0 \tag{7.14}$$

which implicitly gives the temperature dependence of the eigenvalues. Inspection of this expression reveals that

- $E_a > E_{as} \Rightarrow \frac{k_s R}{D}$ decreases as T increases;
- $E_a < E_{as} \Rightarrow \frac{k_s R}{D}$ increases as T increases;
- β_{s1} increases as $\frac{k_s R}{D}$ increases.

Thus the initial eigenvalue increases with temperature for the likely situation $E_a < E_{as}$, implying that the apparent diffusivity increases more strongly with temperature than the true diffusivity, so it is possible that a larger apparent activation energy would be observed for a system with a surface barrier.

Figure 7.3 shows the variation of β_{s1} over the temperature range typical for the cyclohexane/ZSM-5 system used in this work. The activation energy of the surface barrier was chosen to be approxi-

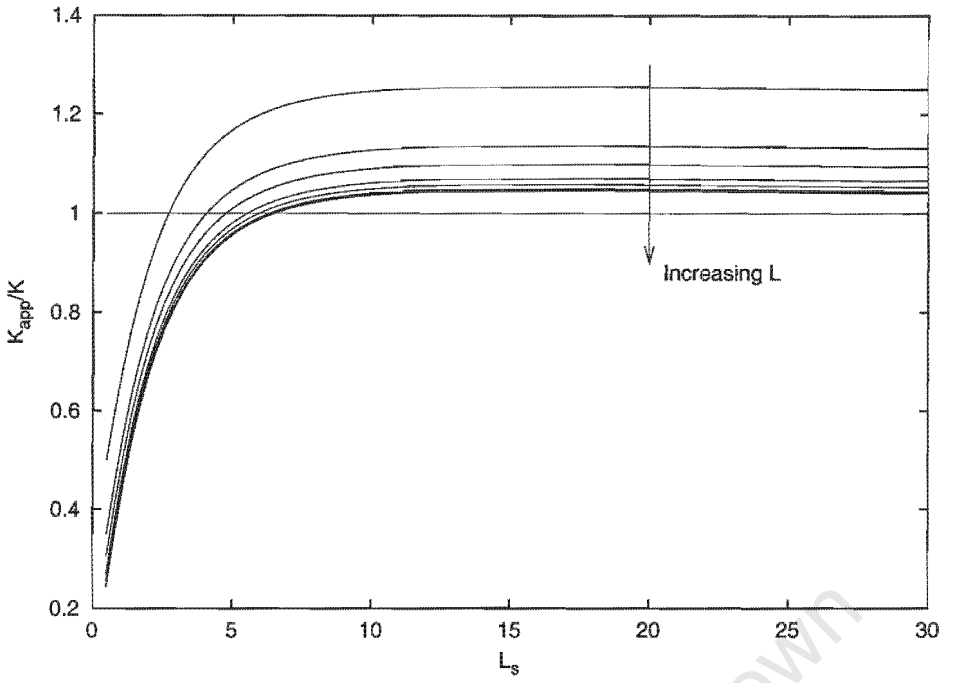

Figure 7.4: Error in apparent value of K relative to true value when using the standard analysis for a system influenced by a surface barrier. Curves are for $L = 10$, 20, 30, 50, 70, 100 and 120.

mately twice that of the activation energy of diffusion, while the ratio of diffusion to surface barrier transport time $k_{s\infty}R/D_\infty$ was chosen largely to give apparently reasonable values of the second term in Equation 7.14; it represents the case in which transport across the surface barrier is orders of magnitude slower than that within the sorbent particle.

The figure indicates that the effect of the surface barrier on the Arrhenius plot for the diffusion coefficient, if significant, is unlikely to simply increase the slope of the usual straight line. Thus the temperature dependence of the diffusivity should appear to deviate from the Arrhenius form if the surface barrier has a major effect.

It is thus probably safe to conclude that the presence of a surface barrier to diffusion would not significantly increase the measured diffusional activation energy, since the Arrhenius plot of the diffusion coefficient is likely to deviate from linearity for a significant surface barrier resistance.

7.1.3 The effect of a surface barrier on adsorption constant

When using the standard model and long time solution method to analyse a desorption curve for a system with a surface barrier, Equations 2.19 and 7.10 can be compared to determine the deviation that could be expected in the apparent parameters so obtained. Considering the intercept terms, it may be seen that the apparent value of L is given by the expression

$$L_{\text{app}} = \frac{L}{L_s^2}\left[\beta_{s1}^2 + L_s\left(L_s - 1\right)\right] \tag{7.15}$$

It may be seen that, for small values of L_s (i.e. large values of D/k_sR and thus large surface

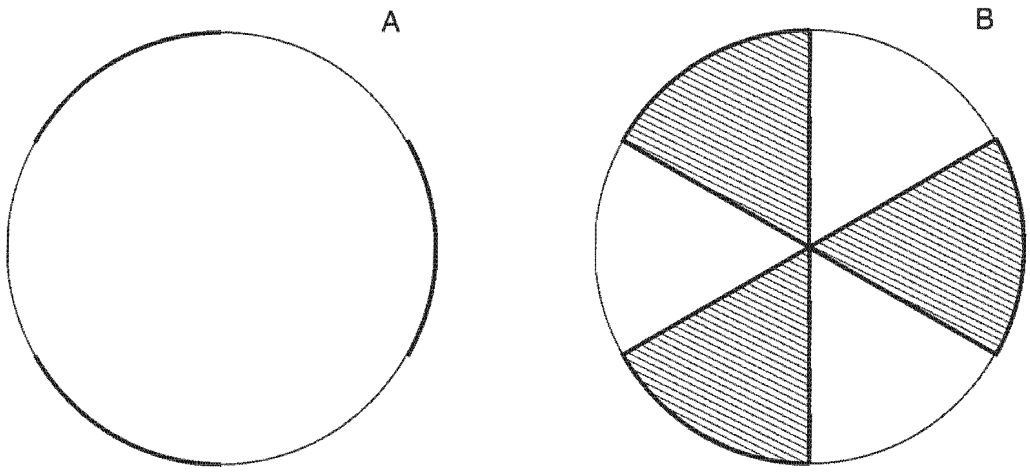

Figure 7.5: Representations of the pore blockage models showing which areas of the sorbent particle do not allow radial diffusive flux.

barrier resistance) the value of L is overestimated. However, due to the underestimation of the diffusion coefficient due to the change in the model eigenvalues, the behaviour of the adsorption constant is not intuitively obvious. This is shown in Figure 7.4, where the error in K is plotted for various 'true' L for a range of L_s, i.e. a range of surface barrier resistance strengths. It may be seen that, for a significant transport barrier (small L_s) at the particle surface, the adsorption constant is underestimated. For what are (presumably) moderate surface resistances, K is slightly overestimated, the error decaying as the surface barrier becomes less significant.

So, if a significant surface barrier were introduced on silanisation, it would be expected that these samples would show a measured value of K lower than the parent sample. This provides a simple method to detect the introduction of pore mouth narrowing provided measurements are available for the unmodified sorbent as a reference.

7.2 Analysis of pore blockage

Two simplistic, extreme cases will be considered, the real description probably lying between the two.

7.2.1 Decrease in surface area for flux

For the first case, assume that pore blockage results in the surface area available for flux of the sorbate out of the sorbent particle being reduced (see A of Figure 7.5). If the catalyst particle has a surface area A, we define the factor α $(0 < \alpha \leq 1)$ such that the modified particle has an area $\alpha^2 A$ available for transport. The fluid phase mass balance is then modified from

$$D \left.\frac{\partial q}{\partial r}\right|_R + \frac{FR}{3V_s K} q|_R = 0 \tag{7.16}$$

to

$$D \left.\frac{\partial q}{\partial r}\right|_R + \frac{FR}{3\alpha^2 V_s K} q|_R = 0 \tag{7.17}$$

The model solution retains the same form as the standard model, except that L is replaced by L' where

$$L' = \frac{FR^2}{3\alpha^2 V_s K D} \tag{7.18}$$

The time scale of the experiment (i.e. the time constant D/R^2) is unchanged, while the convection term is altered. This agrees with the initial assumptions in that the bulk of the catalyst particle is unaffected and only the surface is modified. The boundary condition has been altered without changing the micropore mass balance.

It should be noted that a similar effect could be achieved by decreasing the volume of sorbent, increasing the purge flow rate or decreasing the adsorption constant K. Of these, only the change in K could be physically relevant to the silanisation investigation, since it is possible that silanisation could decrease the adsorption strength of the sorbent. This seems unlikely, however, since the unmodified interior of the particle must be at the same concentration (KC) as if the surface were unmodified, from simple thermodynamic considerations. The surface may have a lower loading, but its capacity relative to the crystal interior is likely to be negligible. It should be remembered that adsorption in zeolites is a pore filling process rather than a simple surface process.

This case will be referred to as model A.

7.2.2 Decrease in total area for flux

For the second case, consider that the particle is made up of successive layers of differential shells, each of which has a similar fraction of its area blocked for flux in the same way as the surface was considered blocked in the case above. One may picture it as the blocked portions of the particle surface casting a 'shadow' toward the centre of the crystal (see B of Figure 7.5). The general mass balance from which Fick's Second Law is derived has the form

$$\frac{\partial}{\partial t} \iiint_V q \, dV = -D \iint_A \nabla q \, dA \tag{7.19}$$

for systems with a constant diffusivity. It is assumed that

$$\iint_{\alpha^2 A} \nabla q \, dA = \alpha^2 \iint_A \nabla q \, dA \tag{7.20}$$

which is reasonable for an isotropic sphere, for which the diffusive flux should be constant at all points on the surface (i.e. q is a function of r only). It then follows that the diffusion equation for a 'partially non-porous' particle can be written as

$$\frac{\partial q}{\partial t} = \alpha^2 D \nabla^2 q \tag{7.21}$$

The fluid phase mass balance takes the same form as the case described above (Equation 7.17).

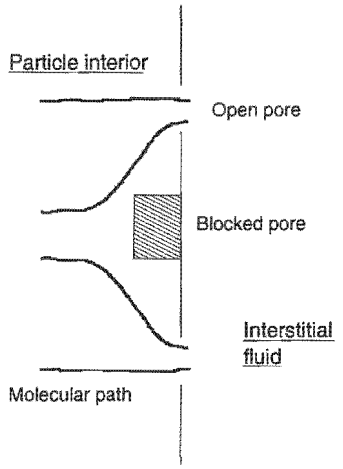

Figure 7.6: Conceptual diffusion paths inside a porous sorbent with a fraction of blocked pore openings.

The model for the ZLC desorption curve is then clearly

$$\frac{C}{C_0} = 2L' \sum_{n=1}^{\infty} \frac{\exp\left(-\beta_n'^2 \alpha^2 \tau\right)}{\beta_n'^2 + L'(L'-1)} \tag{7.22}$$

where L' is defined as in Equation 7.18 and β_n' are given by the roots of

$$\beta_n' \cot \beta_n' + L' - 1 = 0 \tag{7.23}$$

Unlike the previous case, this model does show a change in the experimental time, by a factor α^2.

Note that the particle capacity does not decrease; q is still based on the total particle volume as usual. That is to say, all the pores are still accessible, but not all are amenable to flux. The flux whereby material diffuses out of the 'shaded' regions (in a non-radial direction) so as to exit the particle is not explicitly included in the model.

This case will be referred to as model B.

7.2.3 Effect of pore blockage on measured parameters

Inspection of dimensionless parameters L' and $\alpha^2\tau = \alpha^2 D/R^2$ shows that the difference between model B (Equation 7.22) and the standard model may be expressed as an increase in the representative dimension from the particle radius R to a tortuous length R/α. One may intuitively expect a diffusional trajectory like that shown in Figure 7.6, with the presence of blocked pores causing molecules to diffuse longer distances within the crystal to exit into the gas phase, i.e. the diffusion path is made tortuous by blocking a fraction of the pore mouths. The diffusion time, and so the experimental time, should then increase. Thus the analysis gives the correct qualitative behaviour.

Model A, however, in which only the surface of the crystal was assumed to be affected, indicates that there should not be an increase in the diffusional behaviour of the system, only a modification of the convectional characteristics (as represented by L and L'). Although we would expect a decrease

in the diffusional time constant, due to the extended diffusion path and thus time, this model should not be disregarded. It is in fact far more reasonable that only the pore entrances (i.e. the surface) are affected by silanisation with a bulky agent like TEOS, rather than the entire pore, from entrance to the centre of the crystal, as assumed in Equation 7.22.

The most reasonable explanation of the effect of pore mouth blockage is that the true behaviour lies between these two extremes. It is likely that the diffusional time constant is less severely affected than the dimensionless group L.

For a system conforming to the model A and analysed using the standard ZLC model, one should obtain the true diffusivity and underestimate the adsorption constant. For the case of model B, one should obtain a diffusivity D/α^2 and the true adsorption constant.

7.2.4 Limitations of the pore blockage analyses

In addition to the inaccuracies in the model assumptions described above, there are a number of other implicit assumptions that should be highlighted:

multidimensional geometry as shown in Figure 7.6, the problem is unlikely to remain one dimensional; there will be local concentration gradients in directions other than radial, which are not considered in the model solution;

no capacity decrease the derivation of Equation 7.22 assumes that the sorbent volume available for adsorption does not decrease, contradicting the notion that parts of the crystal are inaccessible to the sorbate molecules.

The standard problem of modelling a system with a discrete channel system (like a zeolite) by using a continuum model is probably amplified in this situation.

7.3 ZLC measurements with cyclohexane/ZSM-5

The experimental method and modification procedure may be found in Chapter 5.

Diffusional time constants for all modified samples are shown in Figure 7.7. The decrease in diffusivity in the silanised samples is clear, particularly in the case of sample Z-L-5/H. Example desorption curves are shown in Figure 7.8 for this and the parent catalyst at identical conditions, again clearly showing the difference in transport rate. The interpretation of the data for samples Z-L-100/- and Z-L-100/-(60h) is not clear (as will be explained below in section 7.3.2) and will be considered separately from the other samples, but they are shown for completeness.

The data for most of the sorbent samples appear consistent with the diffusion model and relatively easily interpreted, as can be seen in Figures 7.8 and 7.9. The data for sample Z-5-L/H are particularly good, being represented by a single line on the Arrhenius plot for experiments run with 7 mg and with 2 mg. Note that Figure 7.9 shows average data at each temperature for sample Z-L-0.5/W: the full data set shows the effect of a crystal size distribution, as discussed in Section 4.2.5.

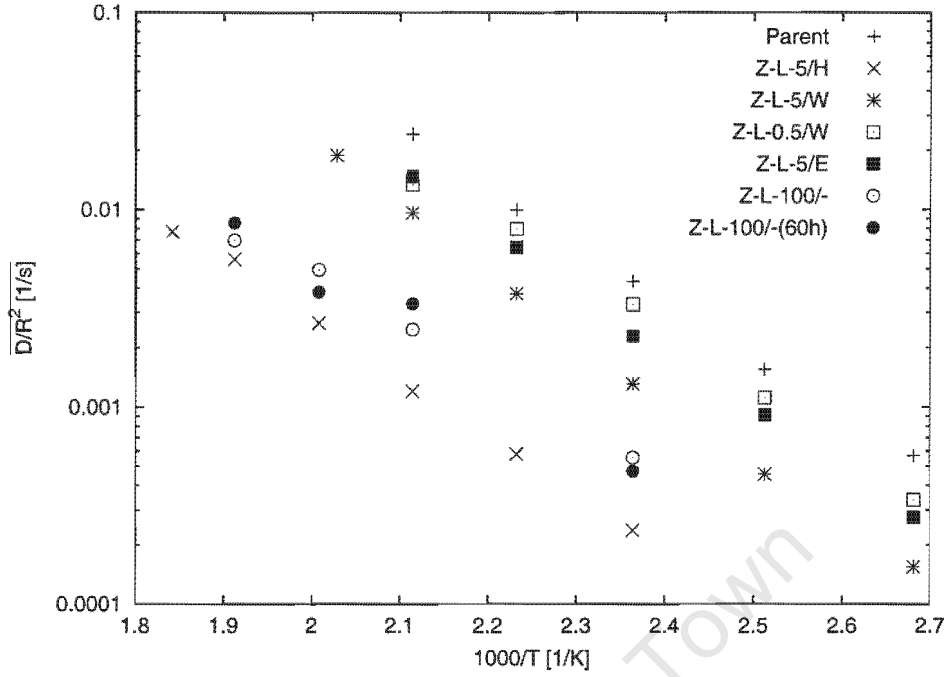

Figure 7.7: Arrhenius plot for the parent and all silanised ZSM-5 samples. Data have been averaged for each temperature.

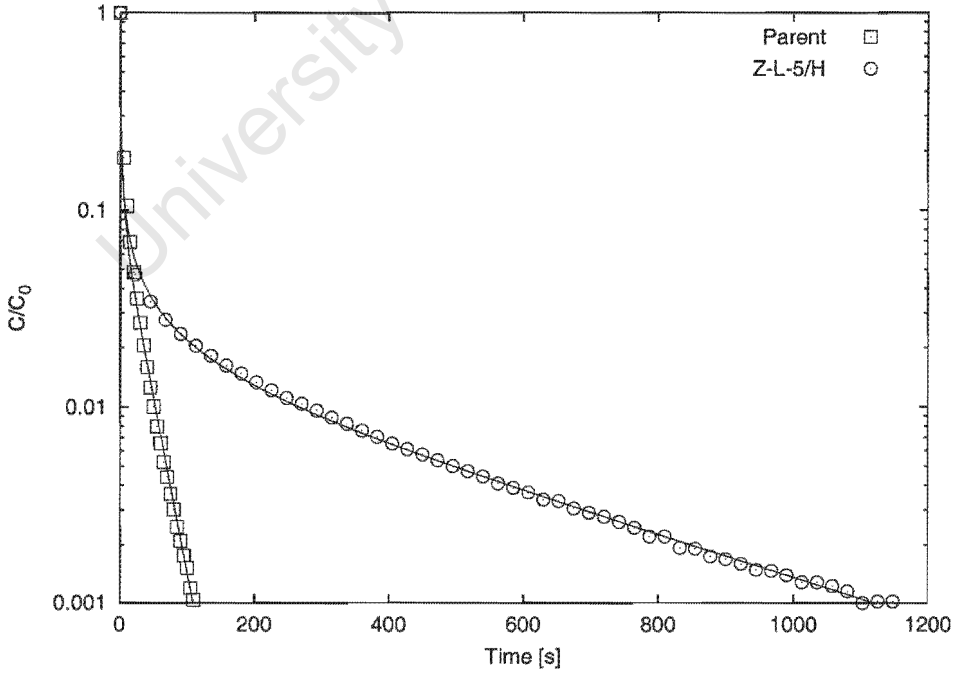

Figure 7.8: Experimental desorption curves and model fits for parent and silanised (Z-L-5/H) catalysts for identical conditions ($T = 150$℃, $F = 93.0\,\mathrm{ml/min}$, $C_0 = 191\,\mathrm{Pa}$).

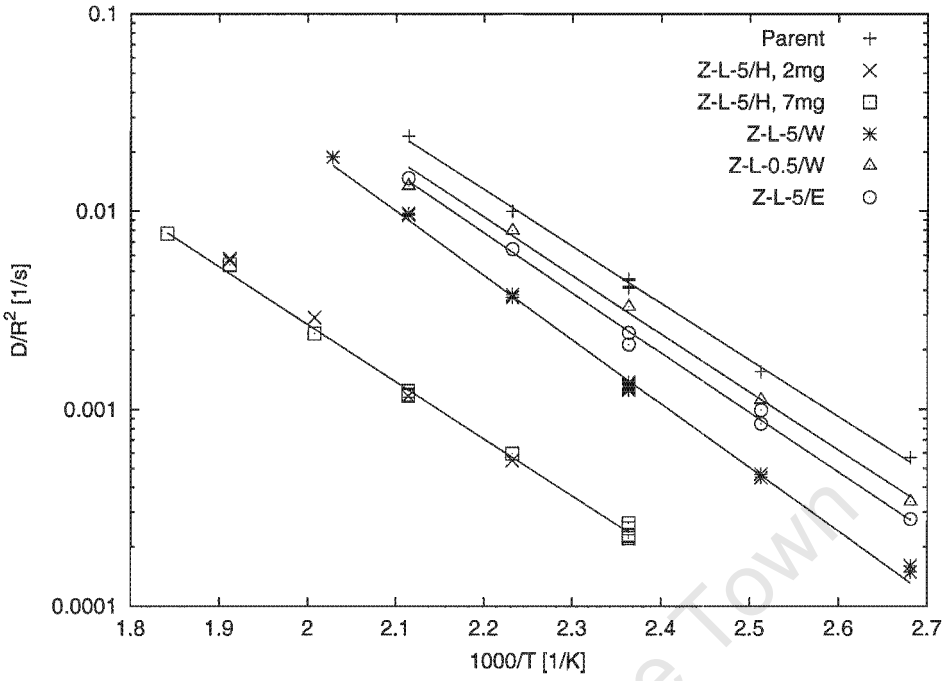

Figure 7.9: Arrhenius plot showing all data (except for sample Z-L-0.5/W, for which average data at each temperature are shown) for samples that have been modified with dilute TEOS.

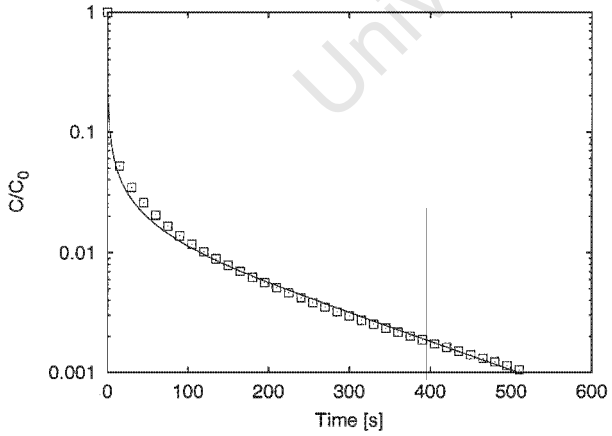

(a) $T = 100$℃, $F = 82.0\,\mathrm{ml/min}$, $C_0 = 191\,\mathrm{Pa}$

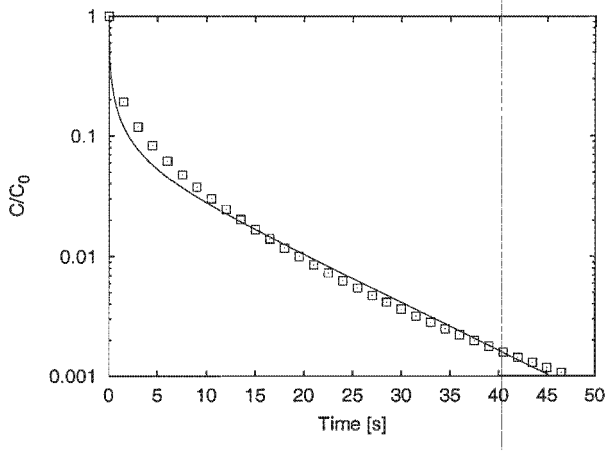

(b) $T = 175$℃, $F = 98.5\,\mathrm{ml/min}$, $C_0 = 191\,\mathrm{Pa}$

Figure 7.10: Sample desorption curves for the parent ZSM-5 sample at the conditions indicated.

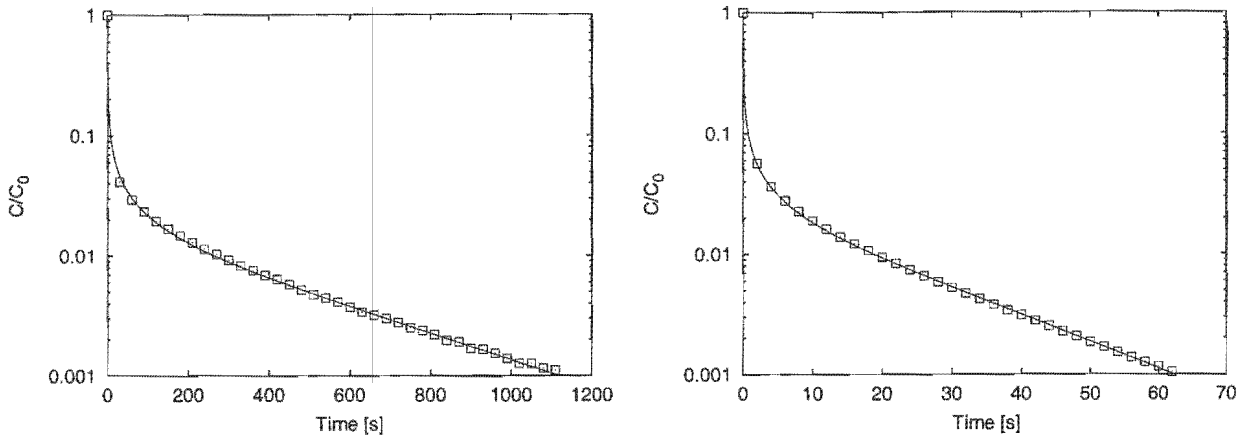

(a) $T = 150℃$, $F = 93.0\,\text{ml/min}$, $C_0 = 191\,\text{Pa}$ (b) $T = 250℃$, $F = 76.6\,\text{ml/min}$, $C_0 = 287\,\text{Pa}$

Figure 7.11: Sample desorption curves for 7 mg of sample Z-L-5/H at the conditions indicated.

Comparison of Figures 7.10 and 7.11 indicates the very good fit of the desorption model to the silanised catalyst data, while the data for the parent sample is somewhat curved. This indicates that sample Z-L-5/H has a very narrow size distribution. It is possible that the presence of diluents during liquid phase silanisation may disperse agglomerated particles (Weber, 1998), with the non-polar *n*-hexane providing the most suitable medium, thus providing the most uniformly sized sample.

7.3.1 Mechanism of transport rate reduction

As illustrated in Figure 7.8, silanisation causes an increase in the time scale of a ZLC experiment. Thus model A, in which only the external surface area of the crystal was considered reduced for flux (Section 7.2.1), may immediately be discounted. This is not surprising, since the principle behind increasing a catalyst's shape selectivity relies on an increase in diffusional resistance, which is characterised by the diffusional time constant. If L were to be interpreted as the initial (dimensionless) concentration gradient at the crystal surface (Ruthven and Brandani, 1997), it may be seen that its increase to L/α^2 is simply an increase of that gradient in order to obtain the same diffusive flux in spite of the reduced available area. This is because the mass balance must hold across the surface, i.e. the rate at which material leaves the surface must equal the rate at which it 'enters', since the surface itself has no volume and thus cannot accumulate any mass.

It has been shown in Section 7.1 that the presence of a surface barrier could cause the temperature dependence of the measured diffusion coefficient, normally linear on an Arrhenius plot, to become concave to the horizontal axis (Figure 7.3). Inspection of Figure 7.9, however, reveals no such tendency. It was also shown that the adsorption constant measured for such a system is likely to be underestimated relative to the true value for a strong surface barrier resistance (i.e. small L_s, Figure 7.4). However, the data shown on Figure 7.12 do not show any such decrease relative to the parent sample, although it is plausible that the scatter (approximately a factor 2.3 difference between the upper and lower data in the worst case) could mask the effect.

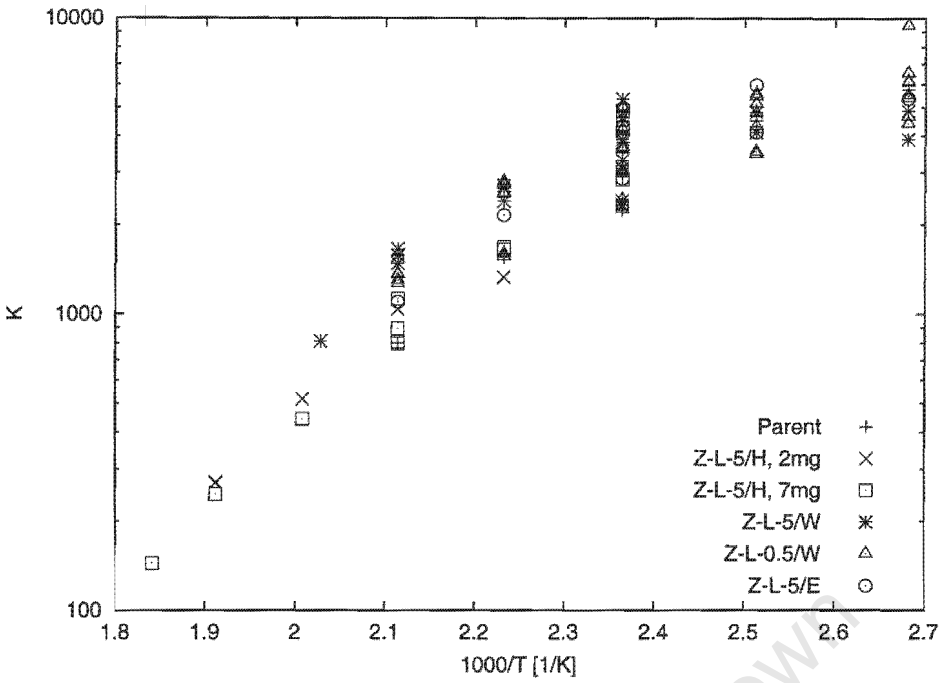

Figure 7.12: Van't Hoff plot showing all adsorption constant data for samples that have been modified with dilute TEOS.

There is therefore no evidence of the introduction of a surface barrier (i.e. pore mouth narrowing) as a result of the silanisation procedure. It should be noted, however, that the two effects mentioned above only would only be noticeable for certain ranges of the dimensionless group D/k_sR. Since reasonable values for this group are not known, it is not certain that these effects would be noticeable experimentally. Also, since the model does not correctly predict the approach to complete surface barrier control, its validity under strong surface resistance conditions is questionable.

Considering model B, in which the total area available to diffusive flux is reduced by a factor α^2 (Section 7.2.2), it is apparent that if this model were appropriate a reduced diffusivity (relative to the parent) should be measured for the silanised catalyst samples while obtaining a constant adsorption constant in all cases. The decrease in the former is shown clearly in Figure 7.9. Also, there is no apparent trend in Figure 7.12; although the data are quite scattered (as discussed above) it is probably reasonable to conclude that the Henry constants of adsorption are constant across all samples.

In order to confirm the apparently good conformance to model B, it should be shown that the decrease in diffusivity tracks the decrease in surface area available for diffusive flux. The surface area data may be obtained by measuring the adsorption capacity for 4-methyl quinoline, which is too big to enter the zeolite pores, as given by temperature programmed desorption. Strictly, this gives the number of acid sites on the external surface; however, it is reasonable to assume that the fractional decrease in external acid sites indicates the fraction of the surface that has been covered with silane and thus the fraction of pore mouths that have been blocked. Thus, the measured diffusion coefficients should lie on the diagonal line shown in Figure 7.13, which shows that there is at least a

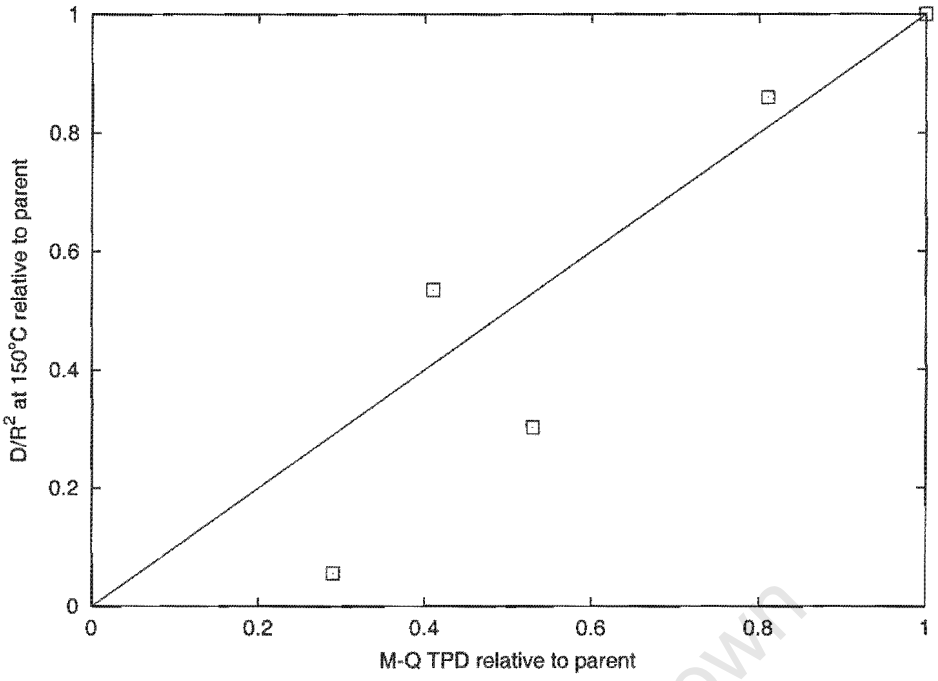

Figure 7.13: Diffusional time constant for cyclohexane in ZSM-5 at 150℃ for modified catalyst samples (relative to parent) as a function of their 4-methyl quinoline temperature programmed desorption capacities (relative to parent). TPD data are from Weber (1998).

qualitative agreement.

The results show that, at least for the liquid phase TEOS deposition performed for the ZSM-5 samples in this work, the decrease in transport rate appears to be a result of pore mouth blocking rather than narrowing.

7.3.2 Sorbents modified with pure TEOS

Figure 7.14 shows the diffusional time constants measured for the sorbents modified using 100% liquid TEOS (i.e. no diluent). The data are widely scattered, although they do seem to be qualitatively consistent. Except for a single point at $T = 225$℃, the data using 4 mg of sample Z-L-100/-(60h) appear to be somewhat lower than that given when using 19 mg of the sorbent; this effect is likely the result of a particle size distribution effect (see Section 4.2.5).

Figure 7.15 shows four example desorption curves at identical temperatures for sample Z-L-100/-(60h), showing the effect of varying flow rate, which is qualitatively correct. Although the initial sorbate concentrations vary for these curves, Figure 7.16 indicates that this parameter does not have a significant effect over the range considered, implying that the adsorption isotherm was probably linear for these experiments. Sample Z-L-100/- shows similar behaviour.

It is evident that the desorption curves for the samples modified without the use of a diluent do not conform to the standard ZLC model, nor to the surface barrier and pore blockage variants presented above. The initial region of the curves show a slow drop in concentration, which becomes slower with decreasing flow rate. This sort of behaviour is only seen for the liquid phase model (Equation 2.44),

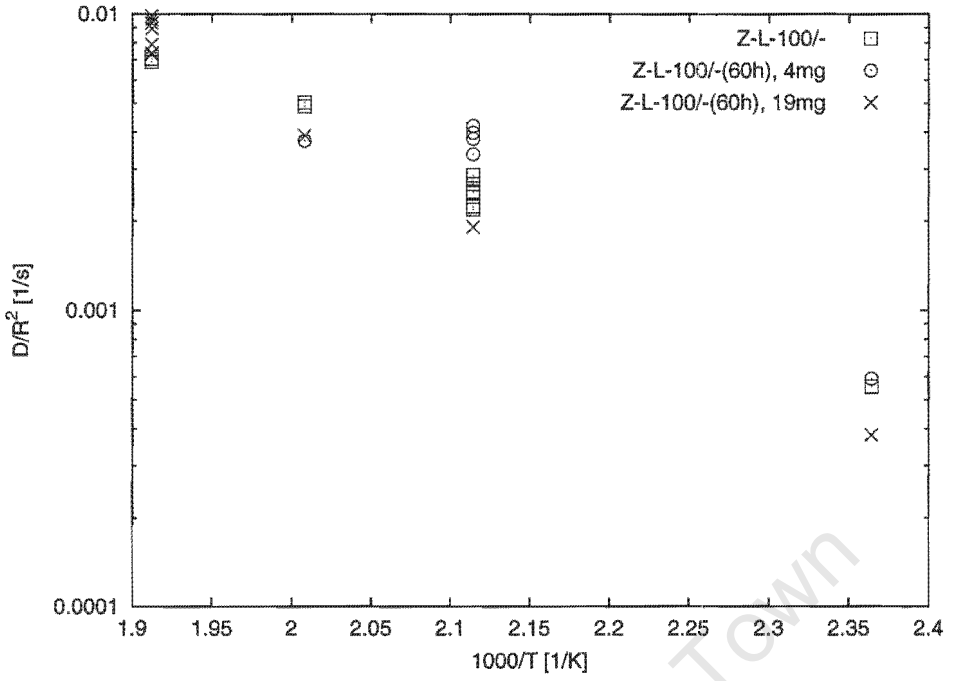

Figure 7.14: Arrhenius plot for ZSM-5 samples modified with pure liquid TEOS.

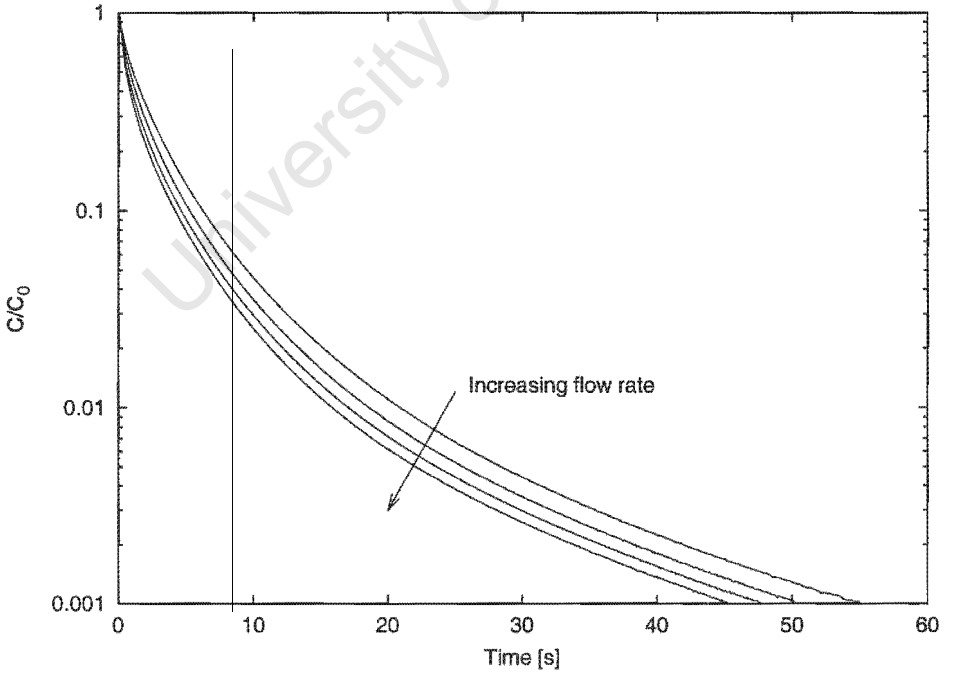

Figure 7.15: Desorption curves for sample Z-L-100/-(60h) at 250℃ and flow rate and initial cyclohexane concentrations as follows: $F = 79.5\,\mathrm{ml/min}$, $C_0 = 207\,\mathrm{Pa}$; $F = 98.7\,\mathrm{ml/min}$, $C_0 = 167\,\mathrm{Pa}$; $F = 117.8\,\mathrm{ml/min}$, $C_0 = 140\,\mathrm{Pa}$; $F = 137.0\,\mathrm{ml/min}$, $C_0 = 120\,\mathrm{Pa}$.

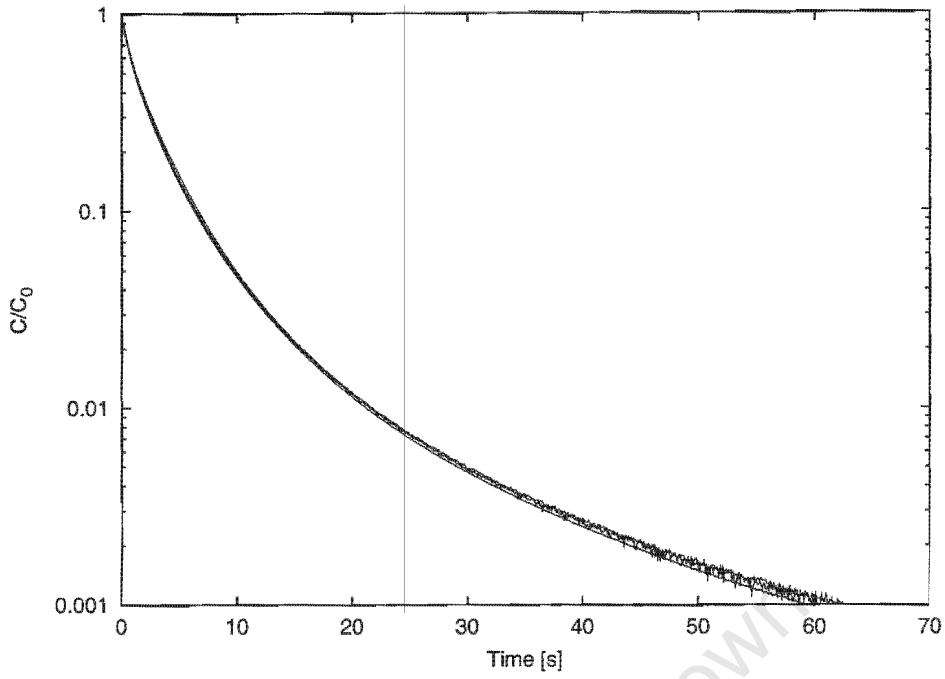

Figure 7.16: Desorption curves for sample Z-L-100/-(60h) at 250°C, 79.5 ml/min and initial cyclohexane concentrations of 207, 482 and 897 Pa.

in which the accumulation of sorbate in the fluid phase cannot be neglected. Although (as pointed out in Section 7.1) the true initial behaviour of a system with strong surface barrier resistance is likely to be an exponential decay, Equation 7.8 indicates that the desorption curve should be independent of purge flow rate. As noted above, the system appears to be in the Henry region of the adsorption isotherm and the unusual shape of the desorption curves is not merely a result of changes in the equilibrium characteristics of the catalyst.

The behaviour of samples Z-L-100/- and Z-L-100-(60h) cannot be reasonably explained by any model considered in this work.

7.4 Conclusions about diffusion in silanised ZSM-5

The effect of depositing an inert silane compound on the external surface of ZSM-5 has been investigated both mathematically and experimentally. Two possible modifications have been considered:

1. narrowing of the pore mouths, modelled as a first order surface barrier;

2. blocking of the pore mouths, interpreted as both a reduction in area available for diffusive flux at the particle surface (model A) as well as throughout the entire particle (with no reduction in adsorption capacity) (model B).

In the surface barrier case, one would expect an analysis based on the standard ZLC model to yield reduced values of both D and K for modified sorbents. For model A, a reduction in surface area

should yield an unchanged D and a reduction in K, while model B would produce a reduced D and an unchanged K.

Experiments were performed with catalyst modified by the liquid phase deposition of both pure and dilute tetraethoxy silane, the parent being Sample C of Chapter 6. It was found that the changes in sorption behaviour of the dilute modified samples corresponded most closely to the pore mouth blockage mechanism in which the area for flux is reduced throughout the particle volume. This is a similar result to the statistical pore blockage model of Theodorou and Wei (1983).

The behaviour of the samples modified with pure TEOS did not conform to any of the diffusion models considered.

Chapter 8

Concluding Remarks

Zero length column chromatography is a simple, reliable method for the measurement of intracrystalline diffusion coefficients in zeolite powder / vapour sorbate systems. The technique is robust against the intrusion of external heat and mass transfer effects by the use of relatively high flow rates and small catalyst samples. Analysis of the desorption curves is simple: the slope of the linear (on semilogarthmic axes) long time region gives the diffusional time constant. Even though the mathematical model for the system assumes a linear adsorption isotherm, this so-called 'long time' analysis gives an accurate result for the diffusional time constant for the case of a Langmuir type isotherm.

The standard analysis is based on the carrier fluid phase being well mixed throughout the sorbent bed, which is reasonable for a physically short column (i.e. with a small Peclet number). By deriving an alternative model with the fluid phase showing plug flow (infinite Peclet number) behaviour, it was shown that the behaviour of the system becomes independent of the flow pattern in the column for the characteristic dimensionless group $L > 15$, irrespective of the physical length of or (axial) flow pattern in the column. This behaviour was verified through use of a third model incorporating finite axial dispersion. This gives a 'zero length' criterion, by which it may be ensured that systems conform to the 'zero length' assumptions of the standard (mixed flow) model.

To investigate the effect of a distribution of sorbent particle sizes (the standard model assumes a monosized sample) on the desorption curve and measured (using the standard model) parameters, a model was derived which incorporates a log-mean distribution of crystal radii. It was found that, for this case, the normally linear (on semilogarithmic axes) tail of the desorption curve became convex to the time axis. This is the expected result, since the slope of that region indicates the diffusional time constant (D/R^2). A varying value of R would thus clearly lead to a varying slope and thus curvature. Analysing such a curve with the standard ZLC model would lead to an underprediction of D/R^2 and an overprediction of L. The deviation, as expected, becomes more severe with an increasing distribution width.

The size distribution model was applied to experimental data, but the fitted distribution width was found to be a function of L, indicating that the model could not describe the data consistently. This is possibly a result of the chosen distribution function not being representative of the sorbent sample. If an experimental size distribution were available, it was shown through a simple mathe-

matical analysis that an adequate description of the desorption curve could be obtained by simply summing the responses of a number of discrete size fractions, weighted by volume fraction.

Finally, numerical analysis indicated that, in the absence of more detailed information, systematic error in the diffusion coefficient caused by analysing a sorbent sample with a size distribution by means of the standard model could be reduced by calculating the mean radius of the particles as the ratio of the total volume of the sample to the total surface area.

For the first part of the experimental study, the sorption rate of cyclohexane in three samples of ZSM-5 of different size and morphology was measured. It was found that the diffusion coefficients obtained using the standard analysis method agreed well with one another and with some literature data. The consistency between the large and small crystals' diffusion coefficients is contradictory to many results in the literature. This was attributed to the fact that most small crystals mentioned in the literature are of an industrial origin and might have been hydrothermally treated, whereas the small particles used in this work were laboratory synthesised with no such post-synthesis modification.

While the individual experimental desorption curves appeared to be well described by the simple model, it was found that the adsorption constant appeared to be a function of purge flow rate. More specifically, L was not directly proportional to flow rate as required by the model, consistent with the expected deviations caused by a crystal size distribution. There were also differences caused by changes in the sorbate concentration during the equilibration stage of the experiment, particularly at low temperatures. This was the result of the presence of a Langmuir shaped adsorption isotherm.

Finally, the effect on the diffusion behaviour of the cyclohexane / ZSM-5 system of depositing a silaceous layer on the external surface of the zeolite was investigated. Models were derived and analysed in order to determine whether the mechanisms of pore mouth narrowing (modelled by using a surface barrier approach) and pore mouth blockage (modelled as a decrease in area available for diffusive flux) could be differentiated. The former case should yield reduced values of diffusion and adsorption constants, while the latter should yield a reduced diffusion coefficient and an unchanged adsorption constant, relative to the unmodified catalyst.

Experiments with samples of ZSM-5 modified by tetraethoxysilane in the liquid phase indicated that there was a significant (up to an order of magnitude, depending on the silanisation procedure) decrease in diffusivity. Although there was scatter in the measured adsorption constants, it appeared that these remained constant for all samples. It would thus appear that, at least for the sorbents used in this work, that the change in transport rate due to silanisation was due to the pore mouth blockage mechanism.

It should be noted that the accuracy of the estimated value of the intracrystalline diffusion constant D is subject to the accuracy of the estimation of the crystal radius R and, indeed, to the applicability of the assumed geometry (spherical in this case), since only the diffusional time constant D/R^2 can be measured.

Bibliography

Anderson, B. G., de Gauw, F. J. M. M., Noordhoek, N. J., IJzendoorn, L. J. V., Santen, R. A. V., and de Voigt, M. J. A. (1998). Mass transfer of alkanes in zeolite packed-bed reactors studied with positron emission profiling (PEP). 1. Experiments. *Industrial and Engineering Chemistry Research*, 37:815–824.

Boniface, H. A. and Ruthven, D. M. (1985). Chromatographic adsorption with sinusoidal input. *Chemical Engineering Science*, 40(11):2053–2061.

Brandani, S. (1996). Analytical solutions for ZLC desorption curves with biporous adsorbent particles. *Chemical Engineering Science*, 51(12):3283–3288.

Brandani, S. (1998). Effects of nonlinear equilibrium on zero length column experiments. *Chemical Engineering Science*, 53(15):2791–2798.

Brandani, S., Cavalcante, C., Guimarães, A., and Ruthven, D. (1998). Heat effects in ZLC experiments. *Adsorption*, 4:275–285.

Brandani, S., Hufton, J., and Ruthven, D. M. (1995a). Self-diffusion of propane and propylene in 5A and 13X zeolite crystals studied by the tracer ZLC method. *Zeolites*, 15(7):624–631.

Brandani, S., Jama, M., and Ruthven, D. (2000a). Diffusion, self-diffusion and counter-diffusion of benzene and *p*-xylene in silicalite. *Microporous and Mesoporous Materials*, 35-36:283–300.

Brandani, S., Jama, M. A., and Ruthven, D. M. (2000b). ZLC measurements under non-linear conditions. *Chemical Engineering Science*, 55:1205–1212.

Brandani, S., Ruthven, D., and Kärger, J. (1995b). Concentration dependence of self-diffusivity of methanol in NaX zeolite crystals. *Zeolites*, 15(6):494–495.

Brandani, S. and Ruthven, D. M. (1995). Analysis of ZLC desorption curves for liquid systems. *Chemical Engineering Science*, 50(13):2055–2059.

Brandani, S. and Ruthven, D. M. (1996a). Analysis of ZLC desorption curves for gaseous systems. *Adsorption*, 2:133–143.

Brandani, S. and Ruthven, D. M. (1996b). Moments analysis of the zero length column method. *Industrial and Engineering Chemistry Research*, 35:315–319.

Bülow, M., Hilgert, W., and Emig, G. (1991). Transport phenomena and reactions in 13X type zeolites. In Öhlmann, G. et al., editors, *Catalysis and Adsorption by Zeolites*, pages 479–490. Elsevier Science Publishers, B.V., Amsterdam.

Cavalcante, Jr., C. L., Brandani, S., and Ruthven, D. M. (1997). Evaluation of the main diffusion path in zeolites from ZLC desorption curves. *Zeolites*, 18(4):282–285.

Cavalcante, Jr., C. L. and Ruthven, D. M. (1995a). Adsorption of branched and cyclic paraffins in silicalite. 1. Equilibrium. *Industrial and Engineering Chemistry Research*, 34:177–184.

Cavalcante, Jr., C. L. and Ruthven, D. M. (1995b). Adsorption of branched and cyclic paraffins in silicalite. 2. Kinetics. *Industrial and Engineering Chemistry Research*, 34:185–191.

Čejka, J., Žilková, N., Wichterlová, B., Eder-Mirth, G., and Lercher, J. A. (1996). Decisive role of transport rate of products for zeolite *para*-selectivity: Effect of coke deposition and external surface silylation on activity and selectivity of HZSM-5 in alkylation of toluene. *Zeolites*, 17:265–271.

Chen, S. Z., Huddersman, K., Keir, D., and Rees, L. V. C. (1988). Synthesis of large uniform crystals of ZSM-5. *Zeolites*, 8:106–109.

Chon, H. and Park, D. H. (1988). Diffusion of cyclohexanes in ZSM-5 zeolites. *Journal of Catalysis*, 114:1–7.

Coulson, J. M. and Richardson, F. F. (1991). *Coulson & Richardson's Chemical Engineering*, volume 2. Pergamon Press, Oxford.

Daubert, T. E. and Danner, R. P. (1991). *Physical and Thermodynamic Properties of Pure Chemicals.* Hemisphere Publishing Company, Washington.

Deisler, P. F. and Wilhelm, R. H. (1953). Diffusion in beds of porous solids: Measurement by frequency responce techniques. *Industrial and Engineering Chemistry*, 45(6):1219–1227.

Eic, M. and Ruthven, D. M. (1988). A new experimental technique for measurement of intracrystalline diffusivity. *Zeolites*, 8:40–45.

Eic, M. and Ruthven, D. M. (1989). Intracrystalline diffusion of linear paraffins and benzene in silicalite studied by the ZLC method. In Jacobs, P. A. and van Santen, R. A., editors, *Zeolites: Facts, Figures, Future*, pages 897–905. Elsevier Science Publishers, B.V., Amsterdam.

Gradshteyn, I. S. and Ryzhik, I. M. (1994). *Table of Integrals, Series and Products.* Academic Press, London, fifth edition. Translated from the Russian by Scripta Technica, Inc.

Grenier, P., Meunier, F., Gray, P. G., Kärger, J., Xu, Z., and Ruthven, D. M. (1994). Diffusion of methanol in NaX crystals: Comparison of IR, ZLC and PFG-NMR measurements. *Zeolites*, 14:242–249.

Haag, W. O., Lago, R. M., and Weisz, P. B. (1982). Transport and reactivity of hydrocarbon molecules in a shape-selective zeolite. *Journal of the Chemical Society, Faraday Discussions*, 72:317.

Han, M., Yin, X., Jin, Y., and Chen, S. (1999). Diffusion of aromatic hydrocarbon in ZSM-5 studied by the improved zero length column method. *Industrial and Engineering Chemistry Research*, 38:3172–3175.

Hibino, T., Niwa, M., and Murakami, Y. (1993). Inactivation of external surface of mordenite and ZSM-5 by chemical vapour deposition of silicon alkoxide. *Zeolites*, 13:518–523.

Hibino, T., Niwa, M., Murakami, Y., Sano, M., Komai, S., and Hanachai, T. (1989). Structure of deposited germanium dioxide which controls the pore-opening size of mordenite. *Journal of Physical Chemistry*, 93:7847–7850.

Hsu, L. K. P. and Haynes, H. W. (1981). Effective diffusivity by the gas chromatography technique: Analysis and application to measurement of diffusion of various hydrocarbons in zeolite NaY. *AIChE Journal*, 27(1):81–91.

Hufton, J. R. and Danner, R. P. (1993). Chromatographic study of alkanes in silicalite: Transport properties. *AIChE Journal*, 39(6):962–974.

Hufton, J. R. and Ruthven, D. M. (1993). Diffusion of light alkanes in silicalite studied by the zero length column method. *Industrial and Engineering Chemistry Research*, 32(10):2379–2386.

Jama, M. A., Delmas, M. P. F., and Ruthven, D. M. (1997). Diffusion of linear and branched C_6 hydrocarbons on silicalite studied by the wall-coated capillary chromatographic method. *Zeolites*, 18:200–204.

Kärger, J. and Ruthven, D. M. (1989). On the comparison between macroscopic and NMR measurements of intracrystalline diffusion in zeolites. *Zeolites*, 9:267–281.

Kärger, J. and Ruthven, D. M. (1992). *Diffusion in Zeolites and Other Microporous Materials*. John Wiley & Sons, Inc., New York.

Kim, J.-H., Ishida, A., Okajima, M., and Niwa, M. (1996). Modification of HZSM-5 by CVD of various silicon compounds and generation of para-selectivity. *Journal of Catalysis*, 161:387–392.

Liang, W., Chen, S., and Peng, S. (1995). A model for the highly *para*-selective reactions in HZSM-5 zeolite catalyst. *Chemical Engineering Science*, 50(15):2391–2396.

Loos, J.-B. W. P., Verheijin, P. J. T., and Moulijn, J. A. (2000). Improved estimation of zeolite diffusion coefficients from zero-length column experiments. *Chemical Engineering Science*, 55:51–65.

Micke, A., Bülow, M., and Kočiřik, M. (1994a). A nonequilibrium surface barrier for sorption kinetics of p-ethyltoluene on ZSM-5 molecular sieves. *J. Phys. Chem.*, 98:924–929.

Micke, A., Kočiřik, M., and Bülow, M. (1993). Theory of zero length column chromatography with the condition of a well-stirred sorbing zone. *Microporous Materials*, 1:363–371.

Micke, A., Kočiřik, M., and Bülow, M. (1994b). Zero length column chromatography to characterise microporous sorbents by means of kinetic data. *Berichte der Bunsen-Gesellschaft für physikalische Chemie*, 98(2):242–248.

Möller, K. P. and O'Connor, C. T. (1994). The measurement of diffusion and adsorption using a jetloop recycle reactor. In Weitkamp, J., Karge, H. G., Pfeifer, H., and Hölderich, W., editors, *Zeolites and Related Microporous Materials: State of the Art 1994*, pages 1201–1208. Elsevier Science Publishers, B.V., Amsterdam.

Möller, K. P. and O'Connor, C. T. (1996). The measurement of diffusion in porous catalysts using a CSTR. *Chemical Engineering Science*, 51(13):3403–3408.

Noordhoek, N. J., IJzendoorn, L. J. V., Anderson, B. G., de Gauw, F. J., Santen, R. A. V., and de Voigt, M. J. (1998). Mass transfer of alkanes in zeolite packed-bed reactors studied with positron emission profiling. 2. Modeling. *Industrial and Engineering Chemistry Research*, 37:825–833.

Perry, R. H., Green, D. W., and Maloney, J. O., editors (1997). *Perry's Chemical Engineer's Handbook*. McGraw-Hill Book Company, London, seventh edition.

Rees, L. V. C. (1994). Exciting new advances in diffusion of sorbates in zeolites and microporous materials. In Weitkamp, J., Karge, H. G., Pfeifer, H., and Hölderich, W., editors, *Zeolites and Related Microporous Materials: State of the Art 1994*, pages 1133–1150. Elsevier Science Publishers, B.V., Amsterdam.

Rodriguez, J. F., Valverde, J. L., and Rodrigues, A. E. (1998). Measurement of effective self-diffusion coefficients in a gel-type cation exchanger by the zero-length-column method. *Industrial and Engineering Chemistry Research*, 37:2020–2028.

Röger, H. P., Krämer, M., Möller, K. P., and O'Connor, C. T. (1998). Effects of in-situ chemical vapour deposition using tetraethoxysilane on the catalytic and sorption properties of ZSM-5. *Microporous and Mesoporous Materials*, 24(4-6):607–614.

Röger, H. P., Manstein, H., Böhringer, W., Möller, K. P., and O'Connor, C. T. (2001). Unravelled from the back: kinetics of alkoxysilane cvd on zeolites and evidence for pore mouth plugging determined from model conversion over stepwise silanised samples. In Galarneau, A., Renzo, F. D., Fajula, F., and Vedrine, J., editors, *Zeolites and Mesoporous Materials at the Dawn of the 21'st Century*, page 142. Elsevier Science Publishers, B.V., Amsterdam.

Ruthven, D. M. (1984). *Principles of Adsorption and Adsorption Processes.* John Wiley & Sons, Inc., New York.

Ruthven, D. M. and Brandani, S. (1997). Measurement of diffusion in microporous solids by macroscopic methods. In Fraissard, J., editor, *Physical Adsorption: Experiment, Theory and Applications*, pages 261–296. Kluwer Academic Publishers, The Netherlands.

Ruthven, D. M., Eic, M., and Richard, E. (1991). Diffusion of C_8 aromatic hydrocarbons in silicalite. *Zeolites*, 11:647–653.

Ruthven, D. M. and Stapleton, P. (1993). Measurement of liquid phase counterdiffusion in zeolite crystals by the ZLC method. *Chemical Engineering Science*, 48(1):89–98.

Ruthven, D. M., Stapleton, P., and Dahlke, K. (1993). Application of the ZLC method to the measurement of intracrystalline counter-diffusion in liquid-zeolite systems. In von Ballmoos, R., Higgins, J. B., and Treacy, M. M. J., editors, *Proceedings of the 9th International Zeolite Conference*, pages 97–103, USA. Reed Publishing.

Ruthven, D. M. and Xu, Z. (1993). Diffusion of oxygen and nitrogen in 5A zeolite crystals and commercial 5A pellets. *Chemical Engineering Science*, 48(18):3307–3312.

Schwan, P. and Möller, K. P. (2001). Analysis of the pulse response in a CSTR for diffusion measurement in bi-porous adsorbent pellets. *Chemical Engineering Science*, 56(8):2821–2830.

Silva, J. A. C. and Rodrigues, A. E. (1996). Analysis of ZLC technique for diffusivity measurements in bidisperse porous adsorbent pellets. *Gas Separation and Purification*, 10(4):207–224.

Silva, J. A. C. and Rodrigues, A. E. (1997). Sorption and diffusion of n-pentane in pellets if 5A zeolite. *Industrial and Engineering Chemistry Research*, 34:493–500.

Silva, J. A. C., Silva, F. A. D., and Rodrigues, A. E. (2001). An analytical solution for the analysis of zero-length-column experiments with heat effects. *Industrial and Engineering Chemistry Research*, 40:3697–3702.

Smith, J. M. (1981). *Chemical Engineering Kinetics.* Chemical Engineering Series. McGraw-Hill Book Company, London, third edition.

Spencer, A. J. M., Parker, D. F., Berry, D. S., England, A. H., Faulkner, T. R., Green, W. A., Holden, J. T., Middleton, D., and Rogers, T. G. (1977). *Engineering Mathematics*, volume 2. Van Nostrand Reinhold Company Limited, New York.

Szostak, R. (1992). *Handbook of Molecular Sieves.* Van Nostrand Reinhold Company Limited, New York.

Theodorou, D. and Wei, J. (1983). Diffusion and reaction in blocked and high occupancy zeolite catalysts. *Journal of Catalysis*, 83:205–224.

Voogd, P., Bekkum, H. V., Shavit, D., and Kouwenhoven, H. W. (1991). Effect of zeolite structure and morphology on intracrystalline n-hexane diffusion in pentasil zeolites studied by the zero-length column method. *Journal of the Chemical Society, Faraday Transactions*, 87(21):3575–3580.

Weber, R. W. (1998). *The Inertisation of the Zeolites ZSM-5, Mordenite and Beta by Chemical Vapour Deposition using Tetraethoxysilane.* PhD thesis, University of Cape Town.

Weber, R. W., Möller, K. P., and O'Connor, C. T. (2000). The chemical vapour and liquid deposition of tetraethoxysilane on ZSM-5, mordenite and beta. *Microporous and Mesoporous Materials*, 35-36:533–543.

Xiao, J. and Wei, J. (1992). Diffusion mechanism of hydrocarbons in zeolites–II. Analysis of experimental observations. *Chemical Engineering Science*, 47:1143.

Yasuda, Y. (1982). Determination of vapour diffusion coefficients in zeolites by the frequency response method. *Journal of Physical Chemistry*, 86(10).

Zhu, W., de Graaf, J. M. V., Broeke, L. J. P. V. D., Kapteijn, F., and Moulijn, J. A. (1998). TEOM: A unique technique for measuring adsorption properties. Light alkanes in silicalite-1. *Industrial and Engineering Chemistry Research*, 37:1934–1942.

Appendix A

Derivation of ZLC Models

This appendix details the solutions (largely in the Laplace Domain) of the various ZLC models for systems with linear adsorption isotherms. In all cases the following assumptions were made:

- initial equilibration followed by perfect step decrease in concentration at zero time;
- spherical, isotropic adsorbent;
- isothermal system;
- no external mass transfer limitations;
- Fickian diffusion with constant diffusivity;
- linear (Henry's Law) adsorption isotherm (i.e. $q(r = R) = KC$).

In addition to the diffusion-limited cases, the models for equilibrium control were also derived.

A.1 Adsorbed phase mass balance

The adsorbed phase mass balance is given by Fick's Second Law in spherical coordinates:

$$\frac{\partial q}{\partial t} = D\left(\frac{\partial^2 q}{\partial r^2} + \frac{2}{r}\frac{\partial q}{\partial r}\right) \tag{A.1}$$

with

$$q(r, t = 0) = q_0 \tag{A.2}$$

$$\frac{\partial q}{\partial r}(r = 0, t) = 0 \tag{A.3}$$

$$q(r = R, t) = KC \tag{A.4}$$

After non-dimensionalising, this may be written

$$\frac{\partial Q}{\partial \tau} = \frac{\partial^2 Q}{\partial X^2} + \frac{2}{X}\frac{\partial Q}{\partial X} \tag{A.5}$$

where

$$Q = \frac{q}{q_0} \tag{A.6}$$

$$X = \frac{r}{R} \tag{A.7}$$

$$\tau = t\frac{D}{R^2} \tag{A.8}$$

The initial condition, based on the assumption of complete equilibration, is

$$Q(X, \tau = 0) = 1 \tag{A.9}$$

while the boundary conditions are

$$\frac{\partial Q}{\partial X}(X = 0, \tau) = 0 \tag{A.10}$$

$$Q(X = 1, \tau) = Y \tag{A.11}$$

where

$$Y = \frac{C}{C_0} \tag{A.12}$$

Equation A.5 may be simplified by the substitution

$$Q = \frac{\alpha}{X} \tag{A.13}$$

to give

$$\frac{\partial \alpha}{\partial \tau} = \frac{\partial^2 \alpha}{\partial X^2} \tag{A.14}$$

The initial condition is then

$$\alpha(X, \tau = 0) = X \tag{A.15}$$

while the boundary conditions may be somewhat simplified:

$$\alpha(X = 0, \tau) = 0 \tag{A.16}$$

$$\alpha(X = 1, \tau) = Y \tag{A.17}$$

Taking the Laplace Transform of Equation A.14 gives

$$\frac{d^2\hat{\alpha}}{dX^2} - s\hat{\alpha} = -X \tag{A.18}$$

This ODE may be easily solved to give

$$\hat{\alpha} = A_1 \exp\left(\sqrt{s}X\right) + A_2 \exp\left(-\sqrt{s}X\right) + \frac{X}{s} \tag{A.19}$$

where A_1 and A_2 are arbitrary constants of integration. Application of the centre boundary condition,

Equation A.16, indicates that

$$A_1 = -A_2 \tag{A.20}$$

after which the second condition, Equation A.17, yields

$$A_1 = \frac{\hat{Y} - 1/s}{\exp(\sqrt{s}) - \exp(-\sqrt{s})} \tag{A.21}$$

to give as the solution, reverting to $\hat{Q}$,

$$\hat{Q} = \left(\hat{Y} - \frac{1}{s}\right) \cdot \frac{1}{X} \cdot \frac{\exp(\sqrt{s}X) - \exp(-\sqrt{s}X)}{\exp(\sqrt{s}) - \exp(-\sqrt{s})} - \frac{1}{s} \tag{A.22}$$

It is not this function, but rather its derivative at $X = 1$ which is required for the solution of the ZLC models, as shown below. Thus, differentiating:

$$\left.\frac{d\hat{Q}}{dX}\right|_{X=1} = \left(\hat{Y} - \frac{1}{s}\right)\left(\sqrt{s}\coth\sqrt{s} - 1\right) \tag{A.23}$$

A.2 Fluid phase mass balance

The fluid phase mass balance is the standard

$$-D_L\frac{\partial^2 C}{\partial z^2} + v\frac{\partial C}{\partial z} + \frac{\partial C}{\partial t} + \left(\frac{1-\varepsilon}{\varepsilon}\right)\frac{\partial \bar{q}}{\partial t} = 0 \tag{A.24}$$

in which, for diffusion control (by simple mass balance and the application of Fick's First Law):

$$\frac{\partial \bar{q}}{\partial t} = \frac{3D}{R}\left.\frac{\partial q}{\partial r}\right|_{r=R} \tag{A.25}$$

and with the initial condition

$$C(z, t=0) = C_0 \tag{A.26}$$

The number and form of the boundary conditions is determined by the specific situation being considered.

Non-dimensionalising, recognising that

$$\frac{1-\varepsilon}{\varepsilon} = \frac{V_s}{V_f} \tag{A.27}$$

and multiplying through by

$$\frac{V_f}{F} = \frac{L_{bed}}{v} \tag{A.28}$$

one obtains

$$-\frac{1}{N_{Pe}}\frac{\partial^2 Y}{\partial Z^2} + \frac{\partial Y}{\partial Z} + \tau_f\frac{\partial Y}{\partial \tau} + \frac{3V_s D}{FR^2}\left.\frac{\partial Q}{\partial X}\right|_{X=1} = 0 \tag{A.29}$$

where

$$Z = \frac{z}{L_{\text{bed}}} \tag{A.30}$$

$$N_{\text{Pe}} = \frac{vL_{\text{bed}}}{D_{\text{L}}} \tag{A.31}$$

$$\tau_{\text{f}} = \frac{V_{\text{f}}D}{FR^2} = \frac{L_{\text{bed}}D}{vR^2} \tag{A.32}$$

The dimensionless initial condition is

$$Y\left(Z, \tau = 0\right) = 1 \tag{A.33}$$

Taking the Laplace Transform of Equation A.29 gives the relation

$$-\frac{1}{N_{\text{Pe}}}\frac{d^2\hat{Y}}{dZ^2} + \frac{d\hat{Y}}{dZ} + s\tau_{\text{f}}\hat{Y} - \tau_{\text{f}} + \frac{3V_{\text{s}}D}{FR^2}\left.\frac{d\hat{Q}}{dX}\right|_{X=1} = 0 \tag{A.34}$$

Substituting Equation A.23:

$$-\frac{1}{N_{\text{Pe}}}\frac{d^2\hat{Y}}{dZ^2} + \frac{d\hat{Y}}{dZ} + G\hat{Y} = \frac{G}{s} \tag{A.35}$$

where

$$G = \tau_{\text{f}}s + \frac{1}{L}\left(\sqrt{s}\coth\sqrt{s} - 1\right) \tag{A.36}$$

$$L = \frac{FR^2}{3V_{\text{s}}KD} \tag{A.37}$$

A.3 Disperse flow model

Equation A.35 has eigenvalues

$$\frac{N_{\text{Pe}} \pm \sqrt{N_{\text{Pe}}^2 + 4GN_{\text{Pe}}}}{2} \tag{A.38}$$

and so the solution of the ODE has the form

$$\hat{Y} = A_3 e^{\frac{1}{2}(N_{\text{Pe}}+H)Z} + A_4 e^{\frac{1}{2}(N_{\text{Pe}}-\text{H})Z} + \frac{1}{s} \tag{A.39}$$

where

$$H = \sqrt{N_{\text{Pe}}^2 + 4GN_{\text{Pe}}} \tag{A.40}$$

and A_3 and A_4 are again arbitrary constants of integration.

We use the Dankwerts boundary conditions for disperse flow:

$$\frac{\partial C}{\partial z}\left(z = L_{\text{bed}}, t\right) = 0 \tag{A.41}$$

$$\frac{\partial C}{\partial z}\left(z = 0, t\right) = \frac{v}{D_{\text{L}}}\left[C\left(z = 0^+, t\right) - C\left(z = 0^-, t\right)\right] \tag{A.42}$$

which may be rewritten, assuming $C(z=0^-,t)=0$ for a perfect step, as

$$\frac{d\hat{Y}}{dZ}(Z=1)=0 \tag{A.43}$$

$$\frac{d\hat{Y}}{dZ}(Z=0)=N_{\mathrm{Pe}}\hat{Y}(Z=0) \tag{A.44}$$

From the condition at $Z=1$ one obtains

$$A_3=-A_4\frac{N_{\mathrm{Pe}}-H}{N_{\mathrm{Pe}}+H}e^{-H} \tag{A.45}$$

and so

$$\hat{Y}=A_4e^{\frac{1}{2}(N_{\mathrm{Pe}}-H)Z}-A_4\frac{N_{\mathrm{Pe}}-H}{N_{\mathrm{Pe}}+H}e^{\frac{1}{2}(N_{\mathrm{Pe}}+H)Z-H}+\frac{1}{s} \tag{A.46}$$

Applying the boundary condition at $Z=0$:

$$A_4=\frac{2N_{\mathrm{Pe}}/s}{(N_{\mathrm{Pe}}-H)(1-e^{-H})-2N_{\mathrm{Pe}}\left(1-\frac{N_{\mathrm{Pe}}-H}{N_{\mathrm{Pe}}+H}\right)e^{-H}} \tag{A.47}$$

Substituting this expression into Equation A.46 at $Z=1$ yields

$$\hat{Y}=\frac{2N_{\mathrm{Pe}}\frac{1}{s}e^{\frac{1}{2}(N_{\mathrm{Pe}}-H)}(2H)}{(N_{\mathrm{Pe}}^2-H^2)(1-e^{-H})-2N_{\mathrm{Pe}}(N_{\mathrm{Pe}}+H)+2N_{\mathrm{Pe}}(N_{\mathrm{Pe}}-H)e^{-H}}+\frac{1}{s} \tag{A.48}$$

Now recognising that

$$N_{\mathrm{Pe}}^2-H^2=-4GN_{\mathrm{Pe}} \tag{A.49}$$

and multiplying the top and bottom of the first term by e^H, it is possible to obtain the following expression for the model in its final form:

$$\hat{Y}=\frac{1}{s}\left[1+\frac{2He^{\frac{1}{2}(N_{\mathrm{Pe}}+H)}}{(N_{\mathrm{Pe}}+2G-H)-(N_{\mathrm{Pe}}+2G+H)e^{H}}\right] \tag{A.50}$$

where

$$G=\tau_{\mathrm{f}}s+\frac{1}{L}\left(\sqrt{s}\coth\sqrt{s}-1\right) \tag{A.51}$$

$$H=\sqrt{N_{\mathrm{Pe}}^2+4GN_{\mathrm{Pe}}} \tag{A.52}$$

$$L=\frac{FR^2}{3V_{\mathrm{s}}KD} \tag{A.53}$$

$$N_{\mathrm{Pe}}=\frac{vL_{\mathrm{bed}}}{D_{\mathrm{L}}} \tag{A.54}$$

$$\tau_{\mathrm{f}}=\frac{V_{\mathrm{f}}D}{FR^2}=\frac{L_{\mathrm{bed}}D}{vR^2} \tag{A.55}$$

A.3.1 Equilibrium control

For the case of negligible diffusion resistance one may write

$$\bar{q}(r,t) = q(t) \text{ only} \tag{A.56}$$

and thus Equation A.24 takes the dimensionless form

$$-\frac{1}{N_{\mathrm{Pe}}}\frac{\partial^2 Y}{\partial Z^2} + \frac{\partial Y}{\partial Z} + \frac{\partial Y}{\partial \tau_{\mathrm{e}}} = 0 \tag{A.57}$$

where

$$\tau_{\mathrm{e}} = \frac{t}{\frac{V_{\mathrm{s}}K}{F} + \frac{V_{\mathrm{f}}}{F}} \tag{A.58}$$

with the same boundary conditions as the diffusion-limited case above. Taking the Laplace Transform:

$$-\frac{1}{N_{\mathrm{Pe}}}\frac{d^2\hat{Y}}{dZ^2} + \frac{d\hat{Y}}{dZ} + p\hat{Y} = 1 \tag{A.59}$$

which has eigenvalues

$$\frac{N_{\mathrm{Pe}} \pm \sqrt{N_{\mathrm{Pe}}^2 + 4pN_{\mathrm{Pe}}}}{2} \tag{A.60}$$

and so Equation A.57 has a solution of the form

$$\hat{Y} = A_3 e^{\frac{1}{2}(N_{\mathrm{Pe}}+I)Z} + A_4 e^{\frac{1}{2}(N_{\mathrm{Pe}}-I)Z} + \frac{1}{p} \tag{A.61}$$

with

$$I = \sqrt{N_{\mathrm{Pe}}^2 + 4pN_{\mathrm{Pe}}} \tag{A.62}$$

Applying the boundary condition at $Z = 1$ yields that

$$A_3 = -A_4 \frac{N_{\mathrm{Pe}} - I}{N_{\mathrm{Pe}} + I} e^{-I} \tag{A.63}$$

and so

$$\hat{Y} = A_4 e^{\frac{1}{2}(N_{\mathrm{Pe}}-I)Z} - A_4 \frac{N_{\mathrm{Pe}} - I}{N_{\mathrm{Pe}} + I} e^{\frac{1}{2}(N_{\mathrm{Pe}}+I)Z-I} \tag{A.64}$$

while the condition at $Z = 0$ indicates

$$A_4 = \frac{2N_{\mathrm{Pe}}/p}{2N_{\mathrm{Pe}}\frac{N_{\mathrm{Pe}}-I}{N_{\mathrm{Pe}}+I}e^{-I} - (N_{\mathrm{Pe}}+I) - (N_{\mathrm{Pe}}-I)e^{-I}} \tag{A.65}$$

Substituting this into Equation A.61 at $Z = 1$ yields

$$\hat{Y} = \frac{2\frac{1}{s}N_{\mathrm{Pe}}e^{\frac{1}{2}(N_{\mathrm{Pe}}-I)}\left(\frac{2I}{N_{\mathrm{Pe}}+I}\right)}{2N_{\mathrm{Pe}}\frac{N_{\mathrm{Pe}}-I}{N_{\mathrm{Pe}}+I}e^{-I} - (N_{\mathrm{Pe}}-I)e^{-I} - (N_{\mathrm{Pe}}+I)} + \frac{1}{p} \tag{A.66}$$

Now multiplying the top and bottom of the left hand term by e^I and by $(N_{\mathrm{Pe}}+I)$, it is possible after simplification to write the solution in its final form:

$$\hat{Y} = \frac{1}{p}\left[1 + \frac{2Ie^{\frac{1}{2}(N_{\mathrm{Pe}}+I)}}{(N_{\mathrm{Pe}}+2p-I)-(N_{\mathrm{Pe}}+2p+I)\,e^I}\right] \tag{A.67}$$

where

$$I = \sqrt{N_{\mathrm{Pe}}^2 + 4pN_{\mathrm{Pe}}} \tag{A.68}$$

$$N_{\mathrm{Pe}} = \frac{vL_{\mathrm{bed}}}{D_{\mathrm{L}}} \tag{A.69}$$

A.4 Plug flow model

In the case of ideal plug flow, D_{L} is zero (i.e. $N_{\mathrm{Pe}} \to \infty$) and so Equation A.35 may be written in the form

$$\frac{d\hat{Y}}{dZ} + G\hat{Y} = \frac{G}{s} \tag{A.70}$$

and the single boundary condition

$$C\,(z=0,t) = 0 \tag{A.71}$$

or, in a more relevant form

$$\hat{Y}\,(Z=0) = 0 \tag{A.72}$$

may be used. Equation A.70 has the single eigenvalue $-G$, and so the solution has the form

$$\hat{Y} = A_5 e^{-GZ} + \frac{1}{s} \tag{A.73}$$

with A_5 being the integration constant.

Applying the boundary condition easily yields that

$$A_5 = -\frac{1}{s} \tag{A.74}$$

and so the full model solution at $Z = 1$ is

$$\hat{Y} = \frac{1}{s}\left[1 - e^{-\tau_{\mathrm{f}}s - \frac{1}{L}\left(\sqrt{s}\coth\sqrt{s}-1\right)}\right] \tag{A.75}$$

A.4.1 Equilibrium control

For negligible diffusion resistance and zero dispersion, Equation A.24 takes the form

$$\frac{\partial Y}{\partial Z} + \frac{\partial Y}{\partial \tau_{\mathrm{e}}} = 0 \tag{A.76}$$

with the same initial and boundary conditions as the diffusion-limited case above. Taking the Laplace Transform yields

$$\frac{d\hat{Y}}{dZ} + p\hat{Y} = 1 \tag{A.77}$$

which has the single eigenvalue $-p$, and so the general solution may easily be written:

$$\hat{Y} = A_6 e^{-pZ} + \frac{1}{p} \tag{A.78}$$

The boundary condition yields

$$A_6 = -\frac{1}{p} \tag{A.79}$$

and so the full Laplace Domain solution at $Z = 1$ is obtained:

$$\hat{Y} = \frac{1}{p}\left[1 - e^{-p}\right] \tag{A.80}$$

This is easily inverted into the (dimensionless) time domain:

$$Y = 1 - \mathbf{H}(\tau_e - 1) \tag{A.81}$$

where $\mathbf{H}$ is the Heaviside function.

A.4.2 Approximation for large L

The Taylor series expansion for an exponential function is

$$e^x = 1 + x + \frac{x^2}{2} + \cdots \tag{A.82}$$

Using the first two terms of such an expansion of Equation A.75 (in which large values of L would make the high order terms negligibly small), yields

$$\hat{Y} \simeq \frac{1}{s}\left[1 - \left\{1 - \tau_f s - \frac{1}{L}\left(\sqrt{s}\coth\sqrt{s} - 1\right)\right\}\right] \tag{A.83}$$

which can be simplified to

$$\hat{Y} = \frac{1}{sL}\left(\sqrt{s}\coth\sqrt{s} - 1\right) \tag{A.84}$$

$$= \frac{1}{sL}\left(\frac{\sqrt{s}\cosh\sqrt{s} - \sinh\sqrt{s}}{\sinh\sqrt{s}}\right) \tag{A.85}$$

neglecting the fluid hold-up (i.e. $\tau_f = 0$).

Following the method of residues (Spencer et al., 1977), it is readily apparent from the second form that this equation has poles at

$$s = 0 \tag{A.86}$$

and at

$$\sqrt{s} = in\pi \tag{A.87}$$

$$\Rightarrow s = -n^2\pi^2 \tag{A.88}$$

where n is a positive integer, since the model uses positive square roots only.

Making the substitution

$$s = -\beta^2 \Rightarrow \sqrt{s} = i\beta \tag{A.89}$$

and substituting this into Equation A.84 yields

$$\hat{Y} = -\frac{1}{\beta^2 L}\left(i\beta \coth i\beta - 1\right) \tag{A.90}$$

Using the relation

$$\coth i\beta = -i \cot \beta \tag{A.91}$$

this may be rewritten in the form

$$\hat{Y} = -\frac{1}{\beta^2}\frac{1}{L}\left(\beta \cot \beta - 1\right) \tag{A.92}$$

The method now states that the time domain solution is given by

$$Y = \sigma_0 + \sum_n \sigma_n \tag{A.93}$$

where

$$\begin{aligned} \sigma_0 &= \lim_{s\to 0} s e^{s\tau}\hat{Y} && \text{(A.94)}\\ &= \lim_{\beta\to 0}\left(-\beta^2\right)\left(e^{-\beta^2\tau}\right)\left(-\frac{1}{\beta^2}\frac{1}{L}\right)\left(\beta\cot\beta - 1\right) && \text{(A.95)}\\ &= 0 && \text{(A.96)} \end{aligned}$$

and

$$\begin{aligned} \sigma_n &= \lim_{s\to n^2\pi^2}\left(s + n^2\pi^2\right)e^{s\tau}\hat{Y} && \text{(A.97)}\\ &= \lim_{\beta\to n\pi}\left(n^2\pi^2 - \beta^2\right)e^{-\beta^2\tau}\left(-\frac{1}{\beta^2}\frac{1}{L}\right)\left(\beta\cot\beta - 1\right) && \text{(A.98)}\\ &= \frac{2}{L}e^{-n^2\pi^2\tau} && \text{(A.99)} \end{aligned}$$

Thus the full time domain solution for large values of L is

$$\hat{Y} = \frac{2}{L}\sum_{n=1}^{\infty} e^{-n^2\pi^2\tau} \tag{A.100}$$

A.5 Crystal size distribution model

This model describes the situation for a CSTR type reactor where the sorbent particles have a distribution of radii, described by a log-normal distribution. The population density function has the form

$$p(\ln R) = \frac{1}{\sqrt{2\pi}\sigma} \exp\left(-\frac{(\ln R - \mu)^2}{2\sigma^2}\right) \tag{A.101}$$

or, equivalently,

$$p(R) = \frac{1}{R\sqrt{2\pi}\sigma} \exp\left(-\frac{(\ln R - \mu)^2}{2\sigma^2}\right) \tag{A.102}$$

For this model we take a slightly different approach when nondimensionaling the governing differential equations by making the substitution (Hsu and Haynes, 1981)

$$R = e^{\mu + \sqrt{2}\sigma\zeta} \tag{A.103}$$

This is necessary (and convenient) because R is not constant for all crystals in the sorbent bed. Fick's Second Law now takes the form

$$\frac{\partial \alpha}{\partial \tau_{\mathrm{m}}} = e^{-2\sqrt{2}\sigma\zeta} \frac{\partial^2 \alpha}{\partial X^2} \tag{A.104}$$

where

$$\tau_{\mathrm{m}} = t\frac{D}{R_{\mathrm{m}}^2} \tag{A.105}$$

and

$$R_{\mathrm{m}} = e^{\mu} \tag{A.106}$$

Taking the Laplace Transform of Equation A.104 now yields

$$e^{-2\sqrt{2}\sigma\zeta} \frac{d^2\hat{\alpha}}{dX^2} - s\hat{\alpha} = -X \tag{A.107}$$

and the desired derivative (as mentioned above in section A.1) may be easily shown to be

$$\left.\frac{d\hat{Q}}{dX}\right|_{X=1} = \left(\hat{Y} - \frac{1}{s}\right)\left[\left(e^{\sqrt{2}\sigma\zeta}\sqrt{s}\right)\coth\left[\left(e^{\sqrt{2}\sigma\zeta}\sqrt{s}\right)\right] - 1\right] \tag{A.108}$$

The fluid phase mass balance takes the form (Hsu and Haynes, 1981)

$$-\frac{V_{\mathrm{s}} D \cdot 4\pi \int_0^\infty R^2 \left.\frac{d\hat{q}}{dr}\right|_{r=R} p(R)dR}{\frac{4}{3}\pi \int_0^\infty R^3 p(R)dR} = F\hat{C} \tag{A.109}$$

Making the usual substitutions, it is a simple matter to reduce this equation to the form

$$-\frac{3V_sKD}{F}\frac{\int_0^\infty R\left.\frac{d\hat{Q}}{dX}\right|_{X=1}p(R)dR}{\int_0^\infty R^3p(R)dR}=\hat{Y} \tag{A.110}$$

and then by further using the substitution Equation A.103 and the fact that

$$p(R)dR=\frac{1}{\sqrt{\pi}}e^{-\zeta^2}d\zeta \tag{A.111}$$

we may write

$$-\frac{V_sKD}{F}\frac{R_m}{\overline{R^3}}\left(\hat{Y}-\frac{1}{s}\right)\int_0^\infty e^{\sqrt{2}\sigma\zeta}\left[\left(e^{\sqrt{2}\sigma\zeta}\sqrt{s}\right)\coth\left(e^{\sqrt{2}\sigma\zeta}\sqrt{s}\right)-1\right]p(\zeta)d\zeta=\hat{Y} \tag{A.112}$$

where

$$\overline{R^3} = \int_0^\infty R^3p(R)dR \tag{A.113}$$

$$= \frac{1}{\sqrt{\pi}}e^{3\mu}\int_{-\infty}^\infty e^{3\sqrt{2}\sigma\zeta-\zeta^2}d\zeta \tag{A.114}$$

The following relation proves useful (Gradshteyn and Ryzhik, 1994, p. 355):

$$\int_{-\infty}^\infty e^{-px^2\pm qx}dx=\frac{\sqrt{\pi}}{|p|}e^{\frac{q^2}{4p^2}} \tag{A.115}$$

from which it may be derived that

$$\overline{R^3}=R_m^3e^{\frac{9}{2}\sigma^2} \tag{A.116}$$

and so we may write

$$-\frac{3V_sKD}{FR_m^2}\left(\hat{Y}-\frac{1}{s}\right)e^{-\frac{9}{2}\sigma^2}\frac{1}{\sqrt{\pi}}\int_{-\infty}^\infty e^{\sqrt{2}\sigma\zeta}\left[\left(e^{\sqrt{2}\sigma\zeta}\sqrt{s}\right)\coth\left(e^{\sqrt{2}\sigma\zeta}\sqrt{s}\right)-1\right]e^{-\zeta^2}d\zeta=\hat{Y} \tag{A.117}$$

which leads to the final form of the model equation:

$$\hat{Y}=\frac{1}{s}\frac{\frac{1}{\sqrt{\pi}L_me^{\frac{9}{2}\sigma^2}}\int_{-\infty}^\infty e^{\sqrt{2}\sigma\zeta}\left[\left(e^{\sqrt{2}\sigma\zeta}\sqrt{s}\right)\coth\left(e^{\sqrt{2}\sigma\zeta}\sqrt{s}\right)-1\right]e^{-\zeta^2}d\zeta}{1+\frac{1}{\sqrt{\pi}L_me^{\frac{9}{2}\sigma^2}}\int_{-\infty}^\infty e^{\sqrt{2}\sigma\zeta}\left[\left(e^{\sqrt{2}\sigma\zeta}\sqrt{s}\right)\coth\left(e^{\sqrt{2}\sigma\zeta}\sqrt{s}\right)-1\right]e^{-\zeta^2}d\zeta} \tag{A.118}$$

where

$$L_m=\frac{FR_m^2}{3V_sKD} \tag{A.119}$$

$$R_m=e^{\mu} \tag{A.120}$$

Appendix B

Experimental Data

B.1 Sample data files

Two types of data files were produced. The first (with a `.txt` extension) contains a list of the experimental conditions. This is convenient to parse using the Fortran code shown in Section C.6.4.

```
wzsm5_1
h-zsm-5
    2
    2
cyclo-c6
 5738
 30.0
14.00
  150
 0.25
 1200
```

The second (with a `.prn` extension) contains the same data in a more verbose manner (suitable for working with in a spreadsheet), followed by the experimental desorption curve itself. Only the time-signal values are considered by the Fortran subroutine in Section C.6.4.

```
"Run Name: wzsm5_1"
"Catalyst: h-zsm-5"
"Catalyst size (microns): "     2
"Catalyst mass (mg): "     2
"Sorbate: cyclo-c6"
"Initial Partial Pressure (Pa): "  5738
"STP Flow Rate (ml/min): "  30.0
"Flow Ratio: " 14.00
```

"Temperature (C): " 150
"Sample Period (secs): " 0.25
"Number of samples: " 1200

"---"
"Run Data"
"---"

"Time (secs)"	"Signal"
0.00	600.31
0.25	599.59
0.50	599.69
0.75	600.70
1.00	600.10
1.25	600.09
1.50	600.93
1.75	600.41
2.00	600.62
.	.
.	.
10.00	600.71
10.25	599.91
10.50	600.51
10.75	606.38
11.00	607.03
11.25	606.15
11.50	432.19
11.75	359.28
12.00	320.24
12.25	292.55
12.50	270.60
12.75	252.25
13.00	236.54
13.25	222.69
13.50	210.36
13.75	199.30
14.00	189.22
14.25	180.15
14.50	171.70

14.75	164.05
15.00	156.95
.	.
.	.
295.00	0.03
295.25	0.04
295.50	0.05
295.75	0.09
296.00	0.05
296.25	0.10
296.50	0.07
296.75	0.08
297.00	0.06
297.25	0.08
297.50	0.07
297.75	0.05
298.00	0.06
298.25	0.08
298.50	0.04
298.75	0.03
299.00	0.07
299.25	0.07
299.50	0.06
299.75	0.08

B.2 AZSM5 (Sample B)

Run name	T (℃)	F (ml/min)	C_0 (Pa)	R (μm)	D/R^2 (1/s)	L	m_s (mg)
azsm5_26	150.	18.6	866.	1.0E-04	2.36E-03	3.33E+01	2.
azsm5_27	150.	27.9	866.	1.0E-04	2.41E-03	4.15E+01	2.
azsm5_28	150.	55.8	866.	1.0E-04	2.55E-03	5.45E+01	2.
azsm5_29	150.	37.2	866.	1.0E-04	2.52E-03	4.47E+01	2.
azsm5_30	150.	14.9	866.	1.0E-04	2.28E-03	3.29E+01	2.
azsm5_31	150.	46.5	866.	1.0E-04	2.50E-03	4.83E+01	2.
azsm5_32	150.	27.9	866.	1.0E-04	2.42E-03	4.03E+01	2.
azsm5_33	150.	46.5	866.	1.0E-04	2.47E-03	5.09E+01	2.
azsm5_34	150.	34.1	473.	1.0E-04	2.44E-03	3.97E+01	2.
azsm5_35	150.	85.2	473.	1.0E-04	2.30E-03	6.61E+01	2.
azsm5_36	150.	85.2	473.	1.0E-04	2.65E-03	5.51E+01	2.
azsm5_37	150.	51.1	473.	1.0E-04	2.57E-03	4.45E+01	2.
azsm5_38	150.	25.6	473.	1.0E-04	2.50E-03	3.34E+01	2.
azsm5_39	150.	68.2	473.	1.0E-04	2.58E-03	5.14E+01	2.
azsm5_40	150.	102.3	473.	1.0E-04	2.68E-03	5.82E+01	2.
azsm5_41	150.	119.3	473.	1.0E-04	2.71E-03	6.12E+01	2.
azsm5_42	150.	9.3	866.	1.0E-04	1.95E-03	3.25E+01	2.
azsm5_43	200.	57.2	473.	1.0E-04	1.28E-02	3.34E+01	2.
azsm5_44	200.	38.1	473.	1.0E-04	1.30E-02	2.55E+01	2.
azsm5_45	200.	114.4	473.	1.0E-04	1.32E-02	5.02E+01	2.
azsm5_46	200.	19.1	473.	1.0E-04	1.33E-02	1.63E+01	2.
azsm5_47	200.	41.6	866.	1.0E-04	1.22E-02	3.03E+01	2.
azsm5_48	200.	15.6	866.	1.0E-04	1.29E-02	1.52E+01	2.
azsm5_49	200.	20.8	866.	1.0E-04	1.22E-02	1.91E+01	2.
azsm5_50	100.	43.7	325.	1.0E-04	3.50E-04	1.46E+02	2.
azsm5_51	100.	45.1	325.	1.0E-04	3.36E-04	1.61E+02	2.
azsm5_52	100.	21.9	325.	1.0E-04	3.26E-04	1.48E+02	2.
azsm5_53	100.	65.6	325.	1.0E-04	3.86E-04	1.45E+02	2.
azsm5_54	125.	46.7	325.	1.0E-04	1.01E-03	6.65E+01	2.
azsm5_55	125.	93.3	325.	1.0E-04	1.15E-03	6.38E+01	2.
azsm5_56	125.	70.0	325.	1.0E-04	1.07E-03	7.03E+01	2.
azsm5_57	150.	49.6	325.	1.0E-04	2.66E-03	4.03E+01	2.
azsm5_58	150.	99.2	325.	1.0E-04	2.71E-03	5.30E+01	2.

continued on next page

Run name	T (℃)	F (ml/min)	C_0 (Pa)	R (μm)	D/R^2 (1/s)	L	m_s (mg)
azsm5_59	175.	52.5	325.	1.0E-04	6.30E-03	3.24E+01	2.
azsm5_60	225.	58.4	325.	1.0E-04	2.57E-02	3.30E+01	2.
Now using 1/4" reactor							
azsm5_61	150.	25.6	495.	1.0E-04	1.66E-03	4.34E+01	3.
azsm5_62	150.	51.1	495.	1.0E-04	1.61E-03	5.98E+01	3.
azsm5_63	150.	51.1	495.	1.0E-04	1.63E-03	5.73E+01	3.
azsm5_64	150.	102.3	549.	1.0E-04	1.71E-03	7.85E+01	3.
azsm5_65	150.	51.1	549.	1.0E-04	1.58E-03	6.39E+01	3.
azsm5_66	150.	68.2	549.	1.0E-04	1.60E-03	7.13E+01	3.
azsm5_67	150.	34.1	549.	1.0E-04	1.60E-03	5.23E+01	3.
azsm5_68	150.	119.3	549.	1.0E-04	1.71E-03	8.27E+01	3.
azsm5_69	150.	85.2	549.	1.0E-04	1.65E-03	7.59E+01	3.
azsm5_70	150.	25.6	549.	1.0E-04	1.43E-03	5.64E+01	3.
azsm5_71	150.	51.1	549.	1.0E-04	1.54E-03	6.92E+01	3.
Top of reactor filled with sand							
azsm5_72	150.	51.1	549.	1.0E-04	1.33E-03	8.08E+01	3.
azsm5_73	150.	25.6	549.	1.0E-04	1.34E-03	6.11E+01	3.
azsm5_74	150.	119.3	549.	1.0E-04	1.49E-03	9.89E+01	3.
azsm5_75	200.	57.2	549.	1.0E-04	7.49E-03	5.52E+01	3.
azsm5_76	200.	28.6	549.	1.0E-04	8.27E-03	3.07E+01	3.
azsm5_77	200.	114.4	549.	1.0E-04	8.13E-03	7.59E+01	3.
azsm5_78	200.	95.3	549.	1.0E-04	8.11E-03	6.81E+01	3.

B.3 BZSM5 (Sample Z-L-5/H)

Run name	T (℃)	F (ml/min)	C_0 (Pa)	R (μm)	D/R^2 (1/s)	L	m_s (mg)
bzsm5_2	200.	69.3	287.	1.0E-04	1.17E-03	2.79E+02	2.
bzsm5_3	250.	76.6	287.	1.0E-04	5.76E-03	2.40E+02	2.
bzsm5_4	250.	76.6	287.	1.0E-04	5.66E-03	2.46E+02	2.
bzsm5_6	225.	73.0	287.	1.0E-04	2.92E-03	2.36E+02	2.
bzsm5_8	175.	65.6	287.	1.0E-04	5.48E-04	4.40E+02	2.
bzsm5_9	200.	69.3	287.	1.0E-04	1.24E-03	8.72E+01	7.
bzsm5_10	200.	104.0	287.	1.0E-04	1.24E-03	1.04E+02	7.
bzsm5_11	200.	52.0	287.	1.0E-04	1.17E-03	7.80E+01	7.
bzsm5_12	200.	52.0	287.	1.0E-04	1.19E-03	7.55E+01	7.
bzsm5_13	150.	46.5	287.	1.0E-04	2.48E-04	1.13E+02	7.
bzsm5_14	175.	65.6	287.	1.0E-04	5.98E-04	9.31E+01	7.
bzsm5_15	175.	65.6	287.	1.0E-04	5.95E-04	9.17E+01	7.
bzsm5_16	250.	76.6	287.	1.0E-04	5.38E-03	8.07E+01	7.
bzsm5_17	150.	93.0	191.	1.0E-04	2.63E-04	1.16E+02	7.
bzsm5_18	150.	69.7	191.	1.0E-04	2.26E-04	1.51E+02	7.
bzsm5_19	150.	139.5	191.	1.0E-04	2.30E-04	1.74E+02	7.
bzsm5_20	150.	116.2	191.	1.0E-04	2.21E-04	1.71E+02	7.
bzsm5_21	270.	79.6	287.	1.0E-04	7.72E-03	1.00E+02	7.
bzsm5_22	225.	73.0	287.	1.0E-04	2.42E-03	9.49E+01	7.

B.4 DZSM5 (Sample Z-L-5/W)

Run name	T (℃)	F (ml/min)	C_0 (Pa)	R (μm)	D/R^2 (1/s)	L	m_s (mg)
dzsm5_01	150.	48.8	273.	1.0E-04	1.27E-03	4.02E+01	4.
dzsm5_02	150.	48.8	273.	1.0E-04	1.28E-03	3.87E+01	4.
dzsm5_03	150.	64.3	207.	1.0E-04	1.29E-03	3.92E+01	4.
dzsm5_04	150.	64.3	207.	1.0E-04	1.29E-03	3.92E+01	4.
dzsm5_05	150.	79.8	167.	1.0E-04	1.31E-03	3.91E+01	4.
dzsm5_06	175.	84.5	167.	1.0E-04	3.69E-03	2.33E+01	4.
dzsm5_07	175.	100.9	140.	1.0E-04	3.80E-03	2.40E+01	4.
dzsm5_08	125.	75.1	167.	1.0E-04	4.68E-04	8.14E+01	4.
dzsm5_09	125.	60.5	207.	1.0E-04	4.50E-04	7.98E+01	4.
dzsm5_10	100.	56.7	207.	1.0E-04	1.60E-04	1.78E+02	4.
dzsm5_11	200.	106.6	140.	1.0E-04	9.56E-03	1.84E+01	4.
dzsm5_12	200.	123.9	120.	1.0E-04	9.55E-03	2.01E+01	4.
dzsm5_13	150.	110.8	120.	1.0E-04	1.36E-03	3.73E+01	4.
dzsm5_14	150.	79.8	167.	1.0E-04	1.33E-03	3.77E+01	4.
dzsm5_15	150.	95.8	167.	1.0E-04	1.35E-03	3.76E+01	4.
dzsm5_16	150.	53.1	167.	1.0E-04	1.25E-03	3.35E+01	4.
dzsm5_17	150.	111.7	167.	1.0E-04	1.37E-03	4.14E+01	4.
dzsm5_18	150.	63.8	167.	1.0E-04	1.29E-03	3.66E+01	4.
dzsm5_19	100.	42.5	203.	1.0E-04	1.49E-04	1.79E+02	4.
dzsm5_20	200.	123.9	120.	1.0E-04	9.74E-03	1.98E+01	4.
dzsm5_21	200.	148.7	120.	1.0E-04	9.68E-03	2.27E+01	4.
dzsm5_22	220.	129.1	120.	1.0E-04	1.88E-02	2.07E+01	4.

B.5 EZSM5 (Sample Z-L-0.5/W)

Run name	T (°C)	F (ml/min)	C_0 (Pa)	R (μm)	D/R^2 (1/s)	L	m_s (mg)
			Agitated before packing				
ezsm5_01	150.	79.8	167.	1.0E-04	5.42E-03	2.06E+01	3.
ezsm5_02	150.	79.8	167.	1.0E-04	5.55E-03	1.92E+01	3.
ezsm5_03	125.	75.1	167.	1.0E-04	1.95E-03	3.61E+01	3.
ezsm5_04	125.	75.1	167.	1.0E-04	1.87E-03	3.70E+01	3.
ezsm5_05	125.	75.1	167.	1.0E-04	1.89E-03	3.65E+01	3.
ezsm5_06	100.	70.4	167.	1.0E-04	6.37E-04	8.16E+01	3.
ezsm5_07	100.	70.4	167.	1.0E-04	6.20E-04	7.93E+01	3.
ezsm5_08	150.	110.8	120.	1.0E-04	5.82E-03	2.03E+01	3.
ezsm5_09	150.	110.8	120.	1.0E-04	5.73E-03	2.09E+01	3.
ezsm5_10	175.	117.3	120.	1.0E-04	1.44E-02	1.70E+01	3.
ezsm5_11	175.	117.3	120.	1.0E-04	1.46E-02	1.64E+01	3.
			Settled				
ezsm5_12	150.	110.8	120.	1.0E-04	1.68E-03	5.08E+01	3.
ezsm5_13	150.	110.8	120.	1.0E-04	1.71E-03	4.77E+01	3.
ezsm5_14	100.	69.8	167.	1.0E-04	2.29E-04	1.80E+02	3.
ezsm5_15	175.	117.3	120.	1.0E-04	4.50E-03	3.35E+01	3.
ezsm5_16	100.	70.4	167.	1.0E-04	2.32E-04	1.83E+02	3.
ezsm5_17	175.	117.3	120.	1.0E-04	4.54E-03	3.28E+01	3.
ezsm5_18	200.	123.9	120.	1.0E-04	1.11E-02	2.80E+01	3.
ezsm5_19	125.	75.1	167.	1.0E-04	5.98E-04	9.44E+01	3.
ezsm5_20	200.	123.9	120.	1.0E-04	1.14E-02	2.80E+01	3.
			Agitated				
ezsm5_21	150.	110.8	120.	1.0E-04	3.36E-03	2.14E+01	3.
ezsm5_22	150.	110.8	120.	1.0E-04	3.32E-03	2.16E+01	3.
ezsm5_23	125.	75.1	167.	1.0E-04	1.05E-03	4.19E+01	3.
ezsm5_24	125.	75.1	167.	1.0E-04	1.05E-03	4.28E+01	3.
ezsm5_25	175.	117.3	120.	1.0E-04	9.15E-03	1.49E+01	3.
ezsm5_26	175.	117.3	120.	1.0E-04	9.14E-03	1.51E+01	3.
ezsm5_27	100.	97.7	120.	1.0E-04	3.60E-04	9.35E+01	3.
ezsm5_28	100.	70.4	167.	1.0E-04	3.47E-04	1.01E+02	3.
ezsm5_29	150.	110.8	120.	1.0E-04	3.31E-03	2.18E+01	3.

continued on next page

Run name	T (℃)	F (ml/min)	C_0 (Pa)	R (μm)	D/R^2 (1/s)	L	m_s (mg)
ezsm5_30	175.	117.3	120.	1.0E-04	9.19E-03	1.49E+01	3.
			Settled				
ezsm5_31	150.	79.8	167.	1.0E-04	2.21E-03	3.27E+01	3.
ezsm5_32	150.	79.8	167.	1.0E-04	2.19E-03	3.24E+01	3.
ezsm5_33	100.	70.4	167.	1.0E-04	2.69E-04	1.40E+02	3.
ezsm5_34	175.	117.3	120.	1.0E-04	6.26E-03	2.20E+01	3.
ezsm5_35	125.	75.1	167.	1.0E-04	7.28E-04	7.00E+01	3.
ezsm5_36	200.	123.9	120.	1.0E-04	1.59E-02	1.87E+01	3.
ezsm5_37	200.	123.9	120.	1.0E-04	1.59E-02	1.86E+01	3.
ezsm5_38	125.	75.1	167.	1.0E-04	7.31E-04	6.50E+01	3.
ezsm5_39	175.	117.3	120.	1.0E-04	6.31E-03	2.22E+01	3.
ezsm5_40	100.	70.4	167.	1.0E-04	2.44E-04	1.53E+02	3.

B.6 FZSM5 (Sample Z-L-100/-)

Run name	T (℃)	F (ml/min)	C_0 (Pa)	R (μm)	D/R^2 (1/s)	L	m_s (mg)
fzsm5_01	200.	71.9	207.	1.0E-04	2.19E-03	1.66E+02	4.
fzsm5_02	200.	89.2	167.	1.0E-04	2.50E-03	1.62E+02	4.
fzsm5_03	200.	106.6	140.	1.0E-04	2.86E-03	1.52E+02	4.
fzsm5_04	200.	71.9	207.	1.0E-04	2.24E-03	1.62E+02	4.
fzsm5_01	200.	71.9	207.	1.0E-04	2.19E-03	1.66E+02	4.
fzsm5_02	200.	89.2	167.	1.0E-04	2.50E-03	1.62E+02	4.
fzsm5_03	200.	106.6	140.	1.0E-04	2.86E-03	1.52E+02	4.
fzsm5_04	200.	71.9	207.	1.0E-04	2.24E-03	1.62E+02	4.
fzsm5_05	200.	89.2	390.	1.0E-04	2.52E-03	1.56E+02	4.
fzsm5_06	200.	89.2	610.	1.0E-04	2.67E-03	1.53E+02	4.
fzsm5_07	150.	64.3	99.	1.0E-04	5.55E-04	1.65E+02	4.
fzsm5_08	225.	75.7	207.	1.0E-04	4.88E-03	1.44E+02	4.
fzsm5_09	225.	75.7	207.	1.0E-04	5.03E-03	1.37E+02	4.
fzsm5_11	250.	79.5	207.	1.0E-04	6.89E-03	3.16E+01	22.
fzsm5_12	250.	98.7	167.	1.0E-04	7.05E-03	3.62E+01	22.

B.7 GZSM5 (Sample Z-L-5/E)

Run name	T (℃)	F (ml/min)	C_0 (Pa)	R (μm)	D/R^2 (1/s)	L	m_s (mg)
gzsm5_08	125.	118.8	106.	1.0E-04	9.91E-04	6.55E+01	3.
gzsm5_09	175.	133.7	106.	1.0E-04	6.44E-03	3.14E+01	3.
gzsm5_10	200.	141.2	106.	1.0E-04	1.47E-02	2.85E+01	3.
gzsm5_11	100.	70.4	167.	1.0E-04	2.76E-04	1.55E+02	3.
gzsm5_12	150.	79.8	167.	1.0E-04	2.13E-03	3.93E+01	3.
gzsm5_13	150.	79.8	167.	1.0E-04	2.44E-03	3.72E+01	3.
gzsm5_14	125.	75.1	167.	1.0E-04	8.45E-04	7.03E+01	3.

B.8 HZSM5 (Sample Z-L-100/-(60h))

Run name	T (℃)	F (ml/min)	C_0 (Pa)	R (μm)	D/R^2 (1/s)	L	m_s (mg)
hzsm5_01	200.	106.6	140.	1.0E-04	3.98E-03	1.27E+02	4.
hzsm5_02	200.	89.2	167.	1.0E-04	3.80E-03	1.20E+02	4.
hzsm5_03	200.	106.6	140.	1.0E-04	4.20E-03	1.18E+02	4.
hzsm5_04	200.	71.9	207.	1.0E-04	3.37E-03	1.22E+02	4.
hzsm5_05	225.	75.7	207.	1.0E-04	3.74E-03	2.49E+02	4.
hzsm5_06	150.	64.3	207.	1.0E-04	5.90E-04	1.77E+02	4.
hzsm5_07	200.	71.9	207.	1.0E-04	1.91E-03	3.49E+01	19.
hzsm5_08	250.	79.5	207.	1.0E-04	8.92E-03	3.01E+01	19.
hzsm5_09	250.	117.8	140.	1.0E-04	9.58E-03	3.78E+01	19.
hzsm5_10	250.	137.0	120.	1.0E-04	9.84E-03	4.09E+01	19.
hzsm5_11	250.	98.7	167.	1.0E-04	9.33E-03	3.41E+01	19.
hzsm5_12	150.	64.3	207.	1.0E-04	3.81E-04	3.97E+01	19.
hzsm5_14	225.	75.7	207.	1.0E-04	3.89E-03	3.71E+01	19.
hzsm5_15	250.	79.5	482.	1.0E-04	7.32E-03	3.99E+01	19.
hzsm5_16	250.	79.5	897.	1.0E-04	7.37E-03	3.85E+01	19.
hzsm5_17	250.	79.5	207.	1.0E-04	7.89E-03	3.60E+01	19.

B.9 RZSM5 (Sample A)

Run name	T (℃)	F (ml/min)	C_0 (Pa)	R (μm)	D/R^2 (1/s)	L	m_s (mg)
rzsm5_42	200.	52.0	632.	1.2E-03	2.32E-04	1.62E+02	22.
rzsm5_43	200.	52.0	480.	1.2E-03	2.22E-04	1.71E+02	22.
rzsn5_44	200.	52.0	253.	1.2E-03	2.25E-04	1.67E+02	22.
rzsm5_45	200.	52.0	379.	1.2E-03	2.36E-04	1.62E+02	22.
rzsm5_46	200.	52.0	881.	1.2E-03	2.32E-04	1.66E+02	22.
rzsm5_47	250.	51.9	379.	1.2E-03	8.87E-04	1.61E+02	22.
rzsm5_48	200.	52.0	758.	1.2E-03	2.18E-04	1.69E+02	22.
rzsm5_49	200.	52.0	1263.	1.2E-03	2.23E-04	1.76E+02	22.
rzsm5_50	200.	52.0	1404.	1.2E-03	2.31E-04	1.76E+02	22.
rzsm5_51	200.	52.0	2140.	1.2E-03	2.32E-04	2.05E+02	22.
rzsm5_52	200.	52.0	1733.	1.2E-03	2.32E-04	1.94E+02	22.
rzsm5_53	250.	51.9	379.	1.2E-03	8.73E-04	1.64E+02	22.
rzsm5_54	200.	52.0	2785.	1.2E-03	2.32E-04	2.08E+02	22.
rzsm5_55	200.	69.3	379.	1.2E-03	2.31E-04	2.15E+02	22.
rzsm5_56	200.	34.7	379.	1.2E-03	2.21E-04	1.59E+02	22.
rzsm5_57	200.	43.3	379.	1.2E-03	2.44E-04	1.64E+02	22.
rzsm5_58	200.	86.6	379.	1.2E-03	2.37E-04	2.41E+02	22.
rzsm5_59	250.	51.9	574.	1.2E-03	8.83E-04	1.83E+02	22.
rzsm5_60	200.	52.0	379.	1.2E-03	2.19E-04	1.86E+02	22.
rzsm5_61	200.	52.0	379.	1.2E-03	2.27E-04	1.88E+02	22.
rzsm5_62	200.	52.0	379.	1.2E-03	2.35E-04	1.82E+02	22.
rzsm5_63	200.	52.0	379.	1.2E-03	2.32E-04	1.85E+02	22.
rzsm5_64	200.	52.0	379.	1.2E-03	2.26E-04	1.91E+02	22.
rzsm5_65	200.	69.3	379.	1.2E-03	2.35E-04	2.18E+02	22.
rzsm5_66	200.	52.0	379.	1.2E-03	2.50E-04	1.75E+02	22.
rzsm5_67	200.	52.0	379.	1.2E-03	2.43E-04	1.79E+02	20.
rzsm5_68	200.	52.0	379.	1.2E-03	2.47E-04	1.76E+02	20.
rzsm5_69	200.	52.0	379.	1.2E-03	2.34E-04	1.93E+02	20.
rzsm5_70	200.	52.0	379.	1.2E-03	2.33E-04	1.96E+02	20.
rzsm5_71	200.	52.0	379.	1.2E-03	2.49E-04	1.89E+02	20.
rzsm5_72	200.	52.0	379.	1.2E-03	2.40E-04	1.96E+02	20.
rzsm5_74	200.	52.0	379.	1.2E-03	2.18E-04	1.94E+02	20.
rzsm5_75	200.	52.0	379.	1.2E-03	2.42E-04	1.78E+02	20.

continued on next page

Run name	T (℃)	F (ml/min)	C_0 (Pa)	R (μm)	D/R^2 (1/s)	L	m_s (mg)
rzsm5_76	200.	52.0	379.	1.2E-03	2.37E-04	1.79E+02	20.
rzsm5_77	200.	52.0	379.	1.2E-03	2.39E-04	1.77E+02	20.
rszm5_78	200.	52.0	379.	1.2E-03	2.50E-04	1.69E+02	20.
rzsm5_79	200.	52.0	379.	1.2E-03	1.93E-04	2.13E+02	20.
rzsm5_80	200.	52.0	379.	1.2E-03	2.36E-04	1.78E+02	20.
rzsm5_81	200.	52.0	379.	1.2E-03	2.41E-04	1.75E+02	20.
rzsm5_82	200.	52.0	379.	1.2E-03	2.38E-04	1.76E+02	20.
rzsm5_83	200.	52.0	379.	1.2E-03	2.23E-04	1.87E+02	20.
rzsm5_85	200.	52.0	379.	1.2E-03	2.17E-04	1.88E+02	20.
rzsm5_86	200.	52.0	379.	1.2E-03	2.26E-04	1.82E+02	20.
rzsm5_87	200.	52.0	379.	1.2E-03	2.34E-04	1.77E+02	20.
rzsm5_88	200.	52.0	379.	1.2E-03	2.26E-04	1.88E+02	20.
rzsm5_89	175.	49.2	379.	1.2E-03	1.12E-04	2.02E+02	20.
rzsm5_90	225.	54.7	379.	1.2E-03	4.78E-04	1.86E+02	20.
rzsm5_91	270.	59.7	379.	1.2E-03	1.44E-03	1.99E+02	20.
rzsm5_92	240.	56.4	379.	1.2E-03	6.77E-04	1.93E+02	20.
rzsm5_93	150.	46.5	379.	1.2E-03	4.14E-05	2.97E+02	20.

B.10 WZSM5 (Sample C, Parent sample)

Run name	T (℃)	F (ml/min)	C_0 (Pa)	R (μm)	D/R^2 (1/s)	L	m_s (mg)
wzsm5_1	150.	46.5	383.	1.0E-04	4.18E-03	2.43E+01	2.
wzsm5_2	150.	93.0	383.	1.0E-04	4.56E-03	2.82E+01	2.
wzsm5_3	150.	93.0	191.	1.0E-04	4.50E-03	2.42E+01	2.
wzsm5_4	200.	104.0	191.	1.0E-04	2.41E-02	2.64E+01	2.
wzsm5_5	100.	82.0	191.	1.0E-04	5.67E-04	1.23E+02	2.
wzsm5_6	175.	98.5	191.	1.0E-04	9.98E-03	3.10E+01	2.
wzsm5_7	125.	87.5	191.	1.0E-04	1.55E-03	6.11E+01	2.
wzsm5_8	150.	93.0	191.	1.0E-04	4.10E-03	3.82E+01	2.

Appendix C

Selected Fortran Code

This appendix includes some of the Fortran77 code used in the course of this work. It is mostly a collection of subroutines which should be called from driver programs with the desired model parameters.

C.1 Standard model fitting program

This is the most used program of those I wrote, for obvious reasons. It reads in two files with experimental data, writes a third file with the normalised data and best-fit model and writes the best-fit model parameters to standard output.

```
C $Id: zlc88opt.port.f 1.3 Thu, 26 Oct 2000 19:54:34 +0200 warwick $
C **********************************************************************
C Program to fit the standard ZLC model to experimental data collected
C using the program apc50cap.exe.
C
C Data file name is read from the standard input (without the extension)
C and results are written to the standard output in the following form:
C
C  RunID Temp.(C) Flow(ml/min@TP) Conc.(Pa) R(cm) D/R**2(1/s) L
C
C The normalised data a fitted model are written to file (same pre-
C extension name as the input files ; . fit extension).
C
C This is a more reliable program than zlc88opt.lbfgs.f, on which it
C is based.
C
C Requires: rddata.o libport zlc88.o objfn.o
C
C **********************************************************************

      program zlc88opt_port

      implicit real*8 (a-h,o-z)

      parameter (n = 2,
```

```
     &       liv = 61,
     &       lv = 78+n*(n+12),
     &       maxpts = 4000,
     &       Clow = 1.d-3,
     &       nstart = 1)

      real*8 d(n), x(n), b(2,n)
      real*8 v(lv), rparm(3)
      real*8 Cexp(4000), C88(4000)
      integer iv(liv), iparm(3)

      integer nerr(2)
      character*40 fname
      character*8 runID
      character*15 sample, gas
      character*44 efname

      external calcf
      external fparm

      common /pie/ pi
      common /zlc/ Cexp

C ***** START OF EXECUTABLE STATEMENTS

      data x / 1.d0, 1.d0 /                    ! Initial guesses
      data d / 1.d0, 1.d0 /                    ! Scale factors for x
      data b(1,1), b(2,1) / 1.d-2, 1.d2 /,     ! Bounds for x
     &     b(1,2), b(2,2) / 1.d-2, 1.d2 /

      pi = 4.d0*datan(1.d0)

      read(*,'(a40)')fname

      call rddata(Cexp,fname,Clow,runID,sample,R,catM,gas,conc,flow,
     &     T,dt,ndata,nend,nerr)

      if (nerr(1).ne.0.or.nerr(2).ne.0) then
         istar = index(fname,' ')
         if (nerr(1).ne.0) then
            efname = fname(1:istar-1)//'.txt'//fname(istar+4:)
         else
            efname = fname(1:istar-1)//'.prn'//fname(istar+4:)
         endif
         write(*,'(a58)')'Error opening '//efname
         stop
      endif

C Calculate default initial guesses for D/R**2 and L

      nmid = nend / 2
      C1 = Cexp(nmid)
      C2 = Cexp(nend)
      t1 = dt * dfloat(nmid)
      t2 = dt * dfloat(nend)

      Dr20 = dlog(C1/C2) / pi**2 / (t2-t1)
```

```
      tstep0 = dt * Dr20
      zlcL0 = 2.d0 / C1 * dexp(-pi**2*Dr20*t1)

      iparm(1) = maxpts
      iparm(2) = nstart
      iparm(3) = nend
      rparm(1) = zlcL0
      rparm(2) = tstep0
      rparm(3) = Clow

      call divset(2,iv,liv,lv,v)
      iv(21) = 0                    ! Suppress all printing

      call dmnfb(n,d,x,b,calcf,iv,liv,lv,v,iparm,rparm,fparm)

      tstep = tstep0 * x(2)
      Dr2 = Dr20 * x(2)
      zlcL = zlcL0 * x(1)
      T = T - 273.d0
      write(*,1000)runID,T,flow,conc,R,Dr2,zlcL

 1000 format(a8,2x,f5.0,2x,f5.1,2x,f5.0,2x,1pe7.1,2x,1pe8.2,2x,1pe8.2)

C Calculate fitted model response

      call zlc88(C88,zlcL,tstep,maxpts,(Clow/10.d0),nnn)

C Write normalised data and fitted model to .fit file

      istar = index(fname,' ')
      efname = fname(1:istar-1)//'.fit'//fname(istar+4:)
      open(unit=1,file=efname,status='unknown',iostat=nerr(1))
      if (nerr(1).eq.0) then
         write(1,'(a11,1pe8.2)')'# D/R**2 = ',Dr2
         write(1,'(a6,1pe8.2)')'# L = ',zlcL
         write(1,*)
         write(1,'(3(a11,2x))')' Time','Data','Model'
         write(1,*)
         write(1,2000)(dt*dfloat(i-1),Cexp(i),C88(i),i=1,nend)
      endif

 2000 format(1pe11.5,2x,1pe11.5,2x,1pe11.5)

      end


C ***** SUBROUTINES


C Dummy subroutine for dmnfb

      subroutine fparm
      return
      end

C Subroutine to calculate objective function
```

```
      subroutine calcf(n,x,nf,f,iparm,rparm,fparm)

      implicit real*8 (a-h,o-z)

      real*8 x(n), rparm(*)
      integer iparm(*)
      real*8 C(4000), Cexp(4000)
      external fparm

      common /pie/ pi
      common /zlc/ Cexp

      zlcL = rparm(1) * x(1)
      tstep = rparm(2) * x(2)
      nstart = iparm(2)
      ndata = iparm(3)

      call zlc88(C,zlcL,tstep,ndata,0.d0,ndum)

      call objfn(C,Cexp,f,nstart,ndata,10.d0)

      return
      end
```

C.2 Standard ZLC model

This is code to produce Equation 2.16.

```
C $Id: zlc88.f 1.7 Tue, 10 Oct 2000 18:52:23 +0200 warwick $
C ***********************************************************************
C subroutine zlc88(C,zlcL,tstep,maxpts,Clow,ndata)
C ***********************************************************************
C
C Subroutine to calculate the response of the standard ZLC model.
C Uses the analytical solution in dimensionless time (t*D/R**2).
C
C The user must supply the named common block pie, containing, oddly
C enough, the variable pi, which must be defined by the calling routine.
C
C Requires: libmach
C
C Variables in calling list:
C     C - vector of C/C0 values (dimensioned maxpts)
C     zlcL - ZLC parameter L = (F*R**2) / (3*Vcat*K*D)
C     tstep - dimensionless time step
C     maxpts - maximum number of points calculated for C
C     Clow - lower limit that C/C0 should be calculated to
C     ndata - number of values calculated for C (returned)
C
C Variables set in zlc88:
C     nsum - number of eigenvalues initially calculated
```

```
C     acc - accuracy for summation for C/C0
C     highL - value over which beta(n) approximated as n*pi
C     bacc - accuracy for Newton's method in finding beta(n)
C
C Common block names used:
C     pie
C
C
C Note on calculation of eigenvalues (beta(n)):
C     an initial number nsum are calculated; if more are required
C     in the actual summation for C/C0, they are generated on the
C     fly in the subroutine conc.
C
C ***********************************************************************

      subroutine zlc88(C,zlcL,tstep,maxpts,Clow,ndata)

      implicit real*8 (a-h,o-z)

      parameter (nsum=1000,
     &     highL=400.d0)

      real*8 C(maxpts),
     &     beta(nsum)

      common /pie/pi

C ***********************************************************************

C Set stopping criteria

      acc=dsqrt(d1mach(4))
      bacc=dsqrt(d1mach(4))

C Calculate vector of beta's

      do 1 i=1,nsum
         if (zlcL.ge.highL) then
            beta(i) = pi * dfloat(i)
         else
            beta(i) = betan(zlcL,i,bacc)
         endif
1     continue

C Sum for normalised concentration

      zlcLL = zlcL * (zlcL - 1.d0)

      C(1) = 1.d0

      i = 1
2     i = i + 1
      t = tstep * dfloat(i-1)
      C(i) = conc(beta,acc,t,zlcL,zlcLL,nsum,highL,bacc)
      if (i.lt.maxpts.and.C(i).gt.Clow) goto 2

      ndata = i
```

```
      return
      end

C
C Function to calculate beta(n) for given n
C Uses Newton's method when close to solution.
C
      real*8 function betan(zlcL,i,bacc)

      implicit real*8 (a-h,o-z)

      common /pie/pi

      di = dfloat(i)
      bold = (di-0.85d0) * pi
      ulimit = di * pi
      blimit = (di-1.d0) * pi

 1    a = 1.d0 / dtan(bold)
           bstep = (bold*a + zlcL - 1.d0) / (a - bold*(1.d0+a*a))
           bnew = bold - bstep
           if (bnew.lt.ulimit.and.bnew.gt.blimit) then
                bold = bnew
           else if (bstep.lt .0.d0) then
                bold = bold + (ulimit-bold)/2.d0
                goto 1
           else
                bold = bold - (bold-blimit)/2.d0
                goto 1
           endif
      if (dabs(bstep).gt.bacc) goto 1

      betan = bold

      return
      end

C
C Function to calculate C/C0 for given time
C
      real*8 function conc(beta,acc,t,zlcL,zlcLL,nsum,highL,bacc)

      implicit real*8 (a-h,o-z)

      real*8 beta(nsum)

      common /pie/pi

      sum = 0.d0

      i = 0
 1    i = i + 1
      if (i.gt.nsum) then
         if (zlcL.ge.highL) then
            beta2 = (pi * dfloat(i))**2
         else
```

```
            beta2 = (betan(zlcL,i,bacc))**2
         endif
      else
         beta2 = beta(i)**2
      endif
      sumd = dexp(-beta2*t) / (beta2+zlcLL)
      sum = sum + sumd
      if (dabs(sumd/sum).gt.acc) goto 1

      conc = 2.d0 * zlcL * sum

      return
      end
```

C.3 Plug flow model

This model is Equation 3.17, discussed in Chapter 3.

```
C $Id: zlcpf.f 1.3 Tue, 10 Oct 2000 18:52:23 +0200 warwick $
C ***********************************************************************
C subroutine zlcpf(C,zlcL,gamma,tstep,maxpts,Clow,ndata)
C ***********************************************************************
C
C Subroutine to calculate the response of the plug flow ZLC model by
C inverting the Laplace Domain solution into the time domain using the
C Fast Fourer Transform algorithm. Dimensionless time is used
C (i.e. t*D/R**2)
C
C The user must supply the named common block pie, containing, oddly
C enough, the variable pi, which must be defined by the calling routine.
C
C Requires: libfftpack , cdcoth.o
C
C Variables in calling list :
C     C - vector of C/C0 values (dimensioned nmax)
C     zlcL - dimensionless parameter L = (F*R**2) / (3*Vcat*K*D)
C     gamma - dimensionless parameter
C             gamma = Vf / (3*Vcat*K)
C     tstep - dimensionless time step
C     maxpts - maximum number of points calculated for C
C     Clow - lower limit that C/C0 should be calculated to
C     ndata - number of values calculated for C (returned)
C
C Variables set in zlc88f:
C     nfft - number of points for FFT (2 * maxpts)
C            has the effect of doubling the time interval
C
C Common block names used:
C     pie
C
C ***********************************************************************
```

```
      subroutine zlcpf(C,zlcL,gamma,tstep,maxpts,Clow,ndata)

      implicit real*8 (a-h,o-z)

      real*8 wsave(8*maxpts+15)
      complex*16 Cfft(2*maxpts)
      complex*16 one, temp, cdcoth, s, a1, a2

      real*8 C(maxpts)

      common /pie/pi

C ***************************************************************************

      nfft = maxpts * 2
      one = dcmplx(1.d0,0.d0)

      tinter = tstep * dfloat(nfft-1)
      dw = 2.d0 * pi / tinter

      tauf = gamma / zlcL

C  Initialise  fftpack  working array

      call  cffti (nfft,wsave)

C Calculate model frequency reponse

      Cfft(1) = dcmplx((tauf+1.d0/zlcL/3.d0),0.d0)

      do 1 i = 2, nfft/2+1
         s = dcmplx(0.d0,dw*dfloat(i-1))
         temp = cdsqrt(s)
         a1 = temp*cdcoth(temp) - one
         a2 = -tauf*s - a1/zlcL
         Cfft(i) = (one - cdexp(a2)) / s
 1    continue

C Fold and reflect  as required by FFT

      call  fold(nfft,Cfft)

C Call inverse  FFT routine

      call  cfftb(nfft,Cfft,wsave)

      Cfft(1) = 2.d0 * Cfft(1)
      do 2 i = 1, nfft
         Cfft(i) = Cfft(i) /  tinter
 2    continue

C Write complex*16 data into real*8 array to be returned

      i = 0
 3    i = i + 1
      C(i) = dble(Cfft(i))
```

```
      if (i.lt.maxpts.and.C(i).gt.Clow) goto 3

      ndata = i

      return
      end
```

C.4 Disperse flow model

This model is Equation 3.11, discussed in Chapter 3.

```
C $Id: zlcdf.f 1.3 Tue, 10 Oct 2000 18:52:23 +0200 warwick $
C ***********************************************************************
C subroutine zlcdf(C,zlcL,gamma,Pe,tstep,maxpts,Clow,ndata)
C ***********************************************************************
C
C Subroutine to calculate the response of the disperse flow ZLC model by
C inverting the Laplace Domain solution into the time domain using the
C Fast Fourier Transform algorithm. Dimensionless time is used
C (i.e. t*D/R**2).
C
C The user must supply the named common block pie, containing, oddly
C enough, the variable pi, which must be defined by the calling routine.
C
C Requires: libfftpack, cdcoth.o
C
C Variables in calling list:
C     C - vector of C/C0 values (dimensioned nmax) (returned)
C     zlcL - dimensionless parameter; L = (F*R**2) / (3*Vcat*K*D)
C     gamma - dimensionless parameter; gamma = Vf / (3*Vcat*K)
C     Pe - Peclet number; Pe = v * Lbed / DL
C     tstep - dimensionless time step
C     maxpts - maximum number of points calculated for C
C     Clow - lower limit that C/C0 should be calculated to
C     ndata - number of values calculated for C (returned)
C
C Variables set in zlc88f:
C     nfft - number of points for FFT (2 * maxpts)
C            has the effect of doubling the time interval
C
C Common block names used:
C     pie
C
C
C Note: this subroutine can not be used for Pe.eq.0.;
C       maximum Pe is between 630. and 650.
C
C ***********************************************************************

      subroutine zlcdf(C,zlcL,gamma,Pe,tstep,maxpts,Clow,ndata)
```

```
      implicit real*8 (a-h,o-z)

      real*8 wsave(8*maxpts+15)
      complex*16 Cfft(2*maxpts)
      complex*16 one, temp, cdcoth, s, a1, a2, a3, top, bottom

      real*8 C(maxpts)

      common /pie/pi

C *********************************************************************

      nfft = maxpts * 2
      one = dcmplx(1.d0,0.d0)

      tinter = tstep * dfloat(nfft-1)
      dw = 2.d0 * pi / tinter

      tauf = gamma / zlcL

C Initialise fftpack working array

      call cffti (nfft,wsave)

C Calculate model frequency reponse

      Cfft(1) = dcmplx((tauf+1.d0/zlcL/3.d0),0.d0)

      nhalf = nfft/2+1
      do 1 i = 2, nhalf
         s = dcmplx(0.d0,dw*dfloat(i-1))
         temp = cdsqrt(s)
         a1 = temp*cdcoth(temp) - one
         a2 = tauf*s + a1/zlcL
         a3 = cdsqrt(Pe**2 + 4.d0*a2*Pe)
         top = 2.d0*a3*cdexp((Pe+a3)/2.d0)
         bottom = (2.d0*a2+Pe-a3)-(2.d0*a2+Pe+a3)*cdexp(a3)
         Cfft(i) = (one + top/bottom) / s
1     continue

C Fold and reflect as required by FFT

      call fold(nfft,Cfft)

C Call inverse FFT routine

      call cfftb(nfft,Cfft,wsave)

      Cfft(1) = 2.d0 * Cfft(1)
      do 2 i = 1, nfft
         Cfft(i) = Cfft(i) / tinter
2     continue

C Write complex*16 data into real*8 array to be returned

      i = 0
3     i = i + 1
```

```
      C(i) = dble(Cfft(i))
      if (i.lt.maxpts.and.C(i).gt.Clow) goto 3

      ndata = i

      return
      end
```

C.5 Size distribution model

This model is Equation 4.12, discussed in Chapter 4.

```
C $Id: zlcrf.f 1.3 Tue, 10 Oct 2000 18:52:23 +0200 warwick $
C **********************************************************************
C subroutine zlcrf(C,zlcL,sigma,tstep,maxpts,Clow,ndata)
C **********************************************************************
C
C Subroutine to calculate the response of the ZLC model incorporating
C a distribution of crystal sizes (log-normal) by inverting the Laplace
C Domain solution into the time domain using the Fast Fourier Transform
C algorithm. Dimensionless time is used (i.e. t*D/Rm**2).
C
C Mean radius here (Rm) is the exponential of the mean of the normal
C distribution of the logarithm of crystal radius.
C
C The user must supply the named common block pie, containing, oddly
C enough, the variable pi, which must be defined by the calling routine.
C
C Requires: libfftpack, cdcoth.o, gaussq.o, dgamma.a
C
C Variables in calling list:
C     C - vector of C/C0 values (dimensioned nmax) (returned)
C     zlcL - dimensionless parameter; L = (F*Rm**2) / (3*Vcat*K*D)
C     sigma - standard deviation of size distribution
C     tstep - dimensionless time step
C     maxpts - maximum number of points calculated for C
C     Clow - lower limit that C/C0 should be calculated to
C     ndata - number of values calculated for C (returned)
C
C Variables set in zlcrf:
C     nfft - number of points for FFT (2 * maxpts)
C            has the effect of doubling the time interval
C     nherm - number of points for Hermite quadrature
C
C Common block names used:
C     pie
C
C **********************************************************************

      subroutine zlcrf(C,zlcL,sigma,tstep,maxpts,Clow,ndata)
```

```
      implicit real*8 (a-h,o-z)

      parameter (kind=4,       ! Hermite rule specifier for gaussq
     &     nherm=30)           ! no. pts for Hermite quadrature
      real*8 z(nherm), w(nherm) ! roots & weights for Hermite quadrature
      real*8 b(nherm)          ! scratch array for Hermite roots
      real*8 endpts(2)         ! must be passed; not used

      real*8 wsave(8*maxpts+15)
      complex*16 Cfft(2*maxpts)
      complex*16 one, cdcoth, s
      complex*16 const, temp1, temp2, f, zint

      real*8 C(maxpts)

      common /pie/pi

C ***********************************************************************

      nfft = maxpts * 2
      one = dcmplx(1.d0,0.d0)
      root2 = dsqrt(2.d0)

      tinter = tstep * dfloat(nfft-1)
      dw = 2.d0 * pi / tinter

C Initialise fftpack working array

      call cffti (nfft,wsave)

C Calculate Hermite roots and weights

      call gaussq(kind,nherm,0.d0,0.d0,0,endpts,b,z,w)

C Calculate model frequency response (outer loop)
C Evaluate integral by Gauss-Hermite quadrature (inner loop)

      Cfft(1) = dcmplx(1.d0/zlcL/3.d0,0.d0)

      const = dcmplx(dsqrt(pi)*zlcL*dexp(4.5d0*sigma**2),0.d0)
      nhalf = nfft/2 + 1
      do 1 i=2, nhalf
         s = dcmplx(0.d0,dw*dfloat(i-1))
         zint = dcmplx(0.d0,0.d0)
         do 2 j=1, nherm
            temp1 = dexp(root2 * sigma * z(j))
            temp2 = temp1 * cdsqrt(s)
            f = temp1 * (temp2*cdcoth(temp2)-one)
            zint = zint + w(j)*f
 2       continue
         Cfft(i) = zint / (const + zint) / s
 1    continue

C Fold and reflect as required by FFT

      call fold(nfft,Cfft)
```

```
C Evaluate inverse FFT

      call cfftb(nfft,Cfft,wsave)

      Cfft(1) = 2.d0 * Cfft(1)
      do 3 i = 1, nfft
         Cfft(i) = Cfft(i) / tinter
 3    continue

C Write complex*16 data to real*8 array to be returned

      i = 0
 4    i = i + 1
      C(i) = dble(Cfft(i))
      if (i.lt.maxpts.and.C(i).gt.Clow) goto 4

      ndata = i

      return
      end
```

C.6 Supplementary functions

C.6.1 `cdcoth()`

Fortran (or possible just g77) doesn't appear to provide a built-in function to calculate the double-precision complex hyperbolic cotangent, so I wrote my own (very rough) one.

```
C $Id: cdcoth.f 1.2 Sat, 10 Jun 2000 23:54:29 +0200 warwick $
C
C Function to calculate complex*16 hyperbolic cotangent.
C Approximated as (1.,0.) for argument.ge.200.

      complex*16 function cdcoth(x)

      implicit complex*16 (a-h,o-z)

      one = dcmplx(1.d0,0.d0)

      if (dble(x).lt.2.d2) then
         temp1 = cdexp(x)
         temp2 = one / temp1
         cdcoth = (temp1+temp2) / (temp1-temp2)
      else
         cdcoth = one
      endif

      return
      end
```

C.6.2 fold()

The FFTPACK library (see Section C.6.6) requires that Fourier domain data be folded about the mid-point before calling the inverse transform subroutine. This small code fragment does just that.

```
C Subroutine to fold data as required by fftpack.

      subroutine fold(nfft,C)

      implicit real*8 (a-h,o-z)
      complex*16 C(*)

      n2 = nfft/2 + 1

C Fold about nfft/2

      do 1 i=n2+1,nfft
         temp1=dble(C(nfft-i+2))
         temp2=-dimag(C(nfft-i+2))
         C(i)=dcmplx(temp1,temp2)
 1    continue

C Retain symmetry if nfft is even

      ntest=2*int(dfloat( nfft )/2.d0+0.6d0)
      if ( nfft .eq. ntest ) then
         temp1=dble(C(n2))
         C(n2)=dcmplx(temp1,0.d0)
      endif

      return
      end
```


C.6.3 objfn()

This is the objection function I used for all model fitting.

```
C $Id: objfn.f 1.3 Thu, 26 Oct 2000 19:54:34 +0200 warwick $
C **********************************************************************
C subroutine objfn(C1,C2,F,nstart,nend,wt)
C **********************************************************************
C Subroutine to calculate the objective function for ZLC desorption
C curves using a weighted sum of logarithmic square errors designed
C to weight the tail of the curve.
C
```

```
C Variables in calling list :
C     C1, C2 - vectors of data
C     F - value of objective function (returned)
C     nstart - initial point to compare
C     nend - final point to compare
C     wt - weighting variable; weighting increases from 1 to this
C
C ***************************************************************************

      subroutine objfn(C1,C2,F,nstart,nend,wt)

      implicit real*8 (a-h,o-z)

      real*8 C1(*), C2(*)

      F = 0.d0

      a = (wt-1.d0) / dfloat(nend-nstart)

      do 1 i=nstart,nend
         weight = 1.d0 + a*dfloat(i-nstart)
         F = F + dlog(C1(i)/C2(i))**2 * weight
1     continue

      return
      end
```

C.6.4 rddata()

This is a simple function I use to read in an experimental desorption curve from two text files: a .PRN file with the time:value data and a .TXT file with data about the conditions of the run (see Section B.1). Data normalisation and removal of dead time is done here.

```
C $Id: rddata.f 1.3 Tue, 10 Oct 2000 18:52:23 +0200 warwick $
C ***************************************************************************
C subroutine rddata(C,fname,Clow,runID,sample,R,catM,gas,conc,flow,
C     &     T,dt,ndata,nend,nerr)
C ***************************************************************************
C
C Subroutine to read experimental ZLC data written by the program
C apc50cap.exe. Dead time (assumed to be .ge.10 secs) is stripped
C from the data; all points .ge.0.97 are forced to 1 (i.e. assumed to
C be part of dead time). All points .lt.1.d-6 are forced to 1.d-6.
C
C Note that the subroutine returns immediately if errors are encountered
C when opening the data files. Both the .txt and .prn files are used.
C The files _MUST_ be in the UNIX format (i.e. NL=CR not NL=CR/LF).
C
C Variables in calling list :
C     C - vector of C/C0 values (arbitrary size) (returned)
C     fname - char*40 name of data file without the extension
```

```
C       Clow – value of C/C0 denoting the 'end' of the experiment
C       runID – char*8 ID of the individual experiment (returned)
C       sample – char*15 type of catalyst (returned)
C       R – radius of the catalyst crystals in cm (returned)
C       catM – mass of catalyst sample in mg (returned)
C       gas – char*15 name of adsorbate (returned)
C       conc – initial sorbate partial pressure in Pa (returned)
C       flow – purge flow rate in ml/min @ TP (returned)
C       T – temperature in K (returned)
C       dt – time step in secs (returned)
C       ndata – total number of data points (less dead time) (returned)
C       nend – number of points for which C.gt.Clow (returned)
C       nerr – integer*2 array denoting success (0) or not of opening
C              run data files (returned)
C              nerr(1) –> .txt file
C              nerr(2) –> .prn file
C
C I/O unit numbers used: 1 (for both .txt and .prn files )
C
C ***************************************************************************

      subroutine rddata(C,fname,Clow,runID,sample,R,catM,gas,conc,flow,
     &     T,dt,ndata,nend,nerr)

      implicit real*8 (a–h,o–z)

      real*8 C(*)
      integer nerr(2)

      character*40 fname
      character*8 runID
      character*15 sample, gas
      character*40 dummy
      character*44 efname

C Append '.txt' to fname and read run info

      istar = index(fname,' ')
      efname = fname(1:istar–1)//'.txt'//fname(istar+4:)
      open(unit=1,file=efname,status='old',iostat=nerr(1))
      if (nerr(1).ne.0) return

      read(1,'(a8)')runID
      read(1,'(a15)')sample     !catalyst type
      read(1,*)R                !actually gives diameter in microns
      R = R / 2.d4              !radius in cm
      read(1,*)catM             !mg
      read(1,'(a15)')gas        !tracer
      read(1,*)conc             !actually initial vapour pressure
      read(1,*)flow             !ml/min @ STP
      read(1,*)ratio
      read(1,*)T                !deg. C
      read(1,*)dt               !secs
      read(1,*)ndata

      conc = conc / (ratio + 1.d0) ! initial partial pressure
      T = T + 273.d0            !Kelvin
```

```
      flow = flow * T / 273.d0  !ml/min @ TP

C Close .txt  file

      close(1)

C Append '.prn' to fname and read run data

      istar  = index(fname,' ')
      efname = fname(1:istar-1)//'.prn'//fname(istar+4:)
      open(unit=1,file=efname,status='old',iostat=nerr(2))
      if (nerr(2).ne.0) return

C Skip text at top of .prn file , then read ndata data points
C Note that 1'st point in C corresponds to t=0

      do 1 i=1,15
         read(1,*)dummy
 1    continue

      do 2 i=1,ndata
         read(1,*)time,C(i)
 2    continue

C Close .prn file

      close(1)

C Average 1'st 10 secs for initial concentration

      C0 = 0.d0
      n = nint(10.d0/dt) + 1
      do 3 i=1,n
         C0 = C0 + C(i)
 3    continue
      C0 = C0 / dfloat(n)

C Normalise concentration data and find dead time
C (C(i).ge.0.97d0) is converted to 1.d0
C (C(i).lt .1.d-6) is converted to 1.d-6
C ndead is the position of the initial time point (less dead time)

      do 4 i=1,ndata
         C(i) = C(i) / C0
         if (C(i).ge.0.97d0) then
            C(i) = 1.d0
            ndead = i
         endif
         if (C(i).lt .1.d-6) C(i) = 1.d-6
 4    continue

C Shift data to remove dead time; modify total number of data points

      do 5 i=1,(ndata-ndead+1)
         C(i) = C(i+ndead-1)
 5    continue
      ndata = ndata - ndead + 1
```

```
C Get default end time

      i = ndata
6     if (C(i).lt.Clow) then
        i = i - 1
        goto 6
      endif
      nend = i

      return
      end
```

C.6.5 d1mach()

This function may be found in the SLATEC mathematics library or the BLAS linear algebra collection, both available from `www.netlib.org`. It essentially gives the machine precision and is used to define convergence criteria. I recommend grabbing the *C* functions from the SLATEC package in Debian GNU/Linux, which make use of *C* library constants.

C.6.6 cffti() and cfftb()

These functions to calculate the inverse complex Fast Fourier Transform are part of FFTPACK, which may be obtained from `www.netlib.org`. Some effort is required to convert the routines from single to double precision.

C.6.7 gaussq()

This is a function to calculate the weighting factors for Gaussian quadrature. Note that this function requires `dgamma()`. Both may be downloaded from `www.netlib.org`.

C.6.8 divset() and dmnfb()

These functions come from the `port` optimisation library (`www.netlib.org`). I have used the routine for double-precision BFGS optimisation. I've found this to be more robust code than `LBFGS`.